System Identification and Adaptive Control of Planar Cable Robots

by

Gokhan Gungor

A thesis
presented to the University of Waterloo
in fulfillment of the
thesis requirement for the degree of
Master of Science
in
Mechanical Engineering

Waterloo, Ontario, Canada, 2014

I hereby declare that I am the sole author of this thesis. This is a true copy of the thesis, including any required final revisions, as accepted by my examiners.

I understand that my thesis may be made electronically available to the public.

Abstract

Cable-based robots generally perform better than other parallel robots with rigid links in terms of wider workspace and higher acceleration of end-effector because of light weight of robot links. Cable robots allow easy installation for outside applications at the expense of the requirement of a precise assembly of its components at the cable anchor points. In this study, system identification and adaptive control of cable planar robots are considered. Firstly, a parametric model is developed for estimation of position errors of anchor points for fully-constrained and redundant planar cable robots. A novel method based on inclusion of virtual cables facilitates the linear separation of the uncertain parameters from the input-output signals for redundant planar robots. A least-squares and gradient based parameter estimation algorithm provide the estimates of the system parameters. Further, this work deals with the design and comparison of three adaptive position control schemes combined with a classical PID controller for fully constrained and redundant planar robots. Then, three Lyapunov based adaptive controllers based on the (i) sliding mode, (ii) PD and (iii) backstepping schemes are designed to compensate for the matrix uncertainties appear in the system dynamics resulting from errors in the anchor point locations. Next, the adaptive controllers are evaluated and compared with a classical PID controller through simulations for a desired 2D singularity-free pose of the mobile platform. Supremacy of the PD control scheme over the aforementioned control schemes is observed through simulations. The least-squares algorithm is compared with the gradient-based method in terms of the speed of convergence of the estimated parameters as well. Finally, we establish linear parametric forms for common friction models, recursive least-squares on-line friction estimator is presented and adaptive friction compensation scheme is designed. The efficiency of this design is discussed via simulation results.

Acknowledgements

I would like to express my sincere gratitude to my supervisor, Dr. Baris Fidan for the guidance and support he has provided throughout my graduate studies. This graduate study could not been completed without his help.

Also, I would like to express my greatest appreciation to Dr. Amir Khajepour for his advise and knowledge he has provided.

I would also like to thank Dr. Sergio Torres Mendez and his family for their endless support.

I would like to thank to Dr. Amir Khajepour and Dr. Eihab M. Abdel-Rahman for the feedback they have given.

My sincere gratitude goes to Kemal Buyukkabasakal for his supports .

I would also like to express my greatest appreciation to Dr. William Melek for his support.

I would also like to thank my family for their love and support, their unconditional encouragement and belief during these years.

Above all, I would like thank God for helping me to overcome all problems I confronted and making everything possible for me.

To my family

Table of Contents

List of Tables

List of Figures

Chapter 1

Introduction

Parallel robots generally have better acceleration and stiffness than serial robots. However, high precision problems are still an issue for accurate parallel manipulator design. Conventional parallel robots usually have limitation about their workspaces and contain singularity inside the workspace region.

Cable-based parallel robots can be favored instead of conventional parallel robots because they can reach wider workspace. Cable robots have some advantages in comparison with conventional parallel robots in industrial applications because of their large workspaces, heavy payload, easy remounting and transportation, and low-inertia [1]. However, this requires a precise assembly of the components that require knowledge of actuator positions of the robot. Error or uncertainty in actuator positions may generate uncertainty in the structure matrix which is transferred as an error in cable tension and length.

Parallel mechanisms generally contain heavy rigid links while cable parallel robot systems can use light flexible wires [2]. They can reach high speeds and acceleration because of the inclusion of cable links which are lighter than conventional robotic links [3]. Despite these advantages of cable robots; they have some disadvantages such as the pull working condition, need for a number cables higher than degrees of freedom (DOF) and work only under tension.

The number of cable links in an actual industrial parallel robots are usually higher than the numbers we consider in this study. The number common strategy for maintaining the positive constraint condition in a cable robot is using more cable than DOF. For example, the NIST robocrane has a suspended mobile platform connected by six cables to a fixed platform [4]. This robot has a large workspace for material handling in warehouse

and storage facilities. The Falcon-7 robot uses a rigid link with seven cables to improve stiffness [5].

The cable robots have different features than other robotic systems in terms of mathematical modeling, designing, and workspace analysis [6] [7]. According to Hiller et al. [8] cable robots can be divided into three different categories: incompletely restrained, completely restrained and redundant restrained. Completely constrained and redundant planar cable robots are studied in this thesis. The number of cables need to be only one more than DOF count to define a completely constrained cable robot. On the other hand, in a redundant parallel robot the number of actuators are more than the number of DOFs [8]. In addition, redundancy in conventional parallel robots are used for avoiding singularities in workspace while in cable robots are used for ensuring necessity cable tension forces in the workspace.

A common strategy for maintaining the positive constraint condition in a cable robot is the addition to the system of more cables are called antagonistic. Distinguish them from the parallel cables, which work along the same direction, principally to support the same payload. Thus, a fully constrained cable robot has only one extra antagonistic cable than DOFs to completely define the position of the mobile platform; for example the Falcon-7 robot [5] has seven cables to completely restrain its six DOFs mobile end-effector. On the other hand, redundant cable robots use two or more antagonistic cables than DOFs in order to fully constraint any motion of the mobile platform; for example, the Charlotte robot [9], has eight cables to fully constrained the spatial movement of its mobile platform.

Redundancy might result favorably to generate stable motion of the robot's mobile platform by changing the cable lengths accordingly and balancing the tensions among cables [10, 11]. However, any force formulation must ensure that all cables are in tension to avoid the mobile platform collapse. These tension formulations, [12–15], are based on the structure matrix which contains parameters related to the geometry of the cable robot, i.e. the length and orientation of cables.

Previous studies on compensating for cable length/orientation errors can be classified into three main approaches: 1) improvement of the mechanical winch device, 2) development of complete mathematical models, and 3) design of alternative control schemes. The work done by Pham et al. [16] are an attempt to improve the cable drive unit by allowing the winch to have a coordinate motion (translation and rotation) while the cable is wound. Kawamura et al. [3] apply a PD control law with gravitational force and internal tension compensation by assuming an accurate measurement of the cable lengths with a nonlinear spring model of the winch and cable elasticities. Fang et al. [17] compensate for cable length errors by modeling the elasticities of both drive units and cables as linear springs.

The authors use this model to calculate the cable tensions in a joint-space motion control without considering any on-line cable length estimation. On the other hand, Kino et al. [18] verify experimentally that a task-space adaptive control is beneficial in compensating for variations in static anchor points.

Adaptive controllers require a parametric model and an adaptive law to adjust the system's controller parameters in response to uncertainty affecting a system's model [19, 20]. The construction of parametric model is based on separation of the uncertain parameters from the measurable input-output signals, such that the parametric model has a linear structure. On-line parameter identification algorithms generate estimates of unknown plant parameters using past and current signal measurements continuously [20]. The adaptive law (parameter estimator) updates the estimated parameters using an on-line algorithm and an estimation error, which might converge to zero. Our focus, in this study, is developing a main framework for parameter identification rather than solving an identification problem for a specific robot. Hence, for brevity, we selected our problem setting to involve less number of cables. This work presents the design and analysis of three indirect adaptive controllers using the modular parameter identification based on methodologies of a proportional derivative adaptive (PDA) controller, backstepping adaptive (BA) and a sliding mode with saturation adaptive (SMsatA) controller. The performance of these three designs are compared with a classical proportional integral derivative (PID) controller when uncertainties in the measurements of anchor points are consider during the motion of the mobile platform.

The study is organized as follows. First, model description of completely constrained and redundant planar cable robotic systems are given. Also, we develop the kinestatic model of the cable robots using loop closure equation. Second, we derive two identification models using three different parameterization methods. Then, recursive least squares and gradient identification algorithms are presented. Further, the adaptive and robust control strategies are designed and analyzed using Lyapunov stability methods. Next, the control strategies are compared via simulation and four performance indexes. Lastly, we establish linear parametric forms for a common friction model, recursive least-squares on-line friction estimator is presented and adaptive friction compensation scheme is designed. Hence, we implement simulation for these design. Finally, the results of this thesis are discussed and summarized.

Chapter 2

Background

A representative physical robotic system is presented in Figure 2.1. The theoretical model of this system is formulated assuming that each cable is always under positive tension for a given pose of the mobile platform.

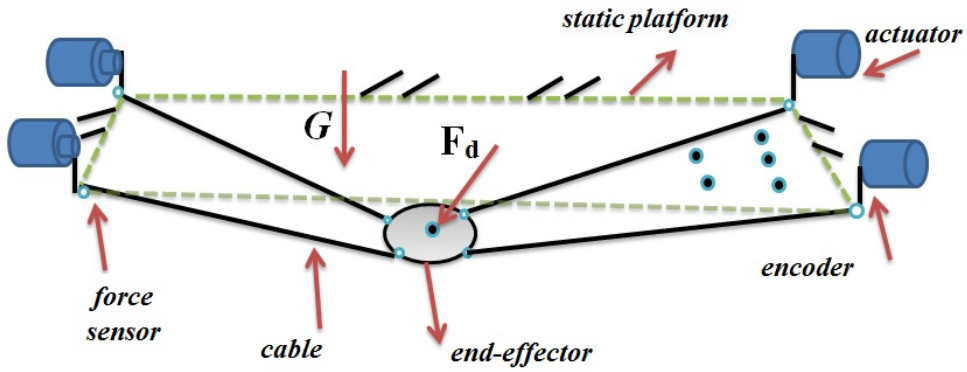

Figure 2.1: Components representation of cable robot.

Consider the Chebychev-Grbler-Kutzbach (or mobility formula) criterion [21] for multi-loop mechanisms with independent closed-loop rigid kinematic chains and the same motion parameters, formulation of number of degree freedom, m, can be written as

$$m = b_p m_{bodies} - \sum_{j=1}^{m_{joints}} (b_p - m_j) \tag{2.1}$$

where m is number of degree of freedom, b_p is motion parameter (b_p=6 for spatial movement and b_p=3 for planar movement), m_{bodies} is number of moving bodies, m_{joints} defines number of joints, m_j describes number of degree of freedom of the j joint. However, this formula (2.1) can not be used for parallelogram and paradoxical mechanisms. Thus, we need to assume the system has only free-singular configurations.

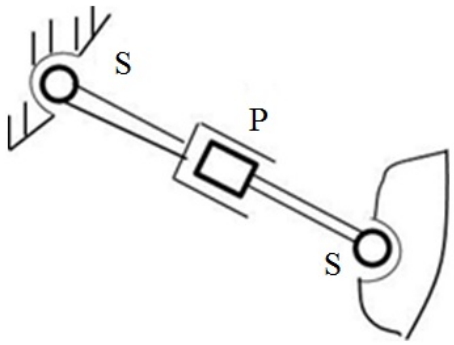

Figure 2.2: Model representation of spatial case.

Based on the model as shown in Figure 2.2, the number of bodies of the each cable is $m_{bodies} = 1\ winch + 1\ rod + 1\ mobile\ platform = 3$, number of joints is $m_{joints} = 2S + 1P = 3$. The spatial cable model can consider in the form of the cable anchor points with the static platform as spherical joints (three constraints), the anchor points with the mobile platform as spherical joints (three constraints), and the change of cable length as prismatic joints (five constraints). Using the Grbler-Kutzbachs formula Eq. (2.1) for spatial motions, the total number of DOF of the system is

$$m = 6m_{bodies} - \sum_{j=1}^{m_{joints}} (6 - m_j) = 6(3) - (2(6-3) + (6-1)) = 18 - 11 = 7. \qquad (2.2)$$

If one of the two links twist is ignored (it does not affect the positioning of the mechanism), the total number of DOF of the system can be written $m = 6$.

Also, the planar model in Figure 2.3 has the cable anchor points with the static platform as revolute joints (two constraint), the anchor points with the mobile platform as revolute joints (two constraints), and the change of cable length as prismatic joints (two constraint). In case of the planar system, we can calculate as follows

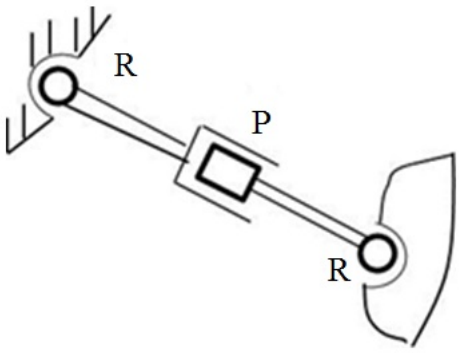

Figure 2.3: Model representation of planar case.

$$m = 3m_{bodies} - \sum_{j=1}^{m_{joints}} (3 - m_j) = 3(3) - ((3-1) + (3-1) + (3-1)) = 9 - 6 = 3. \quad (2.3)$$

Thus, for a spherical and planar fully constrained cable robot, six and three DOF require a minimum of seven cables and four cables to allow the complete motion of the mobile platform, respectively.

Cable elastic properties are modeled by the inclusion of a four linear springs with an axial stiffness coefficient, K_a, and three perpendicular stiffness coefficients, Kp_1, Kp_2 and Kp_3, are presented in [22]. The position and force sensor outputs are represented as the variables l and τ, which measure the cable lengths and tensions, respectively. Finally, disturbances, denoted by $\boldsymbol{F}_d$, represent the external force/moment applied to the mobile platform.

Based on the model as shown in Figure 2.1, a general kinematic and dynamic formulation are developed. Figure 2.4 shows the closure position vectors for a cable ith in a general spatial n cable robot. A coordinate system is fixed at the mass center of the mobile platform, C, and another is fixed at origin of the reference point O. In addition, i denotes the cable number, $\boldsymbol{L}_i$ denotes ith cable's length vector, $\boldsymbol{a}_i$ denotes reference point of the system to the ith anchor's point, $\boldsymbol{p}$ shows the reference frame to the position vector on end effector, $\boldsymbol{r}_i$ is the radius vector of the end effector. $\mathbf{e}_x$, $\mathbf{e}_y$ and $\mathbf{e}_z$ denote the unit vectors in x, y and z directions, respectively. A_i and B_i represent ith anchor's point at the static and mobile platform, respectively.

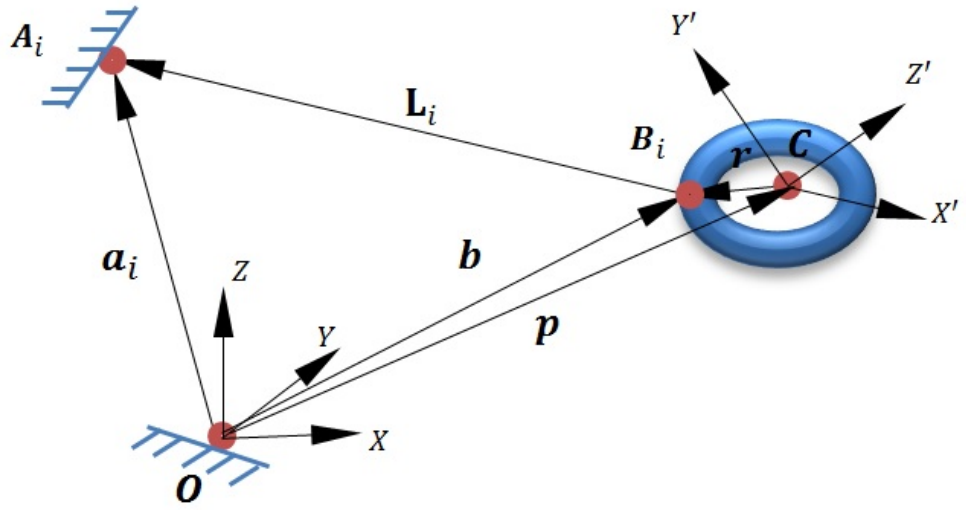

Figure 2.4: Kinematic parameters of cable robot.

Thus, constant vectors $\boldsymbol{a}_i$ and $\boldsymbol{r}_i^{'}$ are placed with respect to the base and the mobile coordinate systems. Using the transformation $\boldsymbol{r}_i = [R]\boldsymbol{r}_i^{'}$, where $[R]$ is the rotation transformation matrix with the using Euler angles for the desired orientation of the mobile box.

The general kinematic models of the robotic systems can be formulated with combination of two below loop closure equations.

$$\overrightarrow{OB_i} = \overrightarrow{OA_i} - \overrightarrow{B_iA_i}, \tag{2.4}$$

$$\overrightarrow{OB_i} = \overrightarrow{OC} + \overrightarrow{CB_i}. \tag{2.5}$$

Substituting the Eq. (2.4) into (2.5), general kinematic model can be expressed as,

$$\overrightarrow{OA_i} = \overrightarrow{OC} + \overrightarrow{CB_i} + \overrightarrow{B_iA_i}. \tag{2.6}$$

General kinematic equation can be written using Eq. (2.6) as

$$\boldsymbol{L}_i = \boldsymbol{a}_i - \boldsymbol{p} - \boldsymbol{r}_i = \boldsymbol{L}_{ix} + \boldsymbol{L}_{iy} + \boldsymbol{L}_{iz}, \qquad \forall i = 1, .., n. \tag{2.7}$$

where

$$\begin{aligned}
\boldsymbol{L}_{ix} &= (a_{ix} - p_x - r_{ix})\mathbf{e}_x, \qquad \forall i = 1, .., n. \\
\boldsymbol{L}_{iy} &= (a_{iy} - p_y - r_{iy})\mathbf{e}_y, \qquad \forall i = 1, .., n. \\
\boldsymbol{L}_{iz} &= (a_{iz} - p_z - r_{iz})\mathbf{e}_z, \qquad \forall i = 1, .., n.
\end{aligned} \tag{2.8}$$

The *ith* cable's length is obtained by applying the 3-norm Euclidian norm to Eq. (2.7) as

$$l_i = \parallel \boldsymbol{a}_i - \boldsymbol{p} - \boldsymbol{r}_i \parallel, \forall i = 1, \cdots, n. \tag{2.9}$$

Eq. (2.9) can be rewritten as

$$l_i = \sqrt{(a_{ix} - p_x - r_{ix})^2 + (a_{iy} - p_y - r_{iy})^2 + (a_{iz} - p_z - r_{iz})^2}, \qquad \forall i = 1, \cdots, n. \tag{2.10}$$

Differentiating equation (2.7) results in

$$\dot{\boldsymbol{L}}_i = \dot{\boldsymbol{p}} + \boldsymbol{\omega}_p \times \boldsymbol{r}_i, \qquad \forall i = 1, \cdots, n. \tag{2.11}$$

where

$$\dot{\boldsymbol{L}}_i = \lim_{\Delta \to 0} \frac{\Delta \boldsymbol{L}_i}{\Delta t} = \dot{l}_i \breve{l}_i + l_i \dot{\breve{l}}_i = \dot{l}_i \breve{l}_i + \boldsymbol{\omega}_i \times l_i \breve{l}_i. \tag{2.12}$$

Hence, the Eq. (2.11) can be rewritten as

$$\dot{l}_i \breve{l}_i + \boldsymbol{\omega}_i \times l_i \breve{l}_i = \dot{\boldsymbol{p}} + \boldsymbol{\omega}_p \times \boldsymbol{r}_i. \tag{2.13}$$

For the mobile box, $\dot{\boldsymbol{p}}$ and $\boldsymbol{\omega}_p$, which are the linear and angular velocities of point C according to reference frame. Expressing each cable vector in its Cartesian components define the unit vector as follows

$$\breve{l}_i = \frac{\boldsymbol{L}_i}{\parallel \boldsymbol{L}_i \parallel} = \breve{l}_{ix} + \breve{l}_{iy} + \breve{l}_{iz}, \tag{2.14}$$

where

$$\breve{l}_{ix} = \frac{(a_{ix} - p_x - r_{ix})}{l_i}\mathbf{e}_x,\ \breve{l}_{iy} = \frac{(a_{iy} - p_y - r_{iy})}{l_i}\mathbf{e}_y,\ and\ \breve{l}_{iz} = \frac{(a_{iz} - p_z - r_{iz})}{l_i}\mathbf{e}_z. \tag{2.15}$$

where $\boldsymbol{L}_i$ shows position vector along the $\breve{l}_i$ which is unit vector. Both sides of the Eq.(2.13) multiply with $\breve{l}_i$ to obtain the rate of the change in the cable length as

$$\dot{l}_i \breve{l}_i \breve{l}_i = \breve{l}_i(\dot{\boldsymbol{p}} + \boldsymbol{\omega}_p \times \boldsymbol{r}_i - \boldsymbol{\omega}_i \times \boldsymbol{L}_i), \tag{2.16}$$

where $\breve{l}_i \breve{l}_i = \| \breve{l}_i \|^2 = 1$ and $\breve{l}_i(-\boldsymbol{\omega}_i \times \boldsymbol{L}_i) = 0$ because $\breve{l}_i \perp (-\boldsymbol{\omega}_i \times \boldsymbol{L}_i)$.

Therefore, the rate of the change in the cable length can be written as follows

$$\dot{l}_i = \breve{l}_i \dot{\boldsymbol{p}} + (\boldsymbol{r}_i \times \breve{l}_i)\boldsymbol{\omega}_p. \tag{2.17}$$

where $\dot{\boldsymbol{p}} = [\dot{p}_x, \dot{p}_y, \dot{p}_z]^T$ and $\boldsymbol{\omega}_p = [\omega_{px}, \omega_{py}, \omega_{pz}]^T$ are the moving platform linear and angular velocity vectors, respectively. Eq. (2.17) can be rewritten in matrix form as

$$\dot{\boldsymbol{l}} = \boldsymbol{J}\boldsymbol{v}_p, \tag{2.18}$$

where $\dot{\boldsymbol{l}} = [l_1 \cdots l_n]^T \in \Re^{n\times 1}$is the cable velocity vector, moving platform velocity vector denoted by $\boldsymbol{v}_p = [\dot{p}_x, \dot{p}_y, \dot{p}_z, \omega_{px}, \omega_{py}, \omega_{pz}]^T \in \Re^{m\times 1}$, and $\boldsymbol{J}$ is an $n \times m$ matrix composed of the the velocity of end-effector and vector of the changing ratio of cables. In addition, rank-deficiency of Jacobian can generate geometrical singularities which occur at the boundaries of the robot workspace. Therefore, the actuators of the robot give more force for providing all cables in tension. However, this can cause damage for the robotic systems.

The static analysis is necessary for all cables in positive tension. The force analysis deals with the problem of finding the forces (cable positive tensions) for a specific equilibrium by the addition of the translation motion.

2.1 Static model

The force analysis is used for a specific equilibrium point of the system to find the forces. The static model analysis can start with the static equilibrium as following. Figure 2.5 shows the free-body diagram for the dynamic study [23].

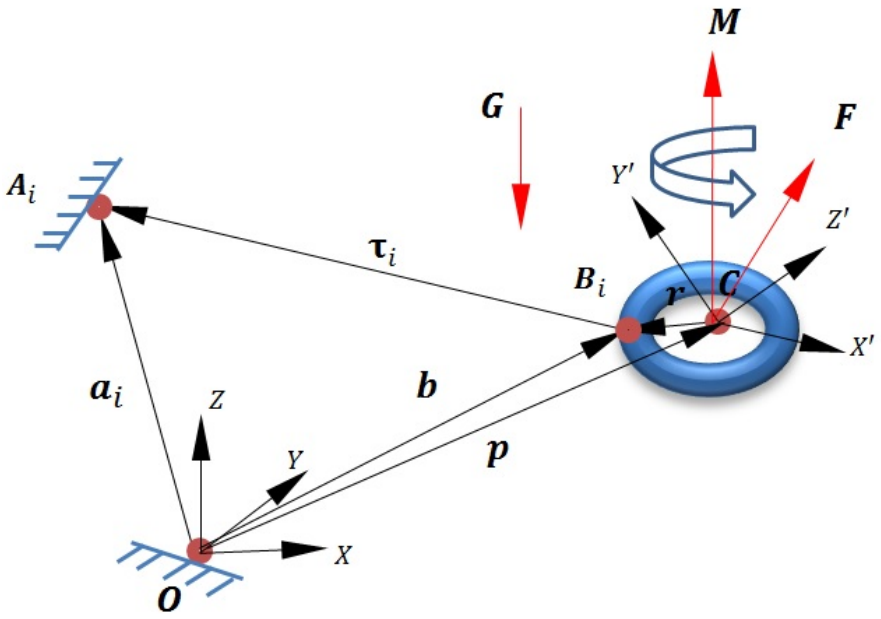

Figure 2.5: Dynamic parameters of cable robot.

This analysis is based in the following assumption:

Assumption 1 Cables are massless and the friction with air is also neglected.
Assumption 2 External forces and moments applied on the mobile platform are constant.
Assumption 3 The gravitational acceleration is acting along the Z axis.

Thus, the mobile box statics force/moment equations are

$$\boldsymbol{F} = \sum_{i=1}^{n} \tau_i (\breve{l}_{ix} + \breve{l}_{iy} + \breve{l}_{iz}),$$

$$\boldsymbol{M} = \sum_{i=1}^{n} \tau_i [(r_i \times \breve{l}_i)_x + (r_i \times \breve{l}_i)_y + (r_i \times \breve{l}_i)_z]. \tag{2.19}$$

where $\boldsymbol{F} = [F_x, F_y, F_z]^T$ and $\boldsymbol{M} = [M_x, M_y, M_z]^T$ are the external forces and moments applied to the mobile platform.

The Eq.(2.19) can be written in matrix form as,

$$\boldsymbol{F}_d = \boldsymbol{A}\boldsymbol{\tau}, \tag{2.20}$$

where

$$\boldsymbol{A} = \begin{bmatrix} breve{l}_{1x} & breve{l}_{2x} & \cdots & breve{l}_{nx} \\ breve{l}_{1y} & breve{l}_{2y} & \cdots & breve{l}_{ny} \\ breve{l}_{1z} & breve{l}_{2z} & \cdots & breve{l}_{nz} \\ (r_1 \times breve{l}_1)_x & (r_2 \times breve{l}_2)_x & \cdots & (r_n \times breve{l}_n)_x \\ (r_1 \times breve{l}_1)_y & (r_2 \times breve{l}_2)_y & \cdots & (r_n \times breve{l}_n)_y \\ (r_1 \times breve{l}_1)_z & (r_2 \times breve{l}_2)_z & \cdots & (r_n \times breve{l}_n)_z \end{bmatrix}. \tag{2.21}$$

The matrix $\boldsymbol{A}$ is called the structure matrix and depends on the parameters of the robot and the pose of the mobile platform. General disturbance force/ moment vector , denoted by $\boldsymbol{F}_d = [F_x, F_y, F_z, M_x, M_y, M_z]^T$, represents external force/moment applied to the mobile platform and as in which $\boldsymbol{\tau} = [\tau_1 \cdots \tau_n]^T$ is the vector of cable tensions. Cable tensions to balance wrench can be found by inverting $\boldsymbol{A}$, ensuring that at least all cable tensions are always positive. However, for fully constrained cable robots, the number of cables n are larger than the degrees of freedom m of the mobile platform; in consequence, $\boldsymbol{A} \, \epsilon \, \Re^{(m \times n)}$, and it may have infinite cable-tension solutions (an under-determined linear system). This solution can be expressed as

$$\boldsymbol{\tau} = \boldsymbol{\tau}_c + \boldsymbol{\tau}_0, \tag{2.22}$$

where $\boldsymbol{\tau}_c \, \epsilon \, \Re^n$ is a given solution that might contain negative tensions, and $\boldsymbol{\tau}_0 \, \epsilon \, \Re^n$ is the homogeneous solution to find a feasible cable tension vector. Any vector solution added to the null vector of $\boldsymbol{A}$ is indeed a solution of Eq. (2.20), such that $\boldsymbol{\tau}_0 = \boldsymbol{N}\boldsymbol{h}$ where $\boldsymbol{N} \, \epsilon \, \Re^{(n \times (n-m))}$ is the nullspace or kernel of $\boldsymbol{A}$ and $\boldsymbol{h}, \epsilon \, \Re^{((n-m))}$ must be determined such that all cable tensions be positive (minimum requirement).

However, in real applications, cable tensions are bounded by lower and upper cable tension limits because lower tension limits maintain cables taut, ensuring a minimum overall stiffness of the robot, and upper tension limits avoid excessive deformation of the cables and the use of big actuators. Here, the minimum 2-norm solution is used to select a point $\boldsymbol{h}$ that minimizes the tensions among all cables while all cable tensions remain bounded; in other words

$$
\begin{aligned}
&min \parallel \boldsymbol{\tau} \parallel \\
&subject\,to\, \boldsymbol{F}_d = \boldsymbol{A}\boldsymbol{\tau},\ and \\
&0 < \tau_{imin} \leq \tau_i \leq \tau_{imax},
\end{aligned} \tag{2.23}
$$

where τ_{max} and τ_{min} are the given upper and lower bound cable tension vectors respectively, and $\boldsymbol{A}^{\dagger} = \boldsymbol{A}^T(\boldsymbol{A}\boldsymbol{A}^T)^{-1}$ denotes the pseudo inverse of $\boldsymbol{A}$. These conditions can be used to generate different workspaces.

2.2 Dynamic model

The dynamic approach used for this cable robot is the Newton-Euler method. The dynamic equations of the mobile box can be developed by using the statics Eq.(2.19) adding the translational and rotational motion about the centroid point. Then, the robot dynamic equations are

$$
\begin{aligned}
\sum_{i=1}^{n} \tau_i \breve{l}_i + \boldsymbol{F} &= m_p \boldsymbol{G} + m_p \boldsymbol{a}_p, \\
\sum_{i=1}^{n} (\boldsymbol{r}_i \times (\tau_i \breve{l}_i)) + \boldsymbol{M} &= \bar{I}\boldsymbol{\alpha} + \boldsymbol{\omega} \times (\bar{I}\boldsymbol{\omega}).
\end{aligned} \tag{2.24}
$$

where m_p is the mass of the mobile box, $\boldsymbol{G} = [0, 0, -m_p G]$ is gravitational acceleration vector; $\bar{I}$ is the 3×3 inertial tensor of the mobile box with respect to the centroid point p, $\boldsymbol{a}_p = [\ddot{p}_x, \ddot{p}_y, \ddot{p}_z]^T$ is the linear acceleration of the mobile box; $\boldsymbol{\omega}_p = [\omega_x, \omega_y, \omega_z]^T$ and $\boldsymbol{\alpha} = [\alpha_x, \alpha_y, \alpha_z]^T$ are the angular velocity and angular acceleration of the mobile box. The mass of the cables and their inertia forces are neglected, which reduces the dynamic equations complexity.

The Eq. (2.24) can be written in matrix form as

$$
\begin{bmatrix} m_p(\boldsymbol{G} + \boldsymbol{a}_p) - \boldsymbol{F} \\ \bar{I}\boldsymbol{\alpha} + \boldsymbol{\omega} \times (\bar{I}\boldsymbol{\omega}) - \boldsymbol{M} \end{bmatrix} = \boldsymbol{A}\boldsymbol{\tau}, \tag{2.25}
$$

where $\boldsymbol{A}$ and $\boldsymbol{\tau}$ have the same meaning as Eq. (2.20).

Thus, the dynamic model of a cable robot can be expressed as,

$$\begin{bmatrix} m_p\ddot{p}_x \\ m_p\ddot{p}_y \\ m_p\ddot{p}_z \\ (\bar{I}\boldsymbol{\alpha}+\boldsymbol{\omega}_p\times(\bar{I}\boldsymbol{w}_p))_x \\ (\bar{I}\boldsymbol{\alpha}+\boldsymbol{\omega}_p\times(\bar{I}\boldsymbol{\omega}_p))_y \\ (\bar{I}\boldsymbol{\alpha}+\boldsymbol{\omega}_p\times(\bar{I}\boldsymbol{\omega}_p))_z \end{bmatrix} = \begin{bmatrix} \breve{l}_{1x} & \breve{l}_{2x} & \cdots & \breve{l}_{nx} \\ \breve{l}_{1y} & \breve{l}_{2y} & \cdots & \breve{l}_{ny} \\ \breve{l}_{1z} & \breve{l}_{2z} & \cdots & \breve{l}_{nz} \\ (r_1\times\breve{l}_1)_x & (r_2\times\breve{l}_2)_x & \cdots & (r_n\times\breve{l}_n)_x \\ (r_1\times\breve{l}_1)_y & (r_2\times\breve{l}_2)_y & \cdots & (r_n\times\breve{l}_n)_y \\ (r_1\times\breve{l}_1)_z & (r_2\times\breve{l}_2)_z & \cdots & (r_n\times\breve{l}_n)_z \end{bmatrix} \begin{bmatrix} \tau_1 \\ \tau_2 \\ \tau_3 \\ \vdots \\ \tau_n \end{bmatrix} + \begin{bmatrix} F_x \\ F_y \\ F_z - m_pG \\ M_x \\ M_y \\ M_z \end{bmatrix}. \tag{2.26}$$

Now, for a constant orientation of the mobile box and supposing free singularity positions and the translation motion is in direction of x and y. In addition, the external force and moment are not applied:

$$\begin{bmatrix} m_p & 0 \\ 0 & m_p \end{bmatrix} \begin{bmatrix} \ddot{p}_x \\ \ddot{p}_y \end{bmatrix} = \begin{bmatrix} \breve{l}_{1x} & \breve{l}_{2x} & \cdots & \breve{l}_{nx} \\ \breve{l}_{1y} & \breve{l}_{2y} & \cdots & \breve{l}_{ny} \end{bmatrix} \begin{bmatrix} \tau_1 \\ \tau_2 \\ \tau_3 \\ \vdots \\ \tau_n \end{bmatrix}. \tag{2.27}$$

Eq. (2.27) is valid if the robotic system can always ensure positive tensions in cables. Thus, the representation form of the dynamic equation in (2.27) can be written as follows

$$\boldsymbol{M}_p\ddot{\boldsymbol{p}} = \boldsymbol{A}\boldsymbol{\tau}, \tag{2.28}$$

where $\boldsymbol{M}_p = [diag(m_p, m_p)]$ represents end-effector diagonal inertia matrix, $\ddot{\boldsymbol{p}} = [\ddot{p}_x, \ddot{p}_y]^T$ is acceleration matrix of end effector, $\boldsymbol{A}$ is an $m \times n$ matrix called as structural matrix and $\boldsymbol{\tau}$ is $n \times 1$ matrix, defines cable tensions.

2.3 Kinematic uncertainties

In this study, we assume the positions of the mobile platform are obtained with a camera mounted above each cable robotic system, the cable tensions and length of the cables are perfectly measured with strain gauges and encoders, respectively. In addition, the system is planar cable robot , its end effector is point mass and no external force on the end-effector. Anchor location errors result in an imprecise mobile platform pose. In

the presence of these kinematic uncertainties, the computation of the structure matrix is not accurate and Eq.(2.21) is replaced with its approximate

$$\hat{\boldsymbol{A}} = f(\hat{a}_{ix}, \hat{a}_{iy}, \boldsymbol{p}, l_i), \qquad \forall i = 1, .., n. \tag{2.29}$$

where $\hat{a}_{ix}$,$\hat{a}_{iy}$ denote the ith estimated anchor points coordinates which generate an approximate structure matrix $\hat{\boldsymbol{A}}$. Substituting Eq. (2.29) into Eq. (2.28), the dynamic model of a cable robot with kinematic uncertainties is

$$\boldsymbol{M}_p\ddot{\boldsymbol{p}} = \hat{\boldsymbol{A}}\boldsymbol{\tau}. \tag{2.30}$$

The feasible workspace under kinematic uncertainties is defined by substituting Eq. (2.25) into Eq. (2.23), and analyzing the upper and lower kinematic uncertainties. In that sense,

$$\begin{array}{ll} \text{Find} & \hat{\boldsymbol{\tau}}_0 = \boldsymbol{N}\boldsymbol{h} \\ \text{subject to} & \hat{\boldsymbol{\tau}}_0 \geq 0 \\ \text{and} & 0 < \tau_{min} \leq \hat{\boldsymbol{\tau}} \leq \tau_{max}. \end{array} \tag{2.31}$$

Chapter 3

Parameter Identification of Planar Cable Robotic Systems

On-line parameter identification algorithm is systematical designed in three main steps: formation of a parameter model, design of adaptive law and establishing conditions for convergence of parameter estimate to their actual values [20]. Fully constrained robots contain only one more number of cables than numbers of DOFs. Fig. 3.1 presents a fully constrained planar cable robot which has two DOFs and three cables. The number of cables of a redundant robot are at least two more than the DOF count. Fig. 3.2 depicts a redundant planar cable robot which has four cables and two degrees of freedom.

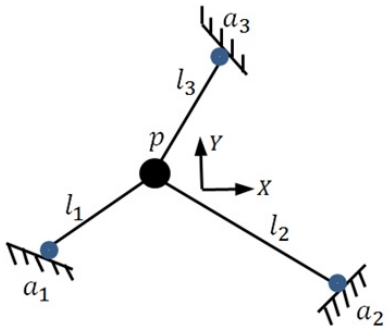

Figure 3.1: Fully-constrained cable robot.

The feasible workspaces of two general planar cable robot configurations in presence of kinematic uncertainties are analyzed. In each configuration, a reference coordinate system

is located in one point inside the static platform and a moving coordinate system is attached to the center of the point-mass mobile platform, p, to describe its translational motions. Cables pass through pulley guides which are placed at anchor points denoted as $\boldsymbol{a}_i$. For each cable i, the cable length l_i is defined between the position of the mobile platform and the anchor point, as shown in Fig. 3.1 and 3.2.

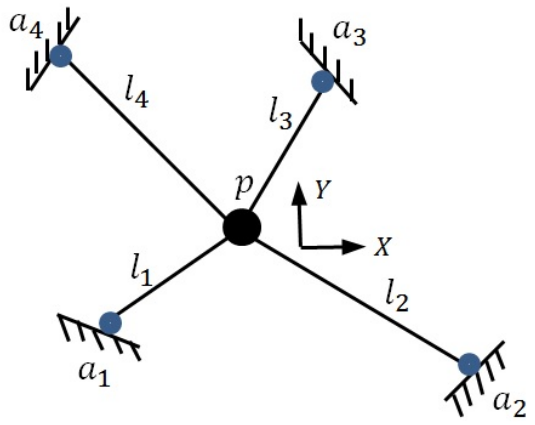

Figure 3.2: A redundant planar cable robot.

The first configuration consist of a planar cable robot with $m = 2$ DOFs and $n = 3$ cables as shown in Fig. 3.1. Without of generality, the location of each anchor point with respect to the reference coordinate system is established based on the following geometric conditions:

$$\begin{aligned} a_{1x} < a_{3x} < a_{2x}, \\ a_{2y} < a_{1y} < a_{3y}. \end{aligned} \tag{3.1}$$

In the second configuration, a redundant planar robotic system is presented in Fig. 3.2. Four cables with variable lengths are used to control the translational motion of the end-effector with respect to a surrounding quadrilateral static platform delimited by the anchor points $\boldsymbol{a}_1$ to $\boldsymbol{a}_4$. A reference coordinate system is located at some point inside the static platform such that the following conditions hold:

$$(a_{1x} + a_{4x}) < (a_{3x} + a_{2x}),$$
$$(a_{1y} + a_{2y}) < (a_{3y} + a_{4y}). \tag{3.2}$$

Conditions as defined in Eq. (3.1) and (3.2) ensure that the cable tensions can work antagonistically and therefore, fully constrained a free-singularity position of the end-effector. In both configurations, it is assumed that the exact position of the end-effector is obtained by means of a camera mounted above each cable robotic system. Also, encoders and strain gauges are used to provide reliable measurement for each cable length l_i and cable tensions τ_i, respectively.

3.1 Parametric model of fully-constrained planar cable robot

As shown in Fig. 3.1, completely constrained planar cable robot force balance equations under zero external force are written as

$$\frac{a_{1x} - p_x}{l_1}\tau_{01} + \frac{a_{2x} - p_x}{l_2}\tau_{02} + \frac{a_{3x} - p_x}{l_3}\tau_{03} = 0,$$
$$\frac{a_{1y} - p_y}{l_1}\tau_{01} + \frac{a_{2y} - p_y}{l_2}\tau_{02} + \frac{a_{3y} - p_y}{l_3}\tau_{03} = 0. \tag{3.3}$$

$$k_1 = \frac{\tau_{02}}{\tau_{01}}, k_2 = \frac{\tau_{03}}{\tau_{01}} \qquad \forall\, k_1, k_2 \ \in \ \Re^+, \tag{3.4}$$

The homogeneous cable tension solutions for the three-cable robot [24] are given by

$$\hat{\tau}_{01} = \alpha l_1(\hat{a}_{2x}\hat{a}_{3y} - \hat{a}_{2x}p_y - \hat{a}_{2y}\hat{a}_{3x} + \hat{a}_{2y}p_x + \hat{a}_{3x}p_y - \hat{a}_{3y}p_x),$$
$$\hat{\tau}_{02} = \alpha l_2(\hat{a}_{1x}\hat{a}_{3y} - \hat{a}_{1x}p_y - \hat{a}_{1y}\hat{a}_{3x} + \hat{a}_{1y}p_x + \hat{a}_{3x}p_y - \hat{a}_{3y}p_y),$$
$$\hat{\tau}_{03} = \alpha l_3(\hat{a}_{1x}\hat{a}_{2y} - \hat{a}_{1x}p_y - \hat{a}_{1y}\hat{a}_{2x} + \hat{a}_{1y}p_x + \hat{a}_{2x}p_y - \hat{a}_{2y}p_y). \tag{3.5}$$

where constant α is selected such that Eq. (2.31) is fulfilled.

3.2 Parametric model of redundant planar cable robot

In order to solve the redundancy and establishing the conditions to select the internal cable tensions, the 4-cable redundant robot kinematics can be transformed to one of the four possible cable triplets as shown in Fig. 3.3.

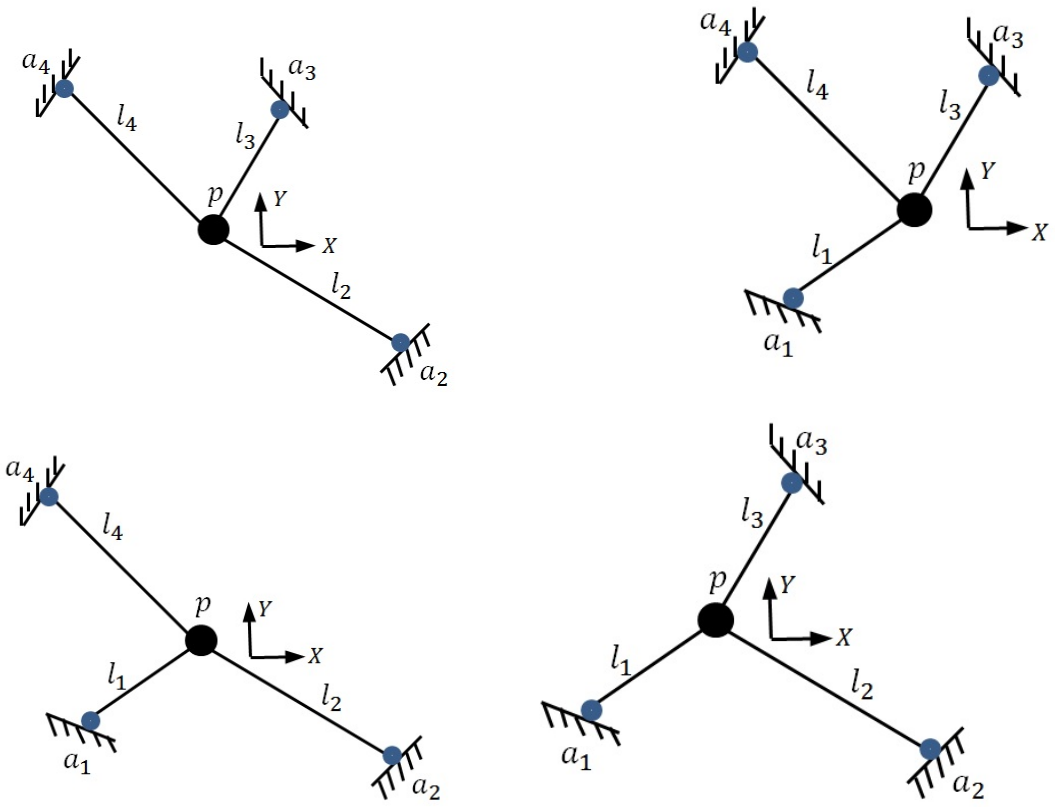

Figure 3.3: Possible cable triplets in the 4-cable redundant manipulators.

Next, we drive a generic parametric model that applies to each of these triplets. Later, we will use an averaging technique to have consensus on the estimation results obtained using each of these four triplets. The below condition is used for formulation of the four possible integer triples $(i\ j\ k)$ of manipulators,

where

$$1 \leq i < j < k \leq 4 \tag{3.6}$$

Force balance equations under zero external force are formulated as

$$\begin{aligned}\frac{a_{ix}-p_x}{l_i}\tau_{0i}+\frac{a_{jx}-p_x}{l_j}\tau_{0j}+\frac{a_{kx}-p_x}{l_k}\tau_{0k}=0,\\ \frac{a_{iy}-p_y}{l_i}\tau_{0i}+\frac{a_{jy}-p_y}{l_j}\tau_{0j}+\frac{a_{ky}-p_y}{l_k}\tau_{0k}=0,\end{aligned} \tag{3.7}$$

$$k_a=\frac{\tau_{0j}}{\tau_{0i}}, k_b=\frac{\tau_{0k}}{\tau_{0i}}\ \forall\ k_a,k_b\in\Re^+. \tag{3.8}$$

The homogeneous cable tension solutions for the four-cable robot [24] are given by

$$\begin{aligned}\hat{\tau}_{01}&=\alpha_1 l_1 l_2(\hat{a}_{4x}p_y+\hat{a}_{3y}p_x-\hat{a}_{3y}\hat{a}_{4x}-\hat{a}_{3x}p_y-\hat{a}_{4y}p_x+\hat{a}_{3x}\hat{a}_{4y}),\\ \hat{\tau}_{02}&=\alpha_2 l_1 l_2(\hat{a}_{4x}p_y+\hat{a}_{3y}p_x-\hat{a}_{3y}\hat{a}_{4x}-\hat{a}_{3x}p_y-\hat{a}_{4y}p_x+\hat{a}_{3x}\hat{a}_{4y}),\\ \hat{\tau}_{03}&=-\alpha_1 l_2 l_3(\hat{a}_{4x}p_y+\hat{a}_{1y}p_x-\hat{a}_{1y}\hat{a}_{4x}-\hat{a}_{1x}p_y-\hat{a}_{4y}p_x+\hat{a}_{4y}\hat{a}_{1x})\\ &\quad-\alpha_2 l_1 l_3(\hat{a}_{4x}p_y+\hat{a}_{2y}p_x-\hat{a}_{2y}\hat{a}_{4x}-\hat{a}_{2x}p_y-\hat{a}_{4y}p_x+\hat{a}_{4y}\hat{a}_{2x}),\\ \hat{\tau}_{04}&=\alpha_1 l_2 l_4(\hat{a}_{1y}p_x+\hat{a}_{3x}p_y-\hat{a}_{3x}\hat{a}_{1y}-\hat{a}_{3y}p_x-\hat{a}_{1x}p_y+\hat{a}_{1x}\hat{a}_{3y})\\ &\quad+\alpha_2 l_1 l_4(\hat{a}_{2y}p_x+\hat{a}_{3x}p_y-\hat{a}_{3x}\hat{a}_{2y}-\hat{a}_{3y}p_x-\hat{a}_{2x}p_y+\hat{a}_{2x}\hat{a}_{3y}),\end{aligned} \tag{3.9}$$

where constant α_1 and α_2 are selected such that Eq. (2.31) is fulfilled.

3.3 Parameter identification of fully-constrained planar cable robot

3.3.1 Parametric model

After separating the unknown parameters from the measured signals, the general static parametric model is obtained [25] as

$$z_m=(\boldsymbol{\theta}_m^*)^T\boldsymbol{\phi},\qquad (m=1,2). \tag{3.10}$$

where

$$z_1=p_x, z_2=p_y. \tag{3.11}$$

Here, z_1 and z_2 are available for measurements.

Unknown parameters can be shown in Eq. (3.12)

$$\boldsymbol{\theta}_1^* = \begin{bmatrix} a_{1x} & a_{2x} & a_{3x} \end{bmatrix}^T,$$

$$\boldsymbol{\theta}_2^* = \begin{bmatrix} a_{1y} & a_{2y} & a_{3y} \end{bmatrix}^T, \tag{3.12}$$

$$\boldsymbol{\phi} = \begin{bmatrix} (\frac{l_2 l_3}{\sigma}) & \frac{k_1 l_1 l_3}{\sigma} & \frac{k_2 l_1 l_2}{\sigma} \end{bmatrix}^T, \tag{3.13}$$

where

$$\sigma = l_2 l_3 + k_1 l_1 l_3 + k_2 l_1 l_2. \tag{3.14}$$

3.3.2 Estimation model

Parametric estimation model can be expressed as:

$$\hat{z}_m = \boldsymbol{\theta}_m^T(t)\boldsymbol{\phi}(t), \qquad (m = 1, 2) \tag{3.15}$$

where $\boldsymbol{\theta_m}(t)$ is the estimate of $\boldsymbol{\theta_m^*}$ at time t

$$\boldsymbol{\theta}_1(t) = \begin{bmatrix} \hat{a}_{1x} & \hat{a}_{2x} & \hat{a}_{3x} \end{bmatrix}^T,$$

$$\boldsymbol{\theta}_2(t) = \begin{bmatrix} \hat{a}_{1y} & \hat{a}_{2y} & \hat{a}_{3y} \end{bmatrix}^T. \tag{3.16}$$

3.3.3 Adaptive laws

In this work, we use a recursive least squares algorithm with forgetting factor and gradient algorithm for each parametric model. The benefit of recursive least squares algorithm as opposed to gradient algorithm can be clear in simulation based comparisons. The adaptive laws are described as follows:

3.3.3.1 Recursive least squares algorithm

The least squares algorithm [20] is obtained by considering the cost function as shown in Eq. (3.17).

$$J(\theta) = \frac{1}{2}\int_0^t e^{-\beta(t-\tau)}\frac{[z_m(\tau) - \boldsymbol{\theta}_m^T(t)\phi(\tau)]^2}{m_s^2(\tau)}d\tau + \frac{1}{2}e^{-\beta t}(\boldsymbol{\theta}_m - \boldsymbol{\theta}_0)^T Q_0(\boldsymbol{\theta}_m - \boldsymbol{\theta}_0), \quad (3.17)$$

where $\boldsymbol{Q}_0 = \boldsymbol{Q}_0^T > 0$, $\beta \geq 0$ are constant values and $\boldsymbol{\theta}_0 = \boldsymbol{\theta}(0)$ is the initial parameter estimate. The local minimum will satisfy as

$$\delta J(\boldsymbol{\theta}_m(t)) = 0 \quad \forall t \geq 0. \quad (3.18)$$

Hence,

$$\delta J(\delta) = e^{-\beta t}\boldsymbol{Q}_0(\boldsymbol{\theta}_m(t) - \boldsymbol{\theta}_0) - \int_0^t e^{-\beta(t-\tau)}\frac{z_m(\tau) - \boldsymbol{\theta}_m^T(t)\boldsymbol{\phi}(\tau)}{m_s^2(\tau)}\boldsymbol{\phi}(\tau)d\tau = 0. \quad (3.19)$$

Then, yield of the non-recursive least squares algorithm is

$$\theta(t) = \boldsymbol{P}_m(t)[e^{-\beta t}\boldsymbol{Q}_0\boldsymbol{\theta}_0 + \int_0^t e^{-\beta(t-\tau)}\frac{z_m(\tau)\boldsymbol{\phi}(\tau)}{m_s^2(\tau)}d\tau]^{-1}. \quad (3.20)$$

where covariance matrix $P(t)$ has form as

$$\boldsymbol{P}_m(t) = [e^{-\beta t}\boldsymbol{Q}_0 + \int_0^t e^{-\beta(t-\tau)}\frac{\phi(\tau)\boldsymbol{\phi}^T(\tau)}{m_s^2(\tau)}d\tau]^{-1}. \quad (3.21)$$

Generally, the recursive LS algorithm with forgetting factor can be defined taking the differential of $\boldsymbol{\theta}(t)$

$$\dot{\boldsymbol{\theta}}_m = \boldsymbol{P}_m\epsilon_m\boldsymbol{\phi}, \boldsymbol{\theta}_m(0) = \boldsymbol{\theta}_0, \qquad (m = 1, 2) \quad (3.22)$$

$$\dot{\boldsymbol{P}}_m = \beta\boldsymbol{P}_m - \boldsymbol{P}_m\boldsymbol{\phi}^T\boldsymbol{P}_m, \boldsymbol{P}_m(0) = \boldsymbol{P}_0 = \boldsymbol{Q}_0^{-1}. \quad (3.23)$$

where $\boldsymbol{P}_m$ for $m = 1, 2$ is the covariance matrix and β is the forgetting factor. The estimation error term ϵ_m is given by

$$\epsilon_m = \frac{z_m - \hat{z}_m}{m_s^2} = \frac{z_m - \boldsymbol{\theta}_m^T(t)}{m_s^2}, \qquad (m = 1, 2) \quad (3.24)$$

where $m_s^2 \geq 1$ is a normalization signal designed to guarantee that

$$\frac{\boldsymbol{\phi}}{m_s^2} \, \epsilon \; with \quad m_s^2 = 1 + \alpha \boldsymbol{\phi}^T \boldsymbol{\phi}, \alpha > 0. \tag{3.25}$$

We can say value of the forgetting factor β has effect the stability properties.

Convergence conditions for the estimate $\boldsymbol{\theta}_m(t)$ to $\boldsymbol{\theta}_m^*$ for the algorithm are established in [20].

3.3.3.2 Gradient algorithms

The gradient algorithm is used for each minimize cost function $J(\theta)$ with the each gradient method.

The cost function is written as

$$J(\boldsymbol{\theta}) = \frac{\epsilon_m^2 m_s^2}{2} = \frac{(z_m - \boldsymbol{\theta}_m^T \boldsymbol{\phi})^2}{2m_s^2}, \tag{3.26}$$

where m_s is the normalizing signal as mentioned in Eq. (3.24). Then, the gradient algorithm has form as

$$\dot{\boldsymbol{\theta}}_m = -\Gamma \Delta J, \tag{3.27}$$

where $\Gamma = \Gamma^T > 0$ is the adaptive gain and ΔJ is $-\dfrac{(z_m - \boldsymbol{\theta}_m^T \boldsymbol{\phi})\phi}{m_s^2} = \epsilon_m \boldsymbol{\phi}$. Thus, we obtain the gradient algorithm as

$$\dot{\boldsymbol{\theta}}_m = \Gamma \epsilon_m \boldsymbol{\phi}, \tag{3.28}$$

where

$$\epsilon_m = \frac{z_m - \hat{z}_m}{m_s^2}, \tag{3.29}$$

where $m_s^2 \geq 1$ is the normalizing signal which is to bound $\boldsymbol{\phi}$ from above. The normalizing signal as mentioned Eq. (3.29) can be expressed as,

$$m_s^2 = 1 + n_s^2, \tag{3.30}$$

where n_s ($n_s \geq 0$) is static normalization signal for providing $\dfrac{\phi}{m_s}$ is bounded from above. Convergence conditions for the estimate $\boldsymbol{\theta}_m(t)$ to $\boldsymbol{\theta}_m^*$ for the algorithm are established in [20].

3.4 Parameter identification of redundant planar cable robot

3.4.1 Parametric model

The general static parametric model for any of the four possible manipulator triples i, j, k can be written in the form of Eq. (3.10) where

$$z_1 = p_x, z_2 = p_y, \tag{3.31}$$

$$\boldsymbol{\theta}_1^* = \begin{bmatrix} a_{ix} & a_{jx} & a_{kx} \end{bmatrix}^T, \tag{3.32}$$

$$\boldsymbol{\theta}_2^* = \begin{bmatrix} a_{iy} & a_{jy} & a_{ky} \end{bmatrix}^T, \tag{3.33}$$

$$\boldsymbol{\phi} = \begin{bmatrix} (\frac{l_j l_k}{\sigma_c}) & \frac{k_a l_i l_k}{\sigma_c} & \frac{k_b l_i l_j}{\sigma_c} \end{bmatrix}^T \tag{3.34}$$

$$\sigma_c = l_j l_k + k_a l_i l_k + k_b l_i l_j, \tag{3.35}$$

3.4.2 Estimation model

Parametric estimation model is again given by using Eq. (3.15) as,

$$\boldsymbol{\theta}_1(t) = \begin{bmatrix} \hat{a}_{ix} & \hat{a}_{jx} & \hat{a}_{kx} \end{bmatrix}^T \tag{3.36}$$

$$\boldsymbol{\theta}_2(t) = \begin{bmatrix} \hat{a}_{iy} & \hat{a}_{jy} & \hat{a}_{ky} \end{bmatrix}^T \tag{3.37}$$

3.4.3 Adaptive laws

Conditions that are given in section (3.3.3) also hold for this type of cable robot model.

3.5 Simulation

In this section, the robot parameters as listed in Tab. 3.1 are used in order to generate the end effector position signal of the cable robots. In the simulation, the recursive least squares algorithm and the gradient algorithm are used to estimate the values of the anchor points with constant forgetting factor (β=1) and velocity of convergence of the gradient algorithm (Γ=6) for fully-constrained and redundant planar cable robots. This simulation results are based on the established input signals (p_x, p_y), which benefit the motion of the end-effector along the whole feasible workspace of the cable robot.

3.5.1 End effector position signal

The input signals (the pose of the end-effector) must be selected carefully in order to obtain the information that the estimation algorithm needs. The persistent excitation signals are established for fully-constrained and redundant planar cable robots as

$$p_x = \Omega_1 + dw_0 t cos(w_1 t)$$

$$p_y = \Omega_2 + dw_0 t sin(w_1 t) \tag{3.38}$$

Here, we select signal parameters values from the Tab. 3.1 to generate the end effector position signals.

Table 3.1: Parameters of position signals of the systems.

Signal parameters	Fully constrained cable robot	Redundant cable robot
Ω_1	0.83	0.83
Ω_2	-4.33	-4.33
ω_0	9	10
ω_1	π	π
d	0.024	0.03

3.5.2 Parameters of the fully constrained planar robot.

The parameters of fully-constrained planar cable robot of anchor point parameters are given in Tab 3.2

Table 3.2: Parameters of the fully constrained planar cable robot.

Anchor points parameters		
Point	Actual [m]	Initial [m]
a_{1x}	-15	-14.25
a_{1y}	-14	-13.75
a_{2x}	17	16.5
a_{2y}	-13	-12.75
a_{3x}	0.5	0.75
a_{3y}	14	14.25

The 3-cable robot shown in Fig. 3.1 is analyzed in this subsection. The unknown the anchor points are estimated using the recursive least squares algorithm and gradient identification algorithm.

3.5.3 Recursive least squares and gradient algorithms

The fully-constrained planar robot trajectories are established using the position signals for the least squares algorithm in fifteen seconds and gradient algorithm in fourty-two seconds as shown in Fig. 3.4, respectively. Applying the trajectories for both estimation algorithms, we can obtain actual estimation anchor points position as shown in Fig. **??**. In this simulation, we suppose a set of actual and initial values of the anchor points showed in Tab. 3.2.

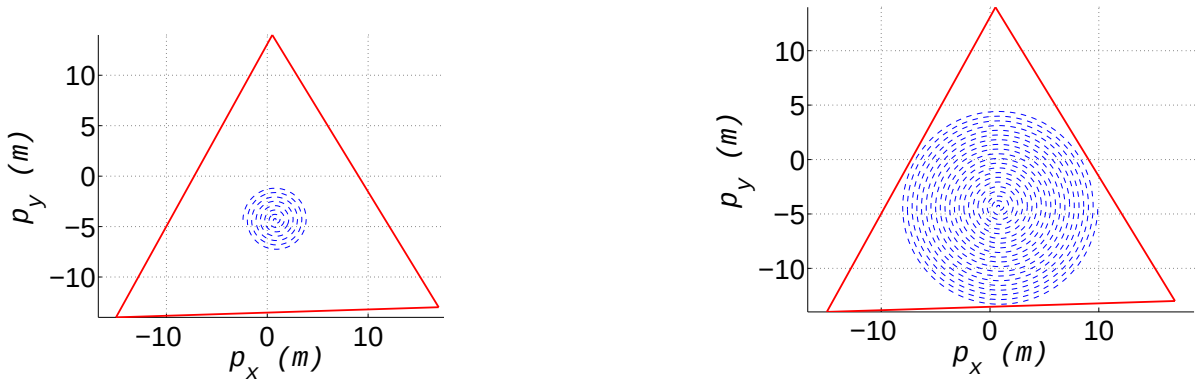

(a) (b)

Figure 3.4: Path of the end-effector fully-constrained planar robot (a) for least squares algorithm and (b) for gradient algorithm.

Fig. 3.5 shows estimated values of the coordinates of the three anchor points to actual anchor points. The recursive least squares algorithm converges to actual values of anchor points in less than 15 seconds. On the other hand, even if the gradient algorithm converges to zero for estimation error of y component of anchor points in less than 15 seconds, however; convergences of the x component of anchor points to their actual values are succeed in more than 30 seconds.

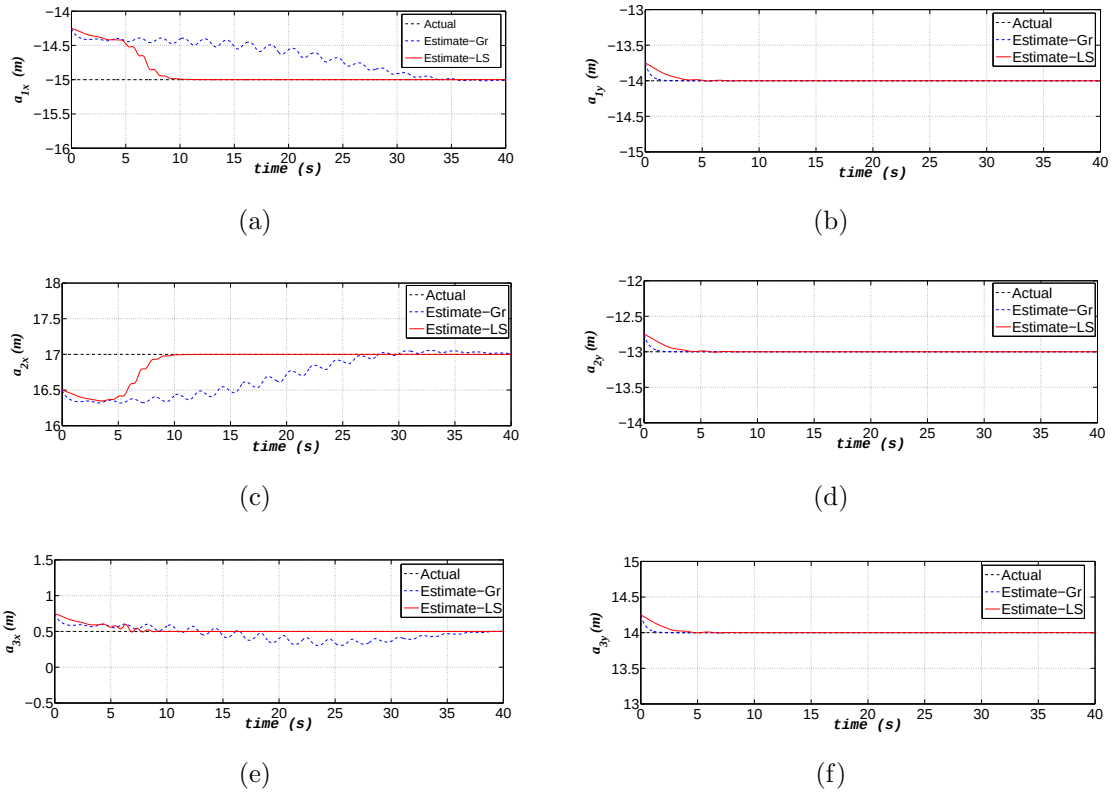

Figure 3.5: Actual and estimated parameters fully-constrained planar robot.

3.5.4 Redundant planar cable robot

In this subsection, we show the estimation of anchor points of the redundant planar cable robot. The recursive least squares and gradient algorithms are applied with setting the initial and actual points. The parameters of redundantly planar cable robot of anchor point are given in Tab 3.3

Table 3.3: Parameters of the redundantly planar cable robot.

Anchor points parameters		
Point	Actual [m]	Initial [m]
a_{1x}	-15	-15.25
a_{1y}	-14	-13.25
a_{2x}	17	16.5
a_{2y}	-13	-13.75
a_{3x}	12	12.5
a_{3y}	14	14.25
a_{4x}	-13	-13.5
a_{4y}	16	15.75

3.5.5 Recursive least squares and gradient algorithms

The redundant planar cable robot trajectories are established using the position signals for least squares algorithm in fifteen seconds and gradient algorithm in fourty seconds as shown in Fig. 3.6, respectively. The position information of end effector of the robot is obtained by these trajectories.

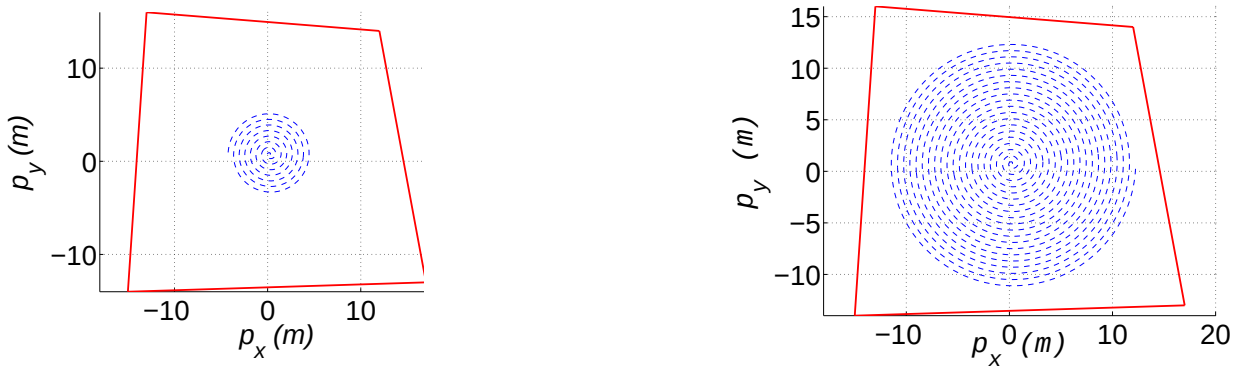

(a) (b)

Figure 3.6: Path of the redundant planar robot end-effector (a) for least squares algorithm and (b) for gradient algorithm.

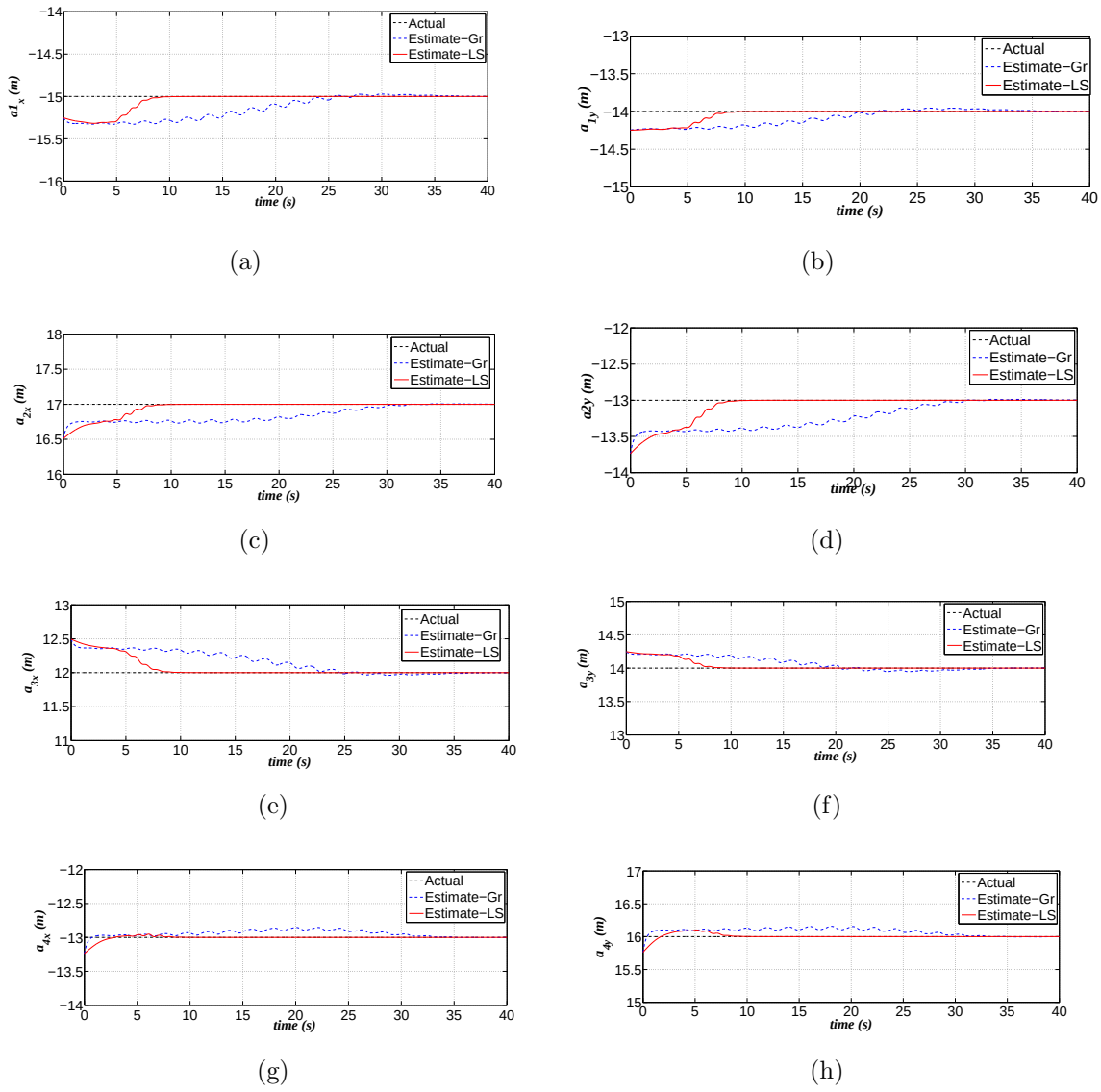

Figure 3.7: Actual and estimated parameters of redundant planar cable robot.

The errors of estimation anchor points of redundant planar cable robot converge to zero with the recursive least squares and gradient algorithms. Fig. 3.7 shows the actual and estimated values of the coordinates of the four anchor points. Fig. 3.7 indicates that convergences of the unknown anchor points to their actual values are achieved less than fifteen seconds with recursive least squares algorithm while the anchor points are estimated

to the actual values in more than 30 seconds with gradient algorithm.

Chapter 4

Adaptive and Robust Controllers

For a pick and place operation, the predominant concern is to make the mobile platform reach a desired target position, $\boldsymbol{p}_d = [p_{xd}, p_{yd}]^T$. Consider the general dynamic formulation of cable robot can be expressed as

$$\boldsymbol{M_p}\ddot{\boldsymbol{p}} = \boldsymbol{A}\boldsymbol{\tau} + \boldsymbol{F}_d, \tag{4.1}$$

where $\boldsymbol{M_p} = [diag(m_p, m_p)]$ represents inertia matrix, $\ddot{\boldsymbol{p}} = [\ddot{p}_x, \ddot{p}_y]^T$, $\boldsymbol{F}_d = [F_x, F_y]^T$ is the disturbance force matrix, $\boldsymbol{A}$ is $2 \times n$ structural matrix and $\boldsymbol{\tau} = [\tau_1 \dots \tau_n]^T$ is $n \times 1$ tension matrix. The general parallel robots motion control scheme can be shown as

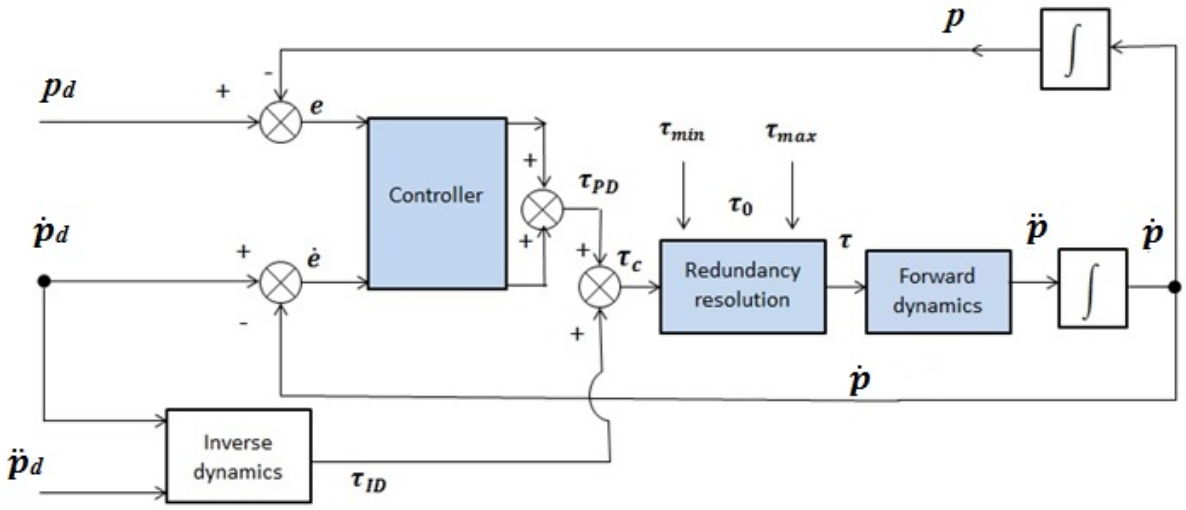

Figure 4.1: General motion feedback control scheme of cable robot.

In the Fig. 4.1 shows the general motion feedback control of cable robot in closed-loop system. Using the closed-loop system, we can generate the position error in respect to desire position. The position error data is directed to controller because it minimizes the position error by building the appropriate commands for actuators [26].

According to [26], the controller calculates the required actuator force and torques to provide the desire motion of the end effector. In general, adaptive and robust controller methods are used for compensation of lack of information. The adaptive and robust control methods provide for keeping closed-loop well performance of the manipulator with different ways although the system contains uncertainties and external disturbances. The adaptive control system is shown in Fig. 4.2.

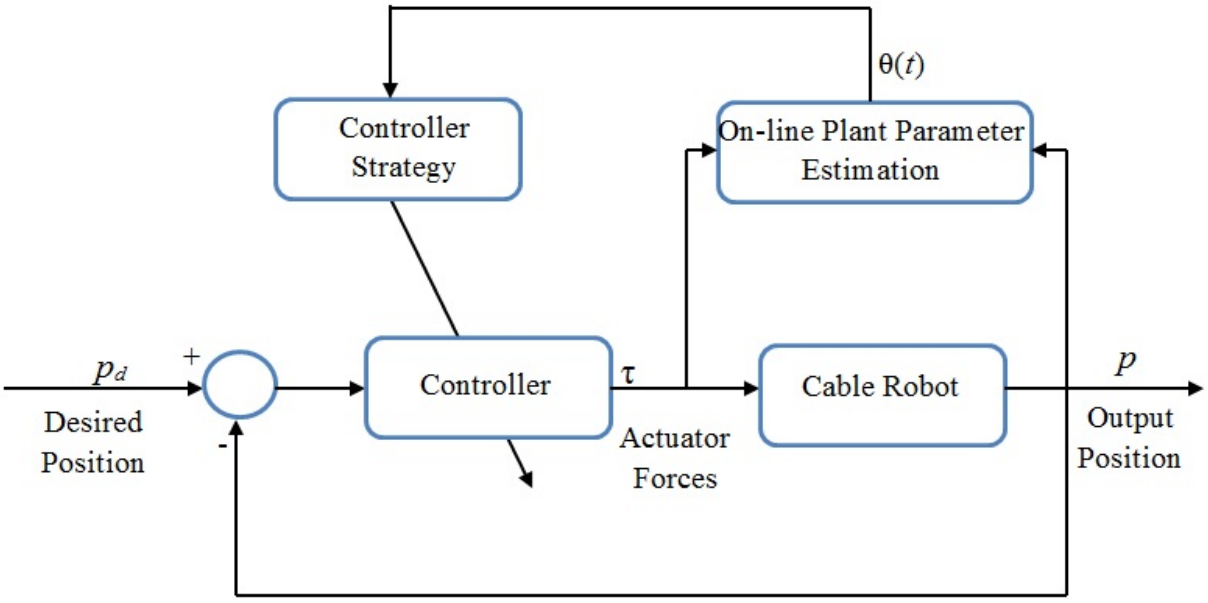

Figure 4.2: Adaptive control with parameter estimation.

In general, the control problem is, for the initial position of the mobile platform $\boldsymbol{p} = [p_x, p_y]^T$, to reach the desired position $\boldsymbol{p}_d = [p_{xd}, p_{yd}]^T$ and stay there as time goes to infinity, and to force the error position, $\boldsymbol{e} = [e_x, e_y]^T$, go to zero at the same time the velocity, $\dot{\boldsymbol{e}}$=$[\dot{e}_x, \dot{e}_y]^T$, goes to zero [25]; that is

$$\boldsymbol{e} = (\boldsymbol{p}(t) - \boldsymbol{p}_d(t)) \to 0 \quad as \quad t \to \infty, \tag{4.2}$$

$$\dot{\boldsymbol{e}}(t) = \dot{\boldsymbol{p}}(t) \to 0 \quad as \quad t \to \infty, \tag{4.3}$$

$$\ddot{\boldsymbol{e}}(t) = \ddot{\boldsymbol{p}}(t) \to 0 \quad as \quad t \to \infty, \tag{4.4}$$

Next, sliding mode (SM), backstepping (B) and proportional derivative (PD) feedback controllers are considered to asymptotically stabilize the cable robot to a desired position of the end-effector while the inputs satisfy all positive tension conditions [24]. The design of the controllers are based on a Lyapunov candidate function $V(\boldsymbol{p}) > 0$, ensuring the Lyapunov function derivative $\dot{V}(\boldsymbol{p})$ is negative definite. The following assumptions are made for the design of each controller in this study.

Assumption 4 : The desired position of the mobile platform, p_d, belongs to the feasible workspace of the cable robot.

Assumption 5 :The pseudo inverse of the structure matrix exists.

4.1 Sliding mode adaptive control

SM control is generally used against the system is exposed to uncertainties and external disturbances. The sliding mode control has two part controller design. The first part involves the design of a sliding surface so that the sliding motion satisfies design specifications. The second is concerned with the selection of a control law that will make the switching surface attractive to the system state [27].

The Fig. 4.3 shows block diagram of SMsatA control system. SM surface systems are designed to drive the system states on to a particular surface which is sliding surface in the state space.

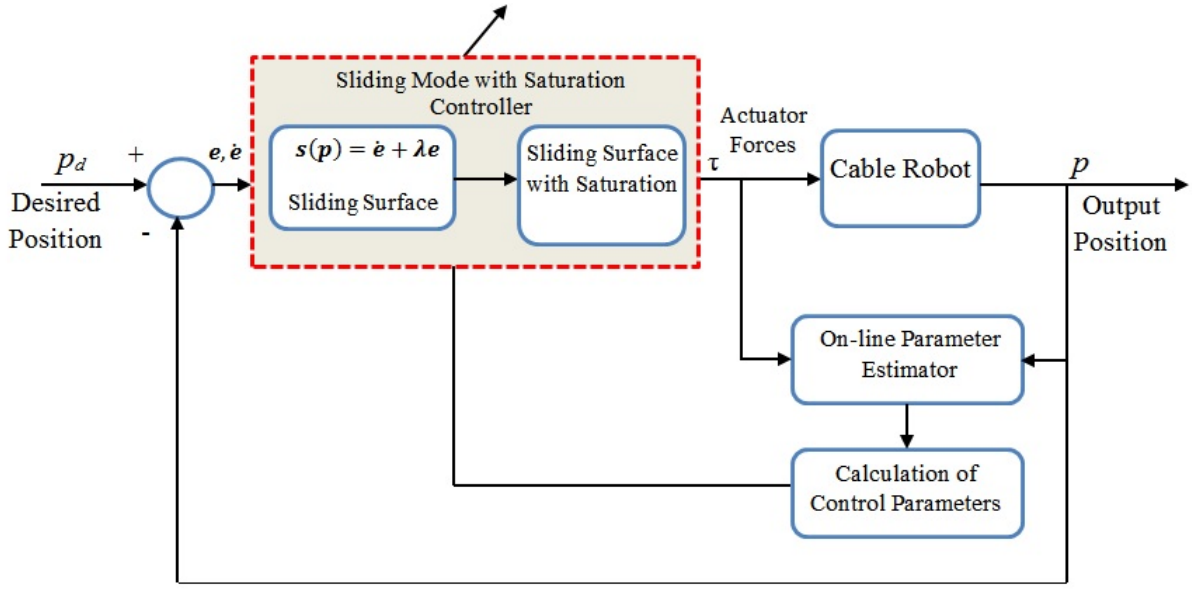

Figure 4.3: Block diagram of adaptive sliding mode with saturation control system.

Reordering the general dynamics Eq. (4.1) after using the assumption (4) and (5) as shown

$$\ddot{\boldsymbol{p}} = [\ddot{p}_x, \ddot{p}_y]^T = \boldsymbol{M}_p^{-1}\boldsymbol{F}_d + \boldsymbol{M}_p^{-1}\boldsymbol{A}\boldsymbol{\tau} = \boldsymbol{M}_p^{-1}(\boldsymbol{F}_d + \boldsymbol{A}\boldsymbol{\tau}). \tag{4.5}$$

The general non-linear equation of motion is obtained as

$$\ddot{\boldsymbol{p}} = f(\boldsymbol{p}) + g(\boldsymbol{p})u, \tag{4.6}$$

where

$$f(\boldsymbol{p}) = \boldsymbol{M}_p^{-1}\boldsymbol{F}_d, \tag{4.7}$$

$$g(\boldsymbol{p}) = \boldsymbol{M}_p^{-1}\boldsymbol{A}, \tag{4.8}$$

$$u = \boldsymbol{\tau}. \tag{4.9}$$

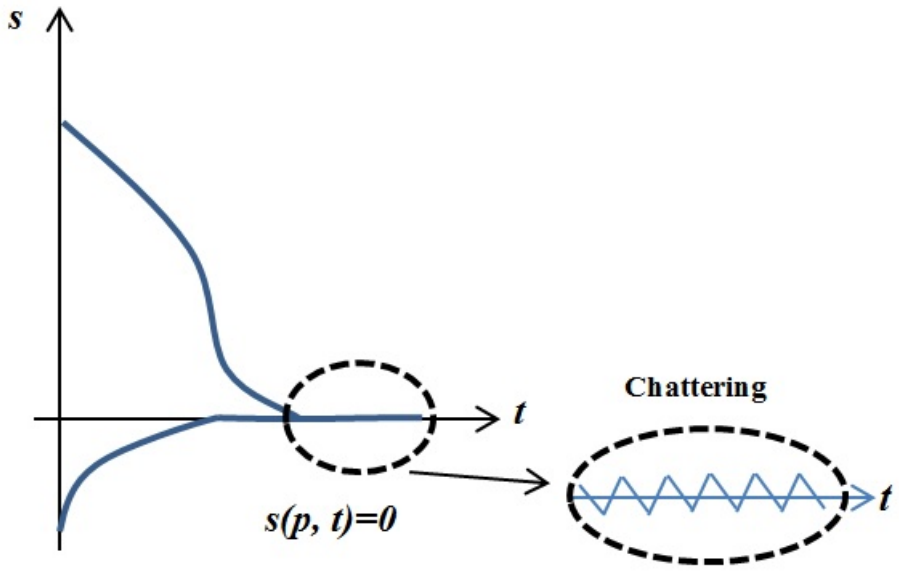

Figure 4.4: Representation of sliding surface with saturation control system.

In the Fig. 4.4, geometrical point of the $s(\boldsymbol{p}, t) = 0$ represents the surface which is called sliding surface in the error space. The sliding surface depends on the tracking error and its certain derivatives. Sliding surface provides the stability for the system that means tracking error might be almost zero in finite time.

An SM controller for a desired constant position of the end-effector is obtained considering a time varying sliding surface is given as

$$\boldsymbol{s}(\boldsymbol{p}) = (\frac{d}{dt} + \boldsymbol{\lambda})\boldsymbol{e} = \dot{\boldsymbol{e}} + \boldsymbol{\lambda}\boldsymbol{e} = 0, \qquad \forall\ \boldsymbol{\lambda} > 0 \tag{4.10}$$

where $\boldsymbol{\lambda} = [diag(\lambda, \lambda)]$ is arbitrary diagonal matrix, and defines the unique pole of the resulting reduced dynamics of the system when in sliding and sliding surface is an $s(\boldsymbol{p})$

The derivative of sliding surface is:

$$\dot{\boldsymbol{s}} = \ddot{\boldsymbol{e}} + \lambda\dot{\boldsymbol{e}}. \tag{4.11}$$

Substituting Eq. (4.3) and Eq (4.4) into Eq. (4.11), derivative of sliding surface can be written as

$$\dot{\boldsymbol{s}} = \ddot{\boldsymbol{e}} + \boldsymbol{\lambda}\dot{\boldsymbol{e}} = \boldsymbol{M}_p^{-1}(\boldsymbol{F}_d + \boldsymbol{A}\boldsymbol{\tau}) + \boldsymbol{\lambda}\dot{\boldsymbol{p}}. \tag{4.12}$$

The Lyapunov function is defined as

$$V(\boldsymbol{s}(\boldsymbol{p})) = \frac{1}{2}\boldsymbol{s}^T\boldsymbol{s}. \tag{4.13}$$

Its derivative is desired to satisfy

$$\dot{V}(\boldsymbol{s}(\boldsymbol{p})) = \boldsymbol{s}^T\dot{\boldsymbol{s}} \leq -\boldsymbol{K}_1|\boldsymbol{s}|, \qquad \forall \boldsymbol{p} \neq 0, for\ some\ \boldsymbol{K}_1 > 0. \tag{4.14}$$

This condition will guarantee that the sliding surface is reached in finite time. This can be done by selecting to control law so that the derivative of s satisfies

$$\dot{\boldsymbol{s}} = -\boldsymbol{K}_1 sgn(\boldsymbol{s}), \tag{4.15}$$

where

$$sgn(\boldsymbol{s}) = sgn(\begin{bmatrix}\boldsymbol{s}_1, ..., \boldsymbol{s}_n\end{bmatrix}^T) = \begin{bmatrix}sgn(\boldsymbol{s}_1), ..., sgn(\boldsymbol{s}_n)\end{bmatrix}^T. \tag{4.16}$$

Based on assumption (5) and substituting Eq. (4.12) into Eq. (4.15), the control input is defined as,

$$\boldsymbol{\tau}_c = \boldsymbol{A}^{\dagger}(\boldsymbol{F}_d + \boldsymbol{M}_p(-\boldsymbol{\lambda}\dot{\boldsymbol{p}} - \boldsymbol{K}_1 sgn(\boldsymbol{s}))), \tag{4.17}$$

where $\boldsymbol{\lambda}$=[diag(λ, λ)]and $\boldsymbol{K}_1$=[diag(K_1, K_1)] is a positive constant. This control input satisfied the stability condition. The all-positive cable tension conditions are satisfied by adding the internal cable tensions $\boldsymbol{\tau}_0$ to the control input, as was established in Eq. (2.22). Thus, the SM controller is obtained as

$$\boldsymbol{\tau} = \boldsymbol{A}^{\dagger}(\boldsymbol{F}_d + \boldsymbol{M}_p(-\boldsymbol{\lambda}\dot{\boldsymbol{p}} - \boldsymbol{K}_1 sgn(\boldsymbol{s}))) + \boldsymbol{\tau}_0. \tag{4.18}$$

The inclusion of a discontinuous term; i.e the signum function, in Eq. (4.18) generates the well-known undesired chattering as shown in Fig 4.3. In order to solve the chattering problem, the term $\boldsymbol{K}_1 sgn(\boldsymbol{s})$ is substituted by the smooth term $K_1 sat(\bar{\epsilon}^{-1}\boldsymbol{s})$, in which $\bar{\epsilon}$ is boundary layer thickness,

where

$$sat(\overline{\epsilon}^{-1}\boldsymbol{s}) = \begin{cases} -1 & if \quad \boldsymbol{s} < -\overline{\epsilon} \\ \overline{\epsilon}^{-1}\boldsymbol{s} & if \quad -\overline{\epsilon} < \boldsymbol{s} < \overline{\epsilon} \\ 1 & if \quad \boldsymbol{s} > \overline{\epsilon} \end{cases} \tag{4.19}$$

Then, the sliding mode with saturation (SMsat) controller is expressed as,

$$\boldsymbol{\tau} = \boldsymbol{A}^{\dagger}(\boldsymbol{F}_d + \boldsymbol{M}_p(-\boldsymbol{\lambda}\dot{\boldsymbol{p}} - \boldsymbol{K_1} sat(\overline{\epsilon}^{-1}\boldsymbol{s}))) + \boldsymbol{\tau}_0 \tag{4.20}$$

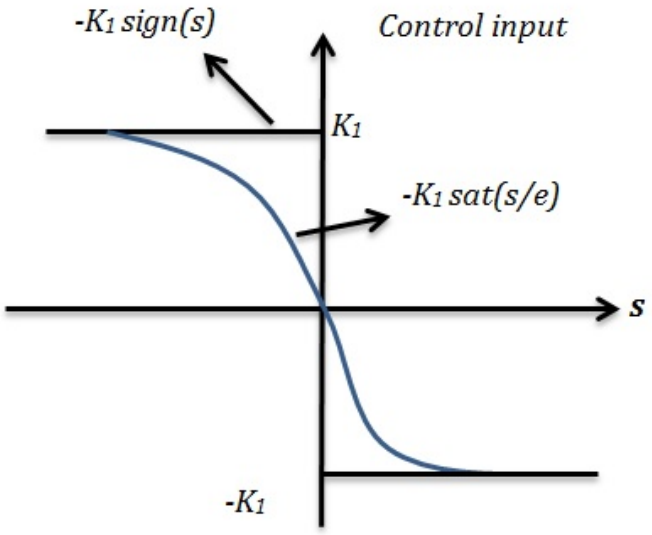

Figure 4.5: The sliding mode with saturation (SMsat) controller.

It is necessary the knowledge of the anchor points in order to apply Eq. (4.20) as a valid control law. If these parameters were unknown, an adaptive control law can be applied. The on-line estimates of the coordinates of the anchor points are obtained to estimate the structure matrix as was established in Eq. (2.29) and Eq. (2.30). The all-positive cable tension condition is satisfied by adding the internal cable tensions defined either in Eq. (3.5) or (3.9). Thus, the SMsatA controller scheme is shown below.

4.1.1 Parametric Model

4.1.1.1 Fully constrained planar cable robot

The general static parametric model is obtained [25] as

$$z_m = (\boldsymbol{\theta}_m^*)^T \boldsymbol{\phi}, \qquad (m = 1, 2). \tag{4.21}$$

where

$$z_1 = p_x, z_2 = p_y. \tag{4.22}$$

Here, z_1 and z_2 are available for measurements.

$$\boldsymbol{\phi} = \begin{bmatrix} (\frac{l_2 l_3}{\sigma}) & \frac{k_1 l_1 l_3}{\sigma} & \frac{k_2 l_1 l_2}{\sigma} \end{bmatrix}^T, \tag{4.23}$$

where

$$\sigma = l_2 l_3 + k_1 l_1 l_3 + k_2 l_1 l_2. \tag{4.24}$$

Unknown parameters can be shown as

$$\boldsymbol{\theta}_1^* = \begin{bmatrix} a_{1x} & a_{2x} & a_{3x} \end{bmatrix}^T,$$

$$\boldsymbol{\theta}_2^* = \begin{bmatrix} a_{1y} & a_{2y} & a_{3y} \end{bmatrix}^T. \tag{4.25}$$

4.1.1.2 Redundant planar cable robot

The general static parametric model for any of the four possible manipulator triples i, j, k can be written in the form Eq. (4.21) where

$$z_1 = p_x, z_2 = p_y, \tag{4.26}$$

z_1 and z_2 are available for measurements.

$$\boldsymbol{\phi} = \begin{bmatrix} (\frac{l_j l_k}{\sigma_c}) & \frac{k_a l_i l_k}{\sigma_c} & \frac{k_b l_i l_j}{\sigma_c} \end{bmatrix}^T \tag{4.27}$$

where

$$\sigma_c = l_j l_k + k_a l_i l_k + k_b l_i l_j. \tag{4.28}$$

Unknown parameters can be written as follows

$$\boldsymbol{\theta}_1^* = \begin{bmatrix} a_{ix} & a_{jx} & a_{kx} \end{bmatrix}^T, \tag{4.29}$$

$$\boldsymbol{\theta}_2^* = \begin{bmatrix} a_{iy} & a_{jy} & a_{ky} \end{bmatrix}^T. \tag{4.30}$$

4.1.2 Estimation Model

4.1.2.1 Fully constrained planar cable robot

Parametric estimation model can be expressed as:

$$\hat{z}_m = \boldsymbol{\theta}_m^T(t)\boldsymbol{\phi}(t), \qquad (m = 1, 2) \tag{4.31}$$

where $\boldsymbol{\theta}_m(t)$ is the estimate of $\boldsymbol{\theta}_m^*$ at time t

$$\boldsymbol{\theta}_1(t) = \begin{bmatrix} \hat{a}_{1x} & \hat{a}_{2x} & \hat{a}_{3x} \end{bmatrix}^T,$$

$$\boldsymbol{\theta}_2(t) = \begin{bmatrix} \hat{a}_{1y} & \hat{a}_{2y} & \hat{a}_{3y} \end{bmatrix}^T. \tag{4.32}$$

4.1.2.2 Redundant planar cable robot

Parametric estimation model is given by Eq. (4.31) for any of the four possible manipulator triples i, j, k as

$$\boldsymbol{\theta}_1(t) = \begin{bmatrix} \hat{a}_{ix} & \hat{a}_{jx} & \hat{a}_{kx} \end{bmatrix}^T, \tag{4.33}$$

$$\boldsymbol{\theta}_2(t) = \begin{bmatrix} \hat{a}_{iy} & \hat{a}_{jy} & \hat{a}_{ky} \end{bmatrix}^T. \tag{4.34}$$

4.1.3 PI algorithm (Adaptive laws)

4.1.3.1 Recursive least squares algorithm

$$\dot{\boldsymbol{\theta}}_m = \boldsymbol{P}_m \epsilon_m \boldsymbol{\phi}, \quad \boldsymbol{\theta}_m(0) = \boldsymbol{\theta}_0 \qquad (m = 1, 2) \tag{4.35}$$

$$\dot{\boldsymbol{P}}_m = \beta \boldsymbol{P}_m - \boldsymbol{P}_m \boldsymbol{\phi}^T \boldsymbol{P}_m, \quad \boldsymbol{P}_m(0) = \boldsymbol{P}_0 = \boldsymbol{Q}_0^{-1}. \tag{4.36}$$

where $\boldsymbol{P}_m$ for $m = 1, 2$ is the covariance matrix and β is the forgetting factor. The estimation error term ϵ_m is given by

$$\epsilon_m = \frac{z_m - \hat{z}_m}{m_s^2} = \frac{z_m - \boldsymbol{\theta}_m^T(t)\boldsymbol{\phi}}{m_s^2}, \qquad (m = 1, 2) \tag{4.37}$$

$m_s^2 \geq 1$ is a normalization signal designed to guarantee that

$$\frac{\boldsymbol{\phi}}{m_s^2} \, \epsilon \; with \quad m_s^2 = 1 + \alpha \boldsymbol{\phi}^T \boldsymbol{\phi}, \quad \alpha > 0. \tag{4.38}$$

4.1.3.2 Gradient algorithm

$$\dot{\boldsymbol{\theta}}_m = \boldsymbol{\Gamma} \epsilon_m \boldsymbol{\phi}, \quad (m = 1, 2) \tag{4.39}$$

where

$$\epsilon_m = \frac{z_m - \hat{z}_m}{m_s^2}, \tag{4.40}$$

where $m_s^2 \geq 1$ is the normalizing signal which is to bound $\boldsymbol{\phi}$ from above. The normalizing signal mentioned Eq. (4.40) can be expressed as

$$m_s^2 = 1 + n_s^2, \tag{4.41}$$

where n_s ($n_s \geq 0$) is static normalization signal for providing $\dfrac{\boldsymbol{\phi}}{m_s}$ is bounded from above. Convergence conditions for the estimate $\boldsymbol{\theta}_m(t)$ to $\boldsymbol{\theta}_m^*$ for the algorithm are established in [20].

4.1.4 Resultant control input

The resultant control input can be define as

$$\hat{\boldsymbol{\tau}} = \hat{\boldsymbol{A}}^{\dagger}(\boldsymbol{F}_d + \boldsymbol{M}_p(-\boldsymbol{\lambda}\dot{\boldsymbol{p}} - \boldsymbol{K_1} sat(\bar{\epsilon}^{-1}\boldsymbol{s}))) + \hat{\boldsymbol{\tau}}_0, \tag{4.42}$$

where $\hat{\boldsymbol{A}}$ is estimation of $\boldsymbol{A}$ which is generated using the estimation scheme presented in the previous section.

4.2 Proportional-derivative adaptive control

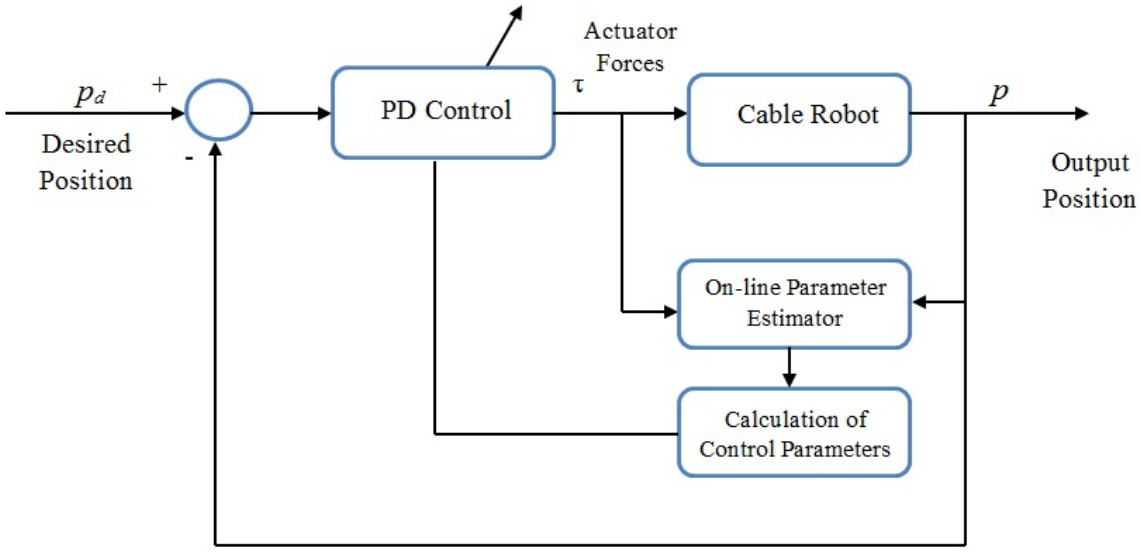

Figure 4.6: PD adaptive control block diagram.

A PD controller can be designed by using the following Lyapunov function and its derivative as

$$V(\boldsymbol{e}, \dot{\boldsymbol{e}}) = \frac{1}{2}\dot{\boldsymbol{e}}^T \boldsymbol{M}_p \dot{\boldsymbol{e}} + \frac{1}{2}\boldsymbol{e}^T \boldsymbol{K}_p \boldsymbol{e}, \quad \forall \quad \boldsymbol{K}_p > 0. \tag{4.43}$$

where $\boldsymbol{K}_p e$ is the proportional feedback effort.

The Krasovskii-LaSalle principle [28] gives a criterion for the asymptotic stability of the system in case $\dot{V}(\boldsymbol{p}) \leq 0$, i.e $\dot{V}(\boldsymbol{p})$ is only negative semi-definite that means it does not assure success asymptotic tracking . In addition we can note $\dot{\boldsymbol{p}}_d$ and $\ddot{\boldsymbol{p}}_d$ are equal zero for constant desired trajectory. Thus, the time derivative of the Lyapunov function can be derived as follows

$$\dot{V}(\boldsymbol{e}, \dot{\boldsymbol{e}}) = \dot{\boldsymbol{e}}^T(\boldsymbol{M}_p\ddot{\boldsymbol{e}} + \frac{1}{2}\dot{\boldsymbol{M}}_p\dot{\boldsymbol{e}} + \boldsymbol{K}_p\boldsymbol{e}), \tag{4.44}$$

where

$$\boldsymbol{M}_p\ddot{\boldsymbol{e}} = \boldsymbol{M}_p\ddot{\boldsymbol{p}} = \boldsymbol{F}_d + \boldsymbol{A}\boldsymbol{\tau}. \tag{4.45}$$

Hence,

$$\dot{V}(\boldsymbol{e}, \dot{\boldsymbol{e}}) = \dot{\boldsymbol{e}}^T(\boldsymbol{F}_d + \boldsymbol{A}\boldsymbol{\tau} + \boldsymbol{K}_p\boldsymbol{e}). \tag{4.46}$$

Selecting the control input $\boldsymbol{\tau_c}$ in Eq. (2.22) as

$$\boldsymbol{\tau_c} = \boldsymbol{A}^\dagger(\boldsymbol{F}_d - \boldsymbol{K}_p\boldsymbol{e} - \boldsymbol{K}_v\dot{\boldsymbol{e}}). \tag{4.47}$$

Eq. (4.46) can be rewritten as

$$\dot{V}(\boldsymbol{e}, \dot{\boldsymbol{e}}) \leq -\dot{\boldsymbol{e}}^T\boldsymbol{K}_v\dot{\boldsymbol{e}}, \quad \forall \quad \boldsymbol{K}_v > 0. \tag{4.48}$$

Thus, the PD control law is obtained as follows

$$\boldsymbol{\tau} = \boldsymbol{A}^\dagger(\boldsymbol{F}_d - \boldsymbol{K}_p\boldsymbol{e} - \boldsymbol{K}_v\dot{\boldsymbol{e}}) + \boldsymbol{\tau}_0. \tag{4.49}$$

where $\boldsymbol{K}_p = [diag(K_p, K_p)]$ is proportional gain matrix and $\boldsymbol{K}_v = [diag(K_v, K_v)]$ represents derivative gain matrix . The internal cable tension vector $\boldsymbol{\tau}_0$, is added to the control law in order to ensure the always positive cable tension conditions. The above control law is valid if all parameters are known.

Again, when the structure matrix $\boldsymbol{A}$ is unknown; its estimate $\hat{\boldsymbol{A}}$ is generated using the estimation scheme presented in the previous section and the certainty equivalence approach is used. The internal cable tensions are defined by either in Eq. (3.5) or (3.9). Thus, the PDA controller scheme is shown below.

4.2.1 Parametric Model

4.2.1.1 Fully constrained planar cable robot

The general static parametric model is obtained [25] as

$$z_m = (\boldsymbol{\theta}_m^*)^T \boldsymbol{\phi}, \qquad (m = 1, 2). \tag{4.50}$$

where

$$z_1 = p_x, z_2 = p_y. \tag{4.51}$$

Here, z_1 and z_2 are available for measurements.

$$\boldsymbol{\phi} = \begin{bmatrix} (\frac{l_2 l_3}{\sigma}) & \frac{k_1 l_1 l_3}{\sigma} & \frac{k_2 l_1 l_2}{\sigma} \end{bmatrix}^T, \tag{4.52}$$

where

$$\sigma = l_2 l_3 + k_1 l_1 l_3 + k_2 l_1 l_2. \tag{4.53}$$

Unknown parameters can be written as

$$\boldsymbol{\theta}_1^* = \begin{bmatrix} a_{1x} & a_{2x} & a_{3x} \end{bmatrix}^T,$$

$$\boldsymbol{\theta}_2^* = \begin{bmatrix} a_{1y} & a_{2y} & a_{3y} \end{bmatrix}^T. \tag{4.54}$$

4.2.1.2 Redundant planar cable robot

The general static parametric model for any of the four possible manipulator triples i, j, k can be written in the form Eq. (3.10) where

$$z_1 = p_x, z_2 = p_y, \tag{4.55}$$

z_1 and z_2 are available for measurements.

$$\boldsymbol{\phi} = \begin{bmatrix} (\frac{l_j l_k}{\sigma_c}) & \frac{k_a l_i l_k}{\sigma_c} & \frac{k_b l_i l_j}{\sigma_c} \end{bmatrix}^T \tag{4.56}$$

where

$$\sigma_c = l_j l_k + k_a l_i l_k + k_b l_i l_j. \tag{4.57}$$

Unknown parameters can be written as follows

$$\boldsymbol{\theta}_1^* = \begin{bmatrix} a_{ix} & a_{jx} & a_{kx} \end{bmatrix}^T, \tag{4.58}$$

$$\boldsymbol{\theta}_2^* = \begin{bmatrix} a_{iy} & a_{jy} & a_{ky} \end{bmatrix}^T. \tag{4.59}$$

4.2.2 Estimation Model

4.2.2.1 Fully constrained planar cable robot

Parametric estimation model can be expressed as:

$$\hat{z}_m = \boldsymbol{\theta}_m^T(t)\boldsymbol{\phi}(t), \qquad (m = 1, 2) \tag{4.60}$$

where $\boldsymbol{\theta}_m(t)$ is the estimate of $\boldsymbol{\theta}_m^*$ at time t

$$\boldsymbol{\theta}_1(t) = \begin{bmatrix} \hat{a}_{1x} & \hat{a}_{2x} & \hat{a}_{3x} \end{bmatrix}^T,$$

$$\boldsymbol{\theta}_2(t) = \begin{bmatrix} \hat{a}_{1y} & \hat{a}_{2y} & \hat{a}_{3y} \end{bmatrix}^T. \tag{4.61}$$

4.2.2.2 Redundant planar cable robot

Parametric estimation model is given by Eq. (4.60) for any of the four possible manipulator triples i, j, k as

$$\boldsymbol{\theta}_1(t) = \begin{bmatrix} \hat{a}_{ix} & \hat{a}_{jx} & \hat{a}_{kx} \end{bmatrix}^T, \tag{4.62}$$

$$\boldsymbol{\theta}_2(t) = \begin{bmatrix} \hat{a}_{iy} & \hat{a}_{jy} & \hat{a}_{ky} \end{bmatrix}^T. \tag{4.63}$$

4.2.3 PI algorithm (Adaptive laws)

4.2.3.1 Recursive least squares algorithm

$$\dot{\boldsymbol{\theta}}_m = \boldsymbol{P}_m \epsilon_m \boldsymbol{\phi}, \quad \boldsymbol{\theta}_m(0) = \boldsymbol{\theta}_0 \qquad (m = 1, 2) \tag{4.64}$$

$$\dot{\boldsymbol{P}}_m = \beta \boldsymbol{P}_m - \boldsymbol{P}_m \boldsymbol{\phi}^T \boldsymbol{P}_m, \quad \boldsymbol{P}_m(0) = \boldsymbol{P}_0 = \boldsymbol{Q}_0^{-1}. \tag{4.65}$$

where $\boldsymbol{P}_m$ for $m = 1, 2$ is the covariance matrix and β is the forgetting factor. The estimation error term ϵ_m is given by

$$\epsilon_m = \frac{z_m - \hat{z}_m}{m_s^2} = \frac{z_m - \boldsymbol{\theta}_m^T(t)\boldsymbol{\phi}}{m_s^2}, \qquad (m = 1, 2) \tag{4.66}$$

$m_s^2 \geq 1$ is a normalization signal designed to guarantee that

$$\frac{\boldsymbol{\phi}}{m_s^2} \; \epsilon \; with \quad m_s^2 = 1 + \alpha \boldsymbol{\phi}^T \boldsymbol{\phi}, \alpha > 0. \tag{4.67}$$

4.2.3.2 Gradient algorithm

$$\dot{\boldsymbol{\theta}}_m = \boldsymbol{\Gamma} \epsilon_m \boldsymbol{\phi}, (m = 1, 2) \tag{4.68}$$

where

$$\epsilon_m = \frac{z_m - \hat{z}_m}{m_s^2}, \tag{4.69}$$

where $m_s^2 \geq 1$ is the normalizing signal which is to bound $\boldsymbol{\phi}$ from above. The normalizing signal mentioned Eq. (4.69) can be expressed as

$$m_s^2 = 1 + n_s^2, \tag{4.70}$$

where n_s ($n_s \geq 0$) is static normalization signal for providing $\dfrac{\boldsymbol{\phi}}{m_s}$ is bounded from above. Convergence conditions for the estimate $\boldsymbol{\theta}_m(t)$ to $\boldsymbol{\theta}_m^*$ for the algorithm are established in [20].

4.2.4 Resultant control input

Resultant control input can be define as

$$\hat{\boldsymbol{\tau}} = \hat{\boldsymbol{A}}^{\dagger}(\boldsymbol{F}_d - \boldsymbol{K}_p\boldsymbol{e} - \boldsymbol{K}_v\dot{\boldsymbol{e}}) + \hat{\boldsymbol{\tau}}_0, \tag{4.71}$$

where $\hat{\boldsymbol{A}}$ is estimation of $\boldsymbol{A}$ which is generated using the estimation scheme presented in the previous section.

4.3 Backstepping adaptive control

Lets us consider dynamic equation in Eq.(4.1) with no external force, we can rewrite the system equations in state-space form as

$$\dot{\boldsymbol{p}}_1 = \boldsymbol{p}_2 \tag{4.72}$$
$$\dot{\boldsymbol{p}}_2 = \boldsymbol{M}_p^{-1}\boldsymbol{A}\boldsymbol{\tau}, \tag{4.73}$$

where $\boldsymbol{p} = \boldsymbol{p}_1$ and $\dot{\boldsymbol{p}} = \boldsymbol{p}_2$.

The output of this system is $\boldsymbol{p}_1 = \boldsymbol{p} = [p_x, p_y]^T$ which follows the reference signal. The defining intended errors can be expressed as $\boldsymbol{e}_1 = \boldsymbol{p}_1 - \boldsymbol{p}_d$, $\boldsymbol{e}_2 = \dot{\boldsymbol{p}}_1 - \dot{\boldsymbol{p}}_d$. Then, the state equation of these tracking errors is written as

$$\begin{cases} \dot{\boldsymbol{e}}_1 = \boldsymbol{e}_2 \\ \dot{\boldsymbol{e}}_2 = \boldsymbol{M}_p^{-1}\boldsymbol{A}\boldsymbol{\tau} - \ddot{\boldsymbol{p}}_d \end{cases} \tag{4.74}$$

where $\boldsymbol{M}_p^{-1}\boldsymbol{A}\boldsymbol{\tau} = \bar{u}$.

Define the following new state variables for the design backstepping controller.

$$\begin{aligned} \boldsymbol{z}_1 &= \boldsymbol{p}_1 - \boldsymbol{p}_d = \boldsymbol{e}_1 \\ \boldsymbol{z}_2 &= \boldsymbol{e}_2 - \boldsymbol{e}_{2d} = \boldsymbol{e}_2 + K\boldsymbol{e}_1. \end{aligned} \tag{4.75}$$

where $\boldsymbol{e}_{2d} = -K\boldsymbol{e}_1$ is the desired value of the $\boldsymbol{e}_2$. Taking the derivation of the Eq. (4.75),

$$\begin{aligned} \dot{\boldsymbol{z}}_1 &= \boldsymbol{e}_2 \\ \dot{\boldsymbol{z}}_2 &= \dot{\boldsymbol{e}}_2 + K\dot{\boldsymbol{e}}_1. \end{aligned} \tag{4.76}$$

Substituting the Eq. (4.75) into Eq. (4.76), the new state variable can be written as follows

$$\begin{aligned}\dot{\boldsymbol{z}}_1 &= -K\boldsymbol{z}_1 + \boldsymbol{z}_2,\\ \dot{\boldsymbol{z}}_2 &= \bar{\boldsymbol{u}} - \ddot{\boldsymbol{p}}_d + K(-K\boldsymbol{z}_1 + \boldsymbol{z}_2) = -K^2\boldsymbol{z}_1 + K\boldsymbol{z}_2 + \bar{\boldsymbol{u}} - \ddot{\boldsymbol{p}}_d.\end{aligned} \tag{4.77}$$

Selecting the $\bar{\boldsymbol{u}} = a_1\boldsymbol{z}_1 + a_2\boldsymbol{z}_2 + \ddot{\boldsymbol{p}}_d$ to remove $\ddot{\boldsymbol{p}}_d$, the $\ddot{\boldsymbol{z}}$ can rewrite as

$$\dot{\boldsymbol{z}}_2 = (a_1 - K^2)\boldsymbol{z}_1 + (a_2 + K)\boldsymbol{z}_2. \tag{4.78}$$

We can express the new derivation of the state variable with matrix form as

$$\begin{bmatrix}\dot{z}_1\\ \dot{z}_2\end{bmatrix} = \begin{bmatrix}-K & 1\\ (a_1 - K^2) & (a_2 + K)\end{bmatrix}\begin{bmatrix}z_1\\ z_2\end{bmatrix}. \tag{4.79}$$

Lets propose $a_1 = K^2$ and $a_2 = -2K$. Then, we can rewrite as

$$\begin{bmatrix}\dot{z}_1\\ \dot{z}_2\end{bmatrix} = \boldsymbol{E}\begin{bmatrix}z_1\\ z_2\end{bmatrix}, \tag{4.80}$$

where $\boldsymbol{E} = \begin{bmatrix}-K & 1\\ 0 & -K\end{bmatrix}$.

Backstepping controller back-steps the control $K\boldsymbol{e}_1$ through the integrator as mentioned above. Backstepping controller can be completed by using the following Lyapunov function and its derivative as

$$V(\boldsymbol{z}_1, \boldsymbol{z}_2) = \frac{1}{2}(\boldsymbol{z}_1^T\boldsymbol{z}_1 + \boldsymbol{z}_2^T\boldsymbol{z}_2), \tag{4.81}$$

$$\begin{aligned}\dot{V}(\boldsymbol{z}_1, \boldsymbol{z}_2) &= \boldsymbol{z}_1^T\dot{\boldsymbol{z}}_{\boldsymbol{1}} + \boldsymbol{z}_2^T\dot{\boldsymbol{z}}_2 < 0\\ &= \begin{bmatrix}z_1^T & z_2^T\end{bmatrix}\begin{bmatrix}\dot{z}_1\\ \dot{z}_2\end{bmatrix} < 0\\ &= \begin{bmatrix}z_1^T & z_2^T\end{bmatrix}\boldsymbol{E}\begin{bmatrix}z_1\\ z_2\end{bmatrix} < 0.\end{aligned} \tag{4.82}$$

where $\boldsymbol{E} < 0 \rightarrow$ negative definition. Substituting the equations (4.75) and (4.76) into Eq. (4.82) the derivation of Lyapunov function can be rewritten as

$$\dot{V} = -K^3\boldsymbol{e}_1^2 - K\boldsymbol{e}_2^2 + (1 - 2K^2)\boldsymbol{e}_1\boldsymbol{e}_2 < 0. \tag{4.83}$$

Recalling the $\bar{\boldsymbol{u}}$ in Eq. (4.74) and (4.77), the equilibrium can be defined as follows

$$\bar{\boldsymbol{u}} = \boldsymbol{M}_p^{-1}\boldsymbol{A}\boldsymbol{\tau} = K^2\boldsymbol{z}_1 - 2K\boldsymbol{z}_2 + \ddot{\boldsymbol{p}}_d. \tag{4.84}$$

The input can be defined by $\boldsymbol{\tau}$ is

$$\boldsymbol{\tau} = (K^2\boldsymbol{z}_1 - 2K\boldsymbol{z}_2 + \ddot{\boldsymbol{p}}_d)\boldsymbol{M}_p\boldsymbol{A}^\dagger. \tag{4.85}$$

The general form of the input function can be written with substitution of the Eq.(4.75) into Eq. (4.3)

$$\boldsymbol{\tau}_c = (-K^2\boldsymbol{e}_1 - 2K\boldsymbol{e}_2 + \ddot{\boldsymbol{p}}_d)\boldsymbol{M}_p\boldsymbol{A}^\dagger. \tag{4.86}$$

The internal cable tension vector $\boldsymbol{\tau}_0$, is added to the control law in order to ensure the always positive cable tension conditions. The below control law is valid if all parameters are known.

$$\boldsymbol{\tau} = (-K^2\boldsymbol{e}_1 - 2K\boldsymbol{e}_2 + \ddot{\boldsymbol{p}}_d)\boldsymbol{M}_p\boldsymbol{A}^\dagger + \boldsymbol{\tau}_0. \tag{4.87}$$

Thus, the Backstepping controller scheme is shown below.

4.3.1 Parametric Model

4.3.1.1 Fully constrained planar cable robot

The general static parametric model is obtained [25] as

$$z_m = (\boldsymbol{\theta}_m^*)^T\boldsymbol{\phi}, \qquad (m = 1, 2). \tag{4.88}$$

where

$$z_1 = p_x, z_2 = p_y. \tag{4.89}$$

Here, z_1 and z_2 are available for measurements.

$$\boldsymbol{\phi} = \begin{bmatrix} (\dfrac{l_2 l_3}{\sigma}) & \dfrac{k_1 l_1 l_3}{\sigma} & \dfrac{k_2 l_1 l_2}{\sigma} \end{bmatrix}^T, \tag{4.90}$$

where

$$\sigma = l_2 l_3 + k_1 l_1 l_3 + k_2 l_1 l_2. \tag{4.91}$$

Unknown parameters can be shown as

$$\boldsymbol{\theta}_1^* = \begin{bmatrix} a_{1x} & a_{2x} & a_{3x} \end{bmatrix}^T,$$

$$\boldsymbol{\theta}_2^* = \begin{bmatrix} a_{1y} & a_{2y} & a_{3y} \end{bmatrix}^T. \tag{4.92}$$

4.3.1.2 Redundant planar cable robot

The general static parametric model for any of the four possible manipulator triples i, j, k can be written in the form Eq. (4.88) where

$$z_1 = p_x, z_2 = p_y, \tag{4.93}$$

z_1 and z_2 are available for measurements.

$$\boldsymbol{\phi} = \begin{bmatrix} (\frac{l_j l_k}{\sigma_c}) & \frac{k_a l_i l_k}{\sigma_c} & \frac{k_b l_i l_j}{\sigma_c} \end{bmatrix}^T, \tag{4.94}$$

where

$$\sigma_c = l_j l_k + k_a l_i l_k + k_b l_i l_j. \tag{4.95}$$

Unknown parameters can be written as

$$\boldsymbol{\theta}_1^* = \begin{bmatrix} a_{ix} & a_{jx} & a_{kx} \end{bmatrix}^T, \tag{4.96}$$

$$\boldsymbol{\theta}_2^* = \begin{bmatrix} a_{iy} & a_{jy} & a_{ky} \end{bmatrix}^T. \tag{4.97}$$

4.3.2 Estimation Model

4.3.2.1 Fully constrained planar cable robot

Parametric estimation model can be expressed as:

$$\hat{z}_m = \boldsymbol{\theta}_m^T(t)\boldsymbol{\phi}(t), \qquad (m = 1, 2) \tag{4.98}$$

where $\boldsymbol{\theta}_m(t)$ is the estimate of $\boldsymbol{\theta}_m^*$ at time t

$$\boldsymbol{\theta}_1(t) = \begin{bmatrix} \hat{a}_{1x} & \hat{a}_{2x} & \hat{a}_{3x} \end{bmatrix}^T,$$

$$\boldsymbol{\theta}_2(t) = \begin{bmatrix} \hat{a}_{1y} & \hat{a}_{2y} & \hat{a}_{3y} \end{bmatrix}^T. \tag{4.99}$$

4.3.2.2 Redundant planar cable robot

Parametric estimation model is given by Eq. (4.98) for any of the four possible manipulator triples i, j, k as

$$\boldsymbol{\theta}_1(t) = \begin{bmatrix} \hat{a}_{ix} & \hat{a}_{jx} & \hat{a}_{kx} \end{bmatrix}^T, \tag{4.100}$$

$$\boldsymbol{\theta}_2(t) = \begin{bmatrix} \hat{a}_{iy} & \hat{a}_{jy} & \hat{a}_{ky} \end{bmatrix}^T. \tag{4.101}$$

4.3.3 PI algorithm (Adaptive laws)

4.3.3.1 Recursive Least squares algorithm

$$\dot{\boldsymbol{\theta}}_m = \boldsymbol{P}_m \epsilon_m \boldsymbol{\phi}, \boldsymbol{\theta}_m(0) = \boldsymbol{\theta}_0 \qquad (m = 1, 2) \tag{4.102}$$

$$\dot{\boldsymbol{P}}_m = \beta \boldsymbol{P}_m - \boldsymbol{P}_m \boldsymbol{\phi}^T \boldsymbol{P}_m, \boldsymbol{P}_m(0) = \boldsymbol{P}_0 = \boldsymbol{Q}_0^{-1}. \tag{4.103}$$

where $\boldsymbol{P}_m$ for $m = 1, 2$ is the covariance matrix and β is the forgetting factor. The estimation error term ϵ_m is given by

$$\epsilon_m = \frac{z_m - \hat{z}_m}{m_s^2} = \frac{z_m - \boldsymbol{\theta}_m^T(t)}{m_s^2}, \qquad (m = 1, 2) \tag{4.104}$$

$m_s^2 \geq 1$ is a normalization signal designed to guarantee that

$$\frac{\boldsymbol{\phi}}{m_s^2} \; \epsilon \; with \quad m_s^2 = 1 + \alpha \boldsymbol{\phi}^T \boldsymbol{\phi}, \alpha > 0. \tag{4.105}$$

4.3.3.2 Gradient algorithm

$$\dot{\boldsymbol{\theta}}_m = \boldsymbol{\Gamma} \epsilon_m \boldsymbol{\phi}, (m = 1, 2) \tag{4.106}$$

where

$$\epsilon_m = \frac{z_m - \hat{z}_m}{m_s^2}, \tag{4.107}$$

where $m_s^2 \geq 1$ is the normalizing signal which is to bound $\boldsymbol{\phi}$ from above. The normalizing signal mentioned Eq. (4.107) can be expressed as

$$m_s^2 = 1 + n_s^2, \tag{4.108}$$

where n_s ($n_s \geq 0$) is static normalization signal for providing $\dfrac{\boldsymbol{\phi}}{m_s}$ is bounded from above. Convergence conditions for the estimate $\boldsymbol{\theta}_m(t)$ to $\boldsymbol{\theta}_m^*$ for the algorithm are established in [20].

4.3.4 Resultant control input

Resultant control input can be written as

$$\hat{\boldsymbol{\tau}} = \hat{\boldsymbol{A}}^{\dagger}\boldsymbol{M}_p(-K^2\boldsymbol{e}_1 - 2K\boldsymbol{e}_2 + \ddot{\boldsymbol{p}}_d) + \hat{\boldsymbol{\tau}}_0, \tag{4.109}$$

where $\hat{\boldsymbol{A}}$ is estimation of $\boldsymbol{A}$ which is generated using the estimation scheme presented in the previous section.

4.4 Proportional-integrative-derivative control

PID control is a simple law which is known by its robustness. Cable robots use the following PID control law with the condition of all-positive cable tensions:

$$\boldsymbol{\tau}_{PID} = \boldsymbol{A}^{\dagger}(\boldsymbol{F}_d - K_p\boldsymbol{e} - K_v\dot{\boldsymbol{e}} - K_i\int_0^t -\boldsymbol{e}(T)dT) + \boldsymbol{\tau}_0, \tag{4.110}$$

where $\boldsymbol{K}_r = [diag(K_r, K_r)],\ \forall r = p, v, i$. The all-positive cable tension conditions are also ensured by adding the internal cable tensions to control input. If bounded errors in the measurement of the anchor points are considered during the motion of the mobile platform, the structure matrix $\boldsymbol{A}$ and the internal cable tensions $\boldsymbol{\tau}_0$, used in Eq.(4.110) are affected. Here, the inexact structure matrix $\tilde{\boldsymbol{A}}$ and and the erroneous internal cable tensions $\tilde{\boldsymbol{\tau}}_0$ are established by the initial values of the anchor points. Thus, the PID controller with uncertainties is defined as

$$\tilde{\boldsymbol{\tau}}_{PID} = \tilde{\boldsymbol{A}}^{\dagger}(\boldsymbol{F}_d - \boldsymbol{K}_p\boldsymbol{e} - \boldsymbol{K}_v\dot{\boldsymbol{e}} - \boldsymbol{K}_i\int_0^t \boldsymbol{e}(T)dT) + \tilde{\boldsymbol{\tau}}_0. \tag{4.111}$$

4.5 Simulation

Using the two types of planar cable robots, three types of computer simulations are conducted by using MATLAB. First a parametric estimation of the anchor points is developed by using the gradient algorithm and least squares command given in [14]; then, a fourth-order Runge-Kutta method with a constant step of 1 ms is used to evaluate the performance of the controllers with and without the inclusion of uncertain anchor point coordinates in the system. The mass of the end-effector is m_p=50 Kg. The initial position of the end-effector is located at the origin and the desired position of the end-effector is established at p_{xd}=6 m, p_{yd}=-10.0 m.

In the simulation, the recursive least squares algorithm (3.3.3.1) and the gradient algorithm (3.3.3.2) are used to estimate the values of the anchor points with constant forgetting factor (β=1) and velocity of convergence of the gradient algorithm (Γ=6) for fully-constrained and redundant planar cable robots.

4.5.1 Control schemes comparison setup

A quantifiable criterion based in the L_2 norm of position errors is selected to evaluate the performance of the three controllers.

$$L_2(\boldsymbol{e}) = \sqrt{\frac{1}{t - t_0} \int \parallel \boldsymbol{e}(t) \parallel^2 dt} \tag{4.112}$$

In addition, the maximum position error at the last 5 seconds of the trajectory is included in the evaluation.

$$e_l = \max_{t \in [0,5]} \quad (\parallel \boldsymbol{e}(t) \parallel)$$

For a fair comparison among the controllers, the gains are tuned such that the consumed kinetic energy by each control is similar. The kinetic energy of the mobile platform is:

$$E_k = \int_{\boldsymbol{p}_1}^{\boldsymbol{p}_2} (\boldsymbol{A}\boldsymbol{\tau}).d\boldsymbol{p}, \tag{4.113}$$

where $\boldsymbol{p}_1 = [p_{1x}, p_{1y}]^T$ and $\boldsymbol{p}_2 = [p_{2x}, p_{2y}]^T$ are the initial and final position of the mobile platform, respectively. Assuming no external forces are applied, Eq. 4.113 can be rewritten as follows:

$$E_k = \int_{\boldsymbol{p}_1}^{\boldsymbol{p}_2} \boldsymbol{M}_p \ddot{\boldsymbol{p}} d\boldsymbol{p} = m_p \int_t^T \ddot{\boldsymbol{p}} \frac{d\boldsymbol{p}}{dt} dt = m_p \int_t^T \ddot{\boldsymbol{p}} \dot{\boldsymbol{p}} dt. \tag{4.114}$$

Also, the maximum position error at the first 5 seconds is used to ensure a fair comparison among the controllers. This index is expressed as

$$e_f = \max_{t \in [35,40]} \quad (\| \boldsymbol{e}(t) \|)$$

The above indexes have been implemented in MATLAB together with each of the analyzed controllers.

4.5.2 Fully-constrained planar robot

The robot shown in Figure 3.1 is analyzed in this subsection. The robot parameters used in simulations are listed in Tab. 4.1.

Table 4.1: Parameters of the fully constrained planar robot.

Point	Actual [m]	Initial [m]	Control gains
a_{1x}	-15	-14.25	λ=0.2
a_{1y}	-14	-13.75	K_1=9.0
a_{2x}	17	16.5	$\bar{\epsilon}$=5
a_{2y}	-13	-12.75	K_p=5.0
a_{3x}	0.5	0.75	K_v=30.0
a_{3y}	14	14.25	K_i=0.01

The lower and upper bounds of the anchor points are established 0.25m with respect to the actual values. The constant $\alpha = 0.1$ for the homogeneous solution in Eq.(3.5) is established such that the bounded cable tensions are τ_{min}=200N and τ_{max}=2000N. The control gains were determined by a trail-and-trail-error method in order to ensure controllers do not show overshoots and cable tensions are bounded with respect to the given minimum and maximum values.

The feasible workspace is shown in Fig 4.7.

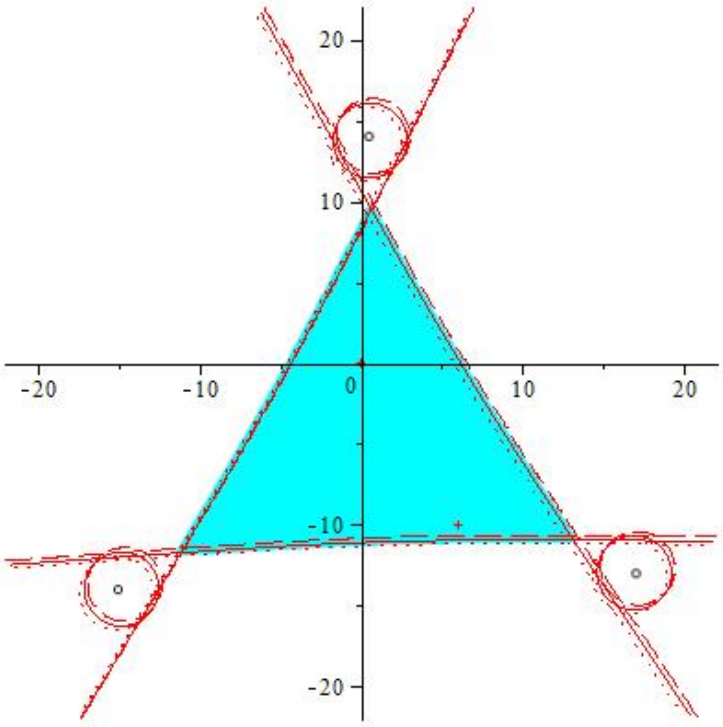

Figure 4.7: Feasible static workspaces with anchor points uncertainties: lower bound values (dot lines), upper bound values (dash lines), and actual values (continuous lines and shaded area).

In the following simulations, the anchor points are estimated on-line and used in the adaptive controllers. The initial values of the parameters, shown in Tab.4.1, are used to compare the adaptive controllers with the PID controller. The simulation results are established of fourty seconds.

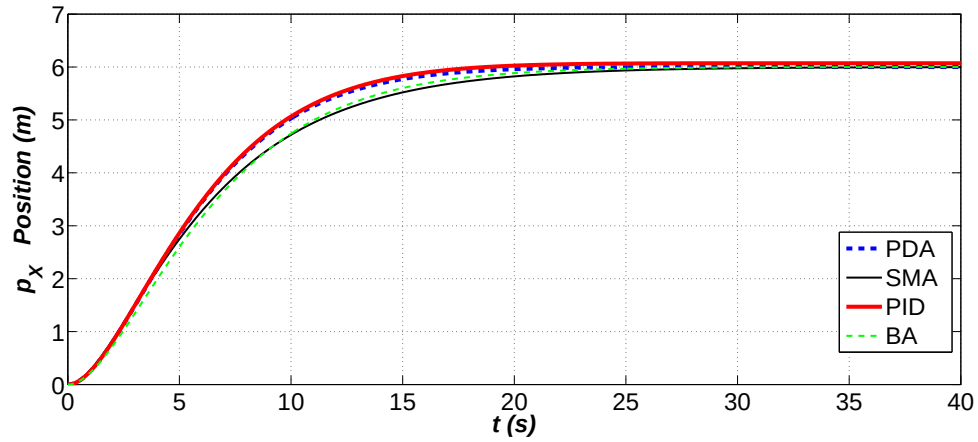

(a)

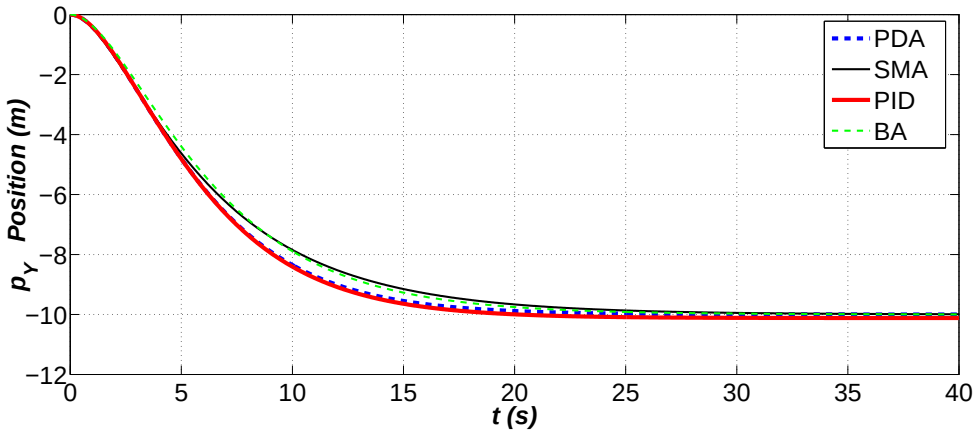

(b)

Figure 4.8: p_x and p_y position controller comparison for the three-cable robot with uncertain parameters.

Although the SMsatA and BA controller does not present shattering they take the maximum time to reach the desired position. The PID controller is the fastest method to achieve the goal position; this contoller presents a small offset, which remains all the time.

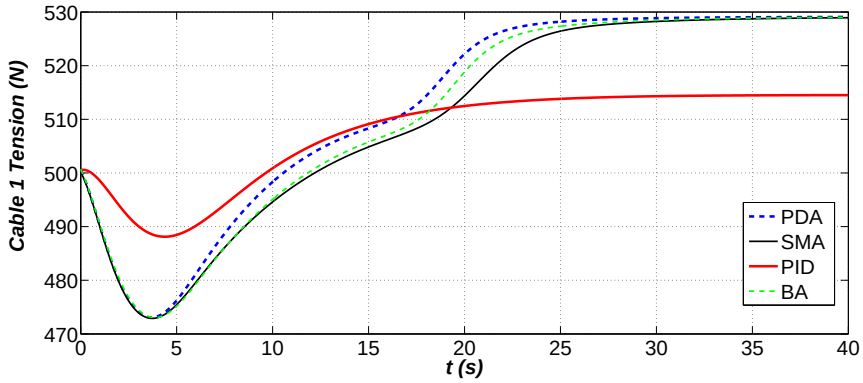

(a)

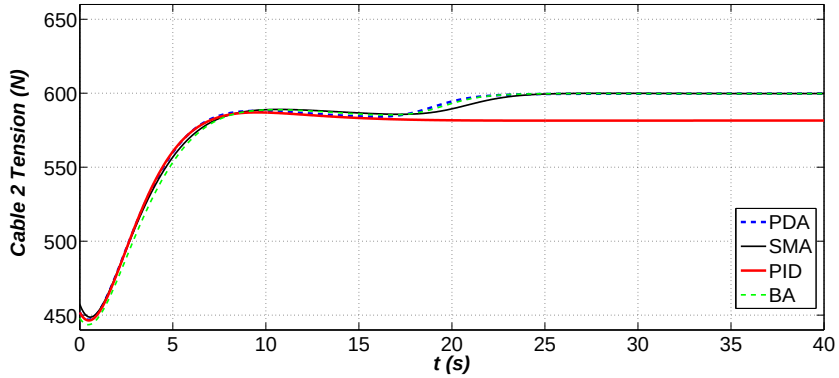

(b)

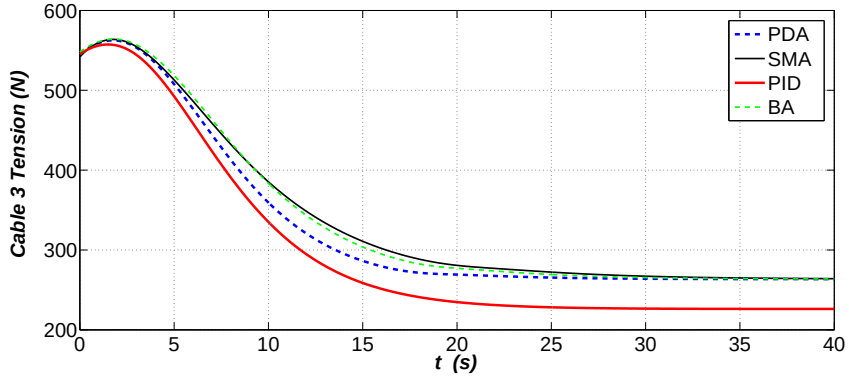

(c)

Figure 4.9: Cable tensions comparison for uncertain parameters.

Bounded positive tension conditions are accomplished in the three controllers. Also, similar cable tension solutions for the three controllers are observed in cable 2 during the 15 seconds. At the desired position, cable 2 achieves the maximum tension which is almost four times below the given maximum bounded tension conditions. In addition, cable 3 reached the minimum tension which is almost two times above the given minimum bounded tension conditions.

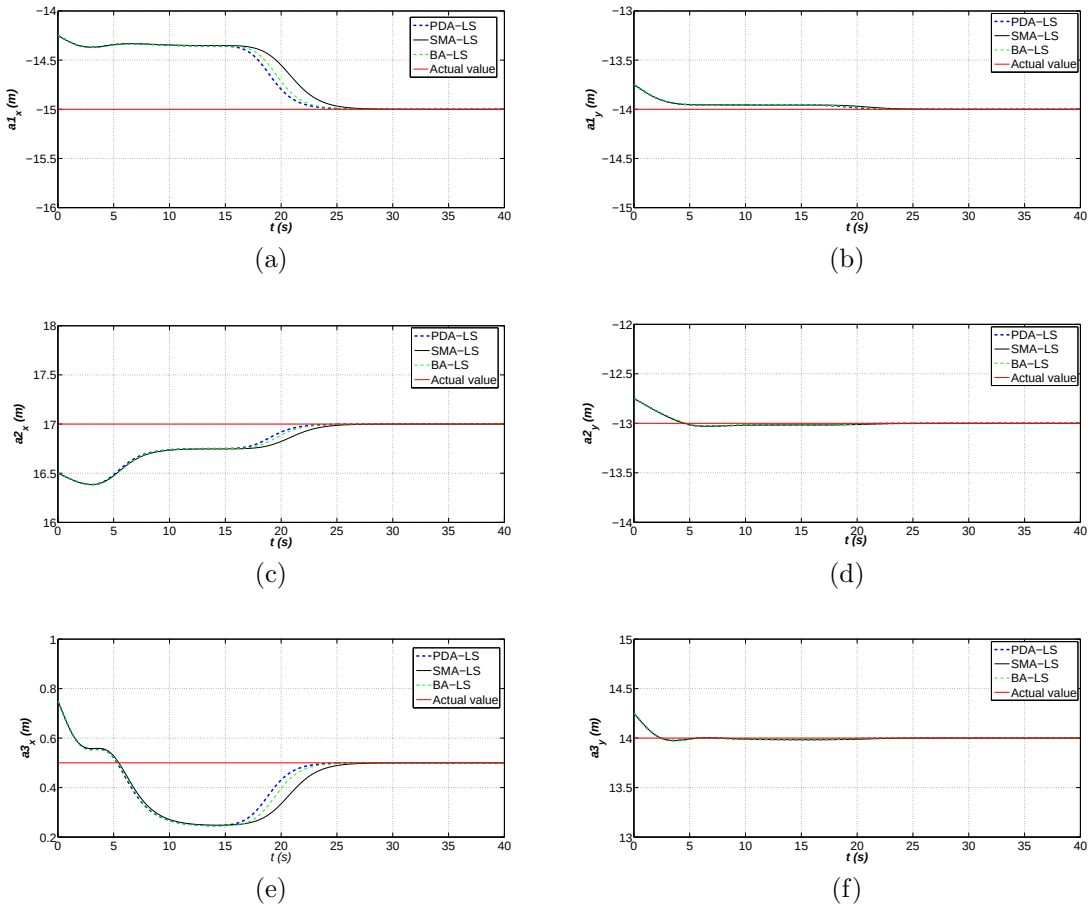

Figure 4.10: Estimated values of the coordinates of the three anchor points to actual anchor points with recursive least squares algorithm.

Fig. 4.10 shows estimated values of the coordinates of the three anchor points to actual anchor's points. The recursive least squares algorithm generally converges to actual values of anchor points in less than 25 seconds.

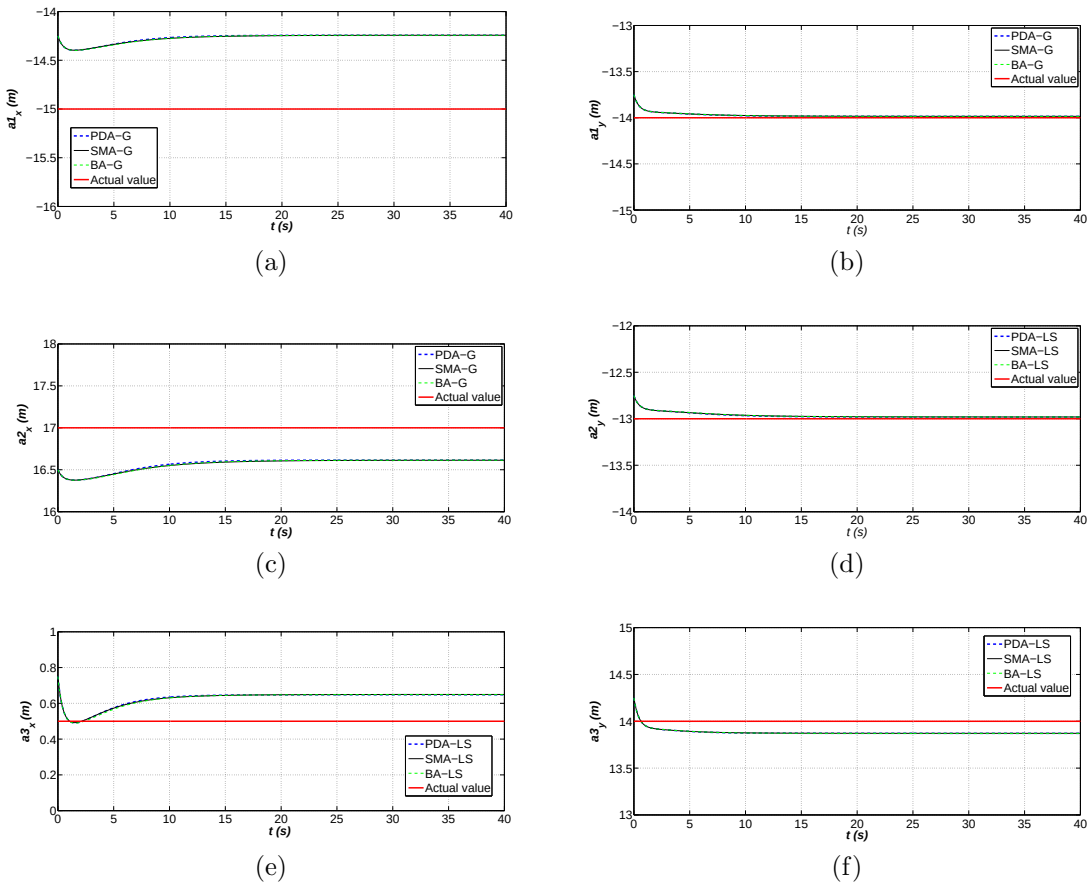

Figure 4.11: Estimated values of the coordinates of the three anchor points to actual anchor points with gradient algorithm.

On the other hand, gradient algorithm converge to anchor point actual values are not succeed in 40 seconds as shown in Fig. 4.11.

The performance of each controller is summarized in Tab. 4.2.

Table 4.2: Comparison of controllers for the 3-cable robot.

W_k	$L_2(\boldsymbol{e})$	e_f	e_l	Controller
1835.265	16.284	0.0018	11.661	PDA
1804.566	16.250	0.137	11.661	PID
1813.381	16.2532	0.021	11.661	SMAsatA
1808.488	16.3084	0.0051	11.661	BA

A fair comparison among the controllers is achieved by observing the similar values of the kinetic energy and initial position error during the first 5s. After the first five seconds of the trajectory, it is observed two main differences among the controllers. First, the largest error is presented by the BA controller. Lastly, the PID presents the worst behavior during the last five seconds

4.5.3 Redundantly planar cable robot

The robot shown in Fig. 3.2 is analyzed in this subsection. The robot parameters used in simulations are listed in Tab. 4.3. Simulation results of fourty seconds are shown below.

Table 4.3: Parameters of the redundantly planar robot.

Point	Actual[m]	Initial[m]	Control gains
a_{1x}	-15	-15.25	λ=0.2
a_{1y}	-14	-13.25	K_1=9.0
a_{2x}	17	16.5	$\bar{\epsilon}$=5
a_{2y}	-13	-13.75	K_p=5.0
a_{3x}	12	12.5	K_v=30.0
a_{3y}	14	14.25	K_i=0.01
a_{4x}	-13	-13.5	
a_{4y}	16	15.75	

The workspace is depicted for $\pm$ 0.25 m varition of the lower and upper bounds of the anchor points with respect to the actual values. Constant $\alpha_1 = \alpha_2 = 0.006$, for the homogeneous solution in Eq. (3.14), are established such that the bounded cable tensions are $\tau_{min} = 50N$, and $\tau_{max} = 2000N$.

The feasible workspace is shown in Fig. 4.12.

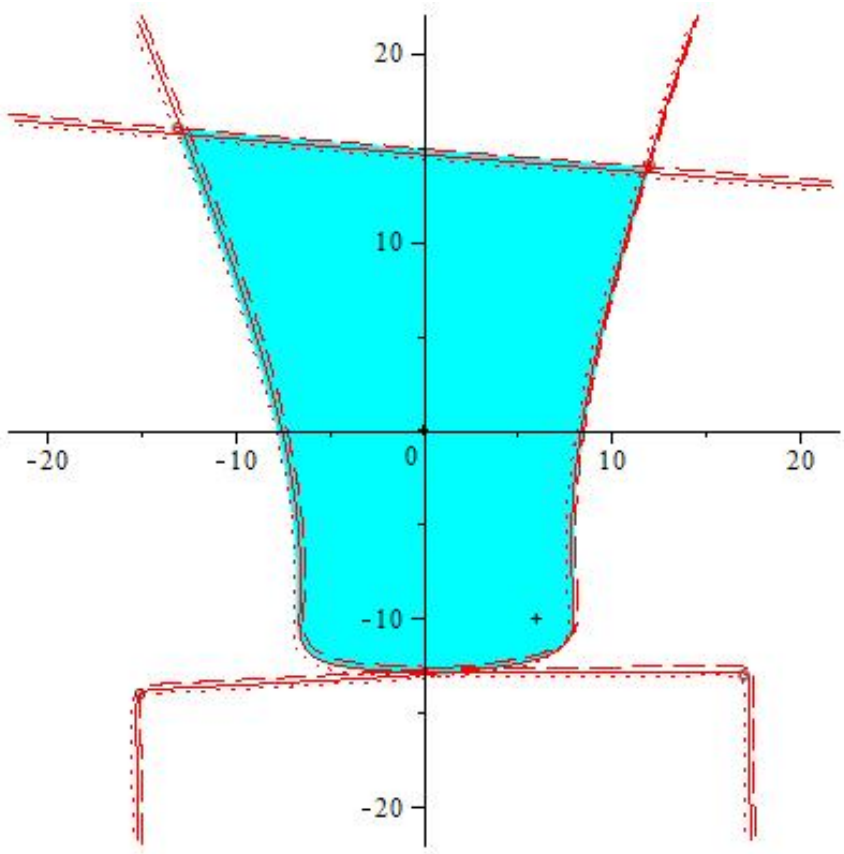

Figure 4.12: Feasible static workspaces with anchor points uncertainties: lower bound values (dot) lines, upper bound values (dash lines), and actual values (continuous lines and shaded area)

Fig. 4.13 shows the tracking motion of the mobile platform supposing uncertain anchor points in the robotic system. The four controllers achieve the regulation goal under the uncertainty of the anchor point coordinates.

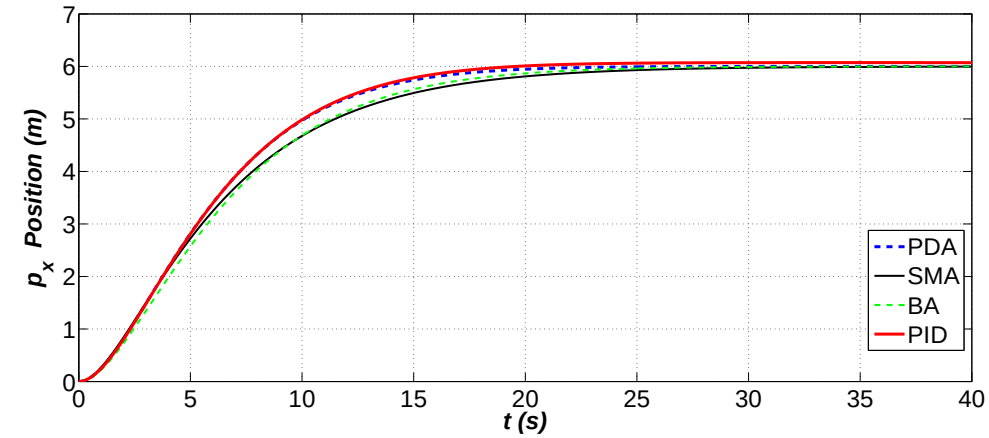

(a)

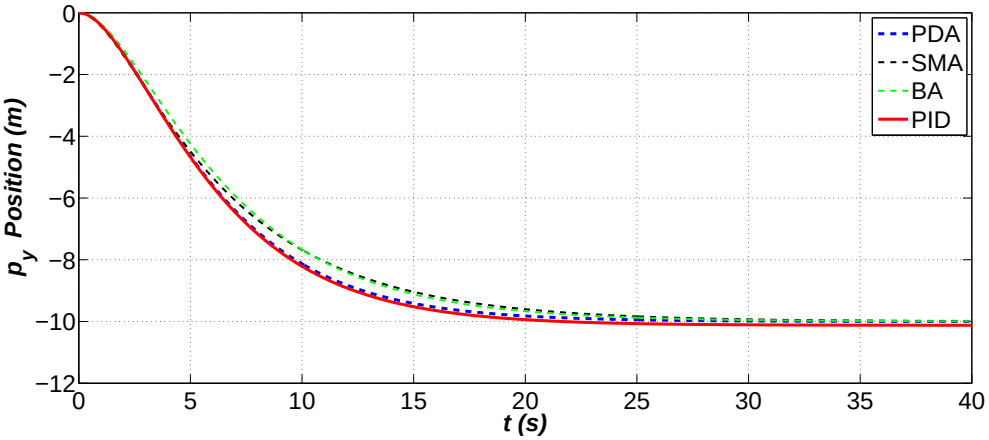

(b)

Figure 4.13: p_x and p_y position controller comparison for the four-cable robot with uncertain parameters.

The SMsatA controller is the last to achieve the desired position. The PDA and PID controller have similar performance during the first ten seconds; however, PID controller present a small offset with respect to the desired position, which remains until the end of the simulation. Although the first regulation control condition is accomplished, it is necessary to verify that the tension in four cables are always positive during all the simulation time. Thus, cable tensions results are shown in Fig 4.14.

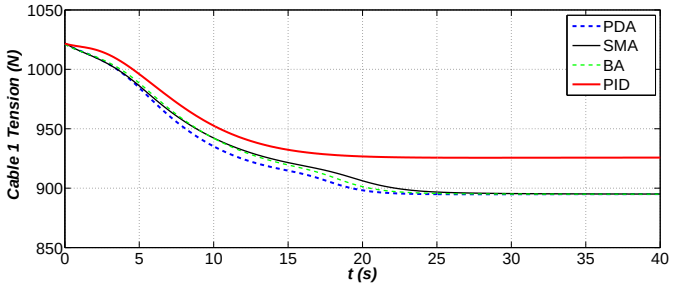

(a)

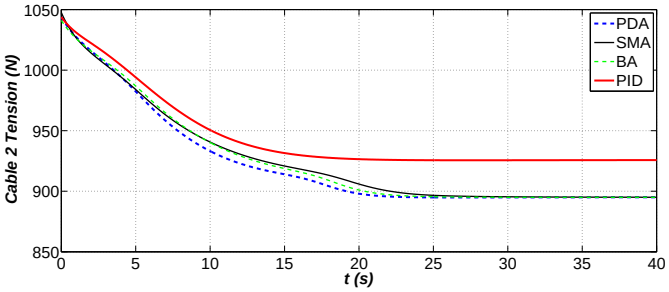

(b)

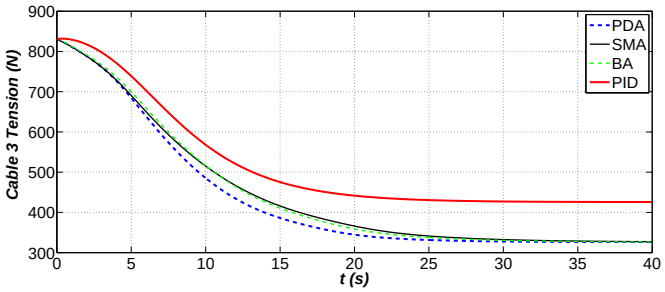

(c)

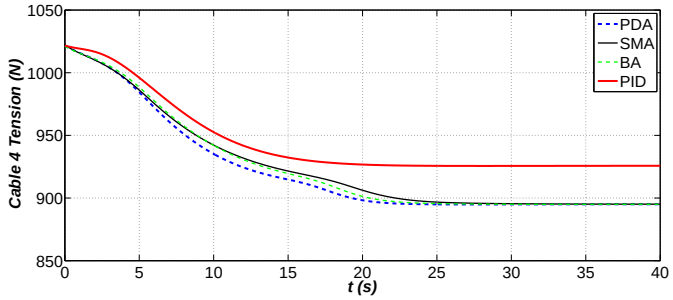

(d)

Figure 4.14: Cable tensions comparison for uncertain parameters.

Positive cable tensions are accomplished for the four controllers. Highest values of the cable tensions are below the given bounded maximum tension value. In addition, minimum cable tensions are above the given bounded minimum tension. Cable 3 reaches the lowest tensions values in four cables. In addition, cable 1 and 2 shows almost similar cable tension results. In the Fig. 4.14, PID controller has generally higher tension value than other controller.

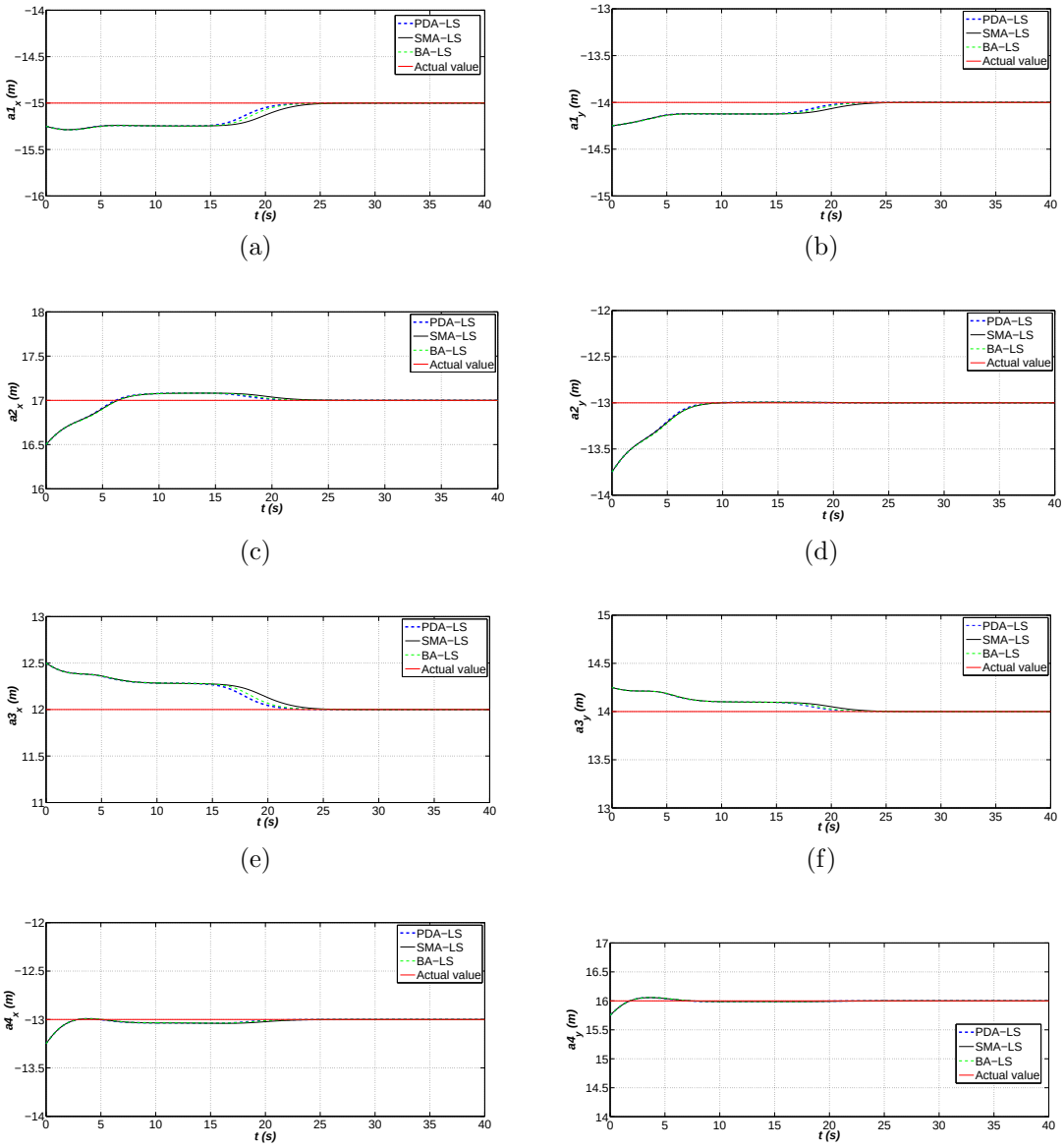

Figure 4.15: Estimated values of the coordinates of the four anchor points to actual anchor points with recursive least squares algorithm.

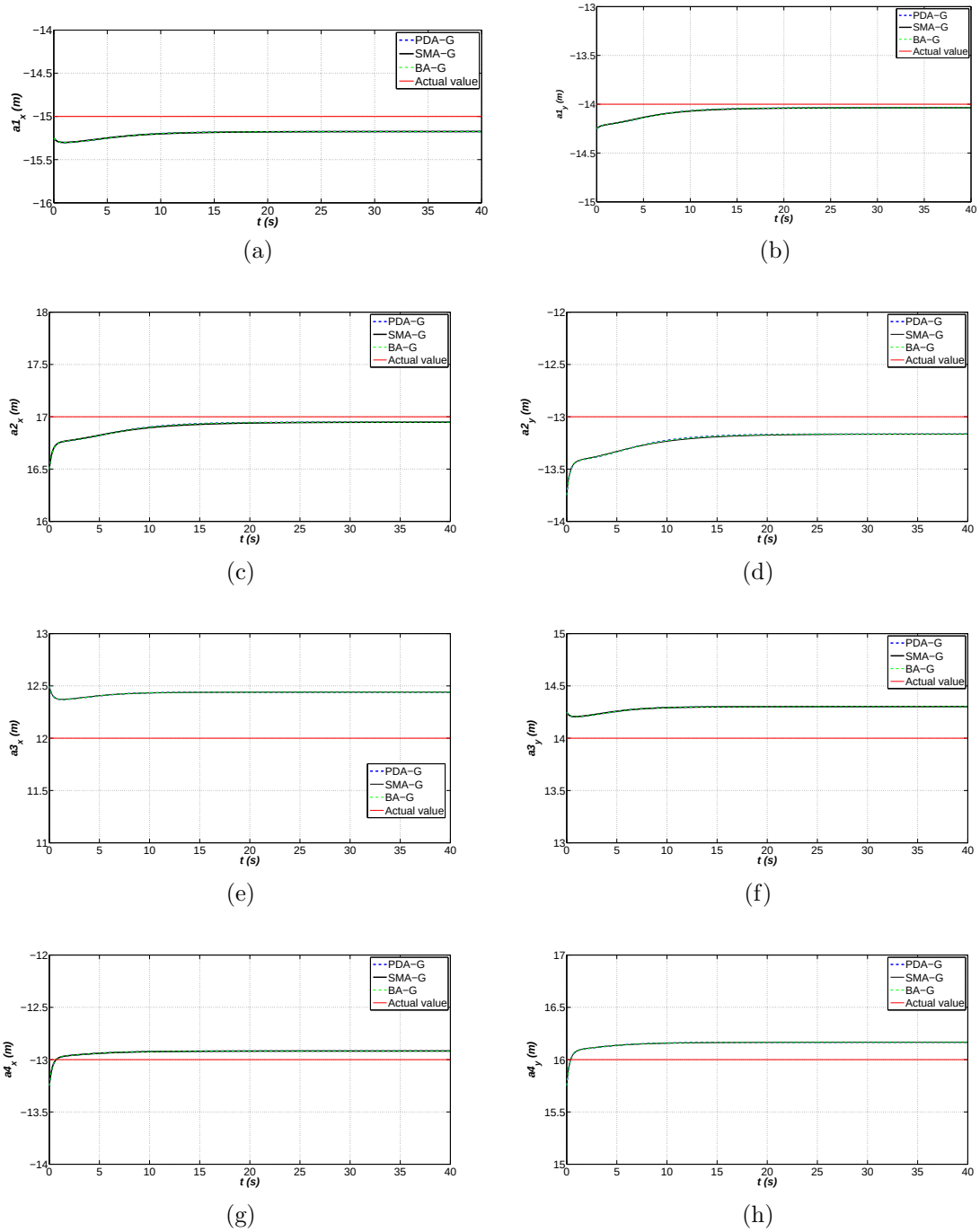

Figure 4.16: Estimated values of the coordinates of the four anchor points to actual anchor points with gradient algorithm.

Figures 4.15 and 4.16 show estimated values of the coordinates of the four anchor points to actual anchor points. The recursive least squares algorithm converges to actual values of anchor points in less than 25 seconds. However, gradient algorithm is not succeed in 40 seconds to converge to actual values of anchor points as shown in Fig. 4.16.

Tab. 4.4 shows the performance indexes for each controller as follows.

Table 4.4: Comparison of controllers for the 4-cable robot.

W_k	$L_2(\boldsymbol{e})$	e_f	e_l	Controller
1679.224	16.51069	0.005104	11.6619	PDA
1685.163	16.44889	0.135	11.6619	PID
1645.779	16.4399	0.025	11.6619	SMAsatA
1653.089	16.5278	0.0094	11.6619	BA

A fair comparison among the controllers is achieved by observing the similar values of the kinetic energy and initial position error during the first 5s. After the first five seconds of the trajectory, two main differences among the controllers are observed. First, the largest error is presented by the BA controller. Lastly, the PID presents the worst behavior during the last five seconds.

Chapter 5

Friction estimation and compensation

Mechanical friction can not be omitted in cable robots because the actuators in the system are affected by mechanical friction such as static and Coulomb friction. Hence, cables can not be in desired tension [2]. In general, we can say the friction raises position error in a trajectory. According to Kino [2], increasing the internal force causes enhancing load on the shafts which is in each actuator unit and pulley as a result, mechanical friction in actuators is increased. We can conclude that even if increasing the internal tension to decrease the position error, this increases directly mechanical friction. That's why as a result precision of position error is increased. The author [2] uses the dither technique to overcome effect of friction. The author in [29] presents tension distribution algorithm with dual-space feed-forward scheme adding viscous and static motor friction effects. Cazalilla et al. [30] use adaptive control approach to identify the friction parameters in actuated joints of 3-DOF parallel manipulator.

Decreasing tracking errors and compensating friction force are crucial components of cable robotic system owing to friction effect. Friction is a disturbance force and it causes tracking error throughout motion. The tracking error can be diminished with friction parameters identification and compensation.

We start the chapter with a short review of the friction models used robotic control design, presented in Section 5.1 [31]. Among these friction models, we use general static friction model with a recursive least squares adaptive law for cable robotic system because of overcome mechanical friction in actuators and then, establish an adaptive motion control scheme based on the adaptive law.

5.1 Friction models

5.1.1 The Capstan friction for pulley

The Capstan friction is a friction formulation between the cables and anchors. The Capstan friction model can define as follows

$$\tau_2 = \tau_1 e^{\mu\beta}. \tag{5.1}$$

In Eq. (5.1) represents a relationship with output τ_1, and input tension of cables on the pulleys. μ is friction coefficient and β is cable angle which is contact with pulley.

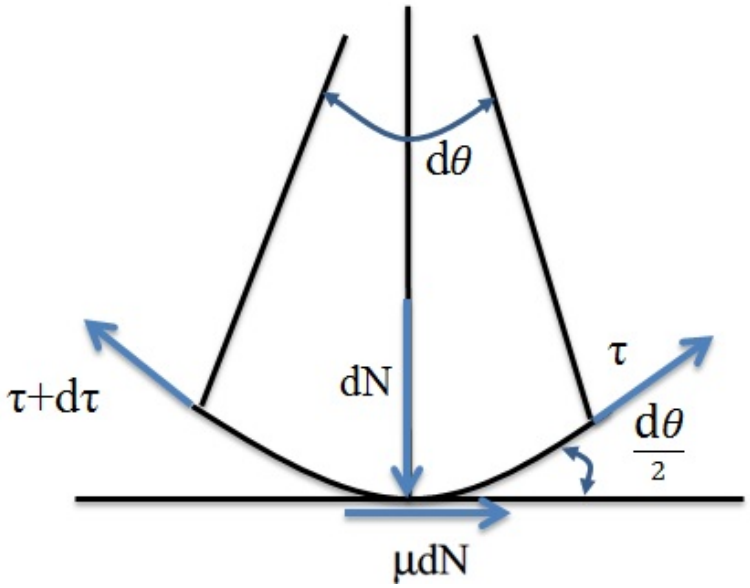

(a)

Figure 5.1: Free body diagram.

Using the free body diagram in Fig. 5.1, the equilibrium forces [32] in direction of x and y can be written respectively as follows

$$\sum \tau_x = \tau cos(\frac{d\theta}{2}) + \mu(dN) - (\tau + d\tau)cos(\frac{d\theta}{2}) = \mu(dN) - d\tau = 0, \tag{5.2}$$

$$\sum \tau_y = dN - (\tau + d\tau)sin(\frac{d\theta}{2}) + \tau sin(\frac{d\theta}{2}) = dN - \tau d\theta = 0. \tag{5.3}$$

Substituting Eq. 5.2 into Eq. 5.3, we can rewrite the equations as follows

$$\frac{d\tau}{\tau} = \mu d\theta. \tag{5.4}$$

Taking the integration of Eq. 5.4 as

$$\int_{\tau_1}^{\tau_2} \frac{d\tau}{\tau} = \int_0^{\beta} \mu d\theta. \tag{5.5}$$

The general Capstan equation can define as

$$\tau_2 = \tau_1 e^{\mu\beta}. \tag{5.6}$$

Based on the Eq. (5.6), we can say the tension on the pulley, the coefficient of friction, angle of contact the pulley affect the friction force.

5.1.1.1 Classical friction models

Classical or static friction models are generally formulated a combination of viscous, static and Coulomb frictions. There are several study about classical friction models in literature. Firstly, Canudat et al. [33] define static friction force as combination of viscous and Coulomb friction forces in Eq.5.7.

$$\tau_f = \begin{cases} \tau_C^+ + \tau_v v & v \geq 0, \\ \tau_C^- + \tau_v v & v < 0. \end{cases} \tag{5.7}$$

In Eq. (5.7), τ_C^+, τ_C^- and τ_v define the Coulomb friction forces and viscous friction force, respectively and v represents the velocity of friction regime. Fig. 5.2 shows two different friction model representations which are Coulomb friction and combination of Coulomb friction and viscous friction, respectively. The fact that for Fig. 5.2b there is slope due to viscous friction in comparison with Coulomb friction.

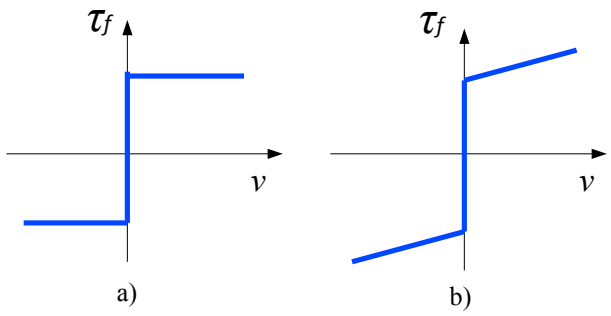

Figure 5.2: Representation of a) Coulomb friction and b) Coulomb+viscous friction models.

Next, Amstrong et. al. [34] define general formulation of static friction as follows

$$\tau_f = \begin{cases} \tau(v) & \text{if } v \neq 0 \\ \tau_e & \text{if } v = 0 \text{ and } |\tau_e| < \tau_S \\ \tau_S sgn(\tau_e) & \text{if } v = 0 \text{ and } |\tau_e| \geq \tau_S \end{cases} \tag{5.8}$$

where τ_e is external force, τ_s is static force and $\tau(v)$ is arbitrary force formulated as

$$\tau(v) = \tau_C + (\tau_S - \tau_C)e^{-|v/v_S|^{\delta_S}} + \tau_v v, \tag{5.9}$$

where v_s is the Stribeck velocity, δ_S defines the shape factor for Stribeck velocity. In addition, [35] presents a static friction model as follows

$$\tau_f = \begin{cases} \tau_S^+ e^{-v/v_{S1}^+} + \tau_C^+(1 - e^{-v/v_{S2}^+}) + \tau_v v & v \geq 0 \\ \tau_S^- e^{-v/v_{S1}^-} + \tau_C^-(1 - e^{-v/v_{S2}^-}) + \tau_v v & v < 0 \end{cases} \tag{5.10}$$

where v_{S1}^+,v_{S2}^-,v_{S1}^+ and v_{S2}^- define the velocity constants.

As shown in Fig. 5.3 d), stribeck friction has negative viscous friction force, which decreases then velocity increases and as velocity continue gets larger then friction force starts increasing. In addition, Fig. 5.3 c) shows extra friction at zero velocity because of static friction effect.

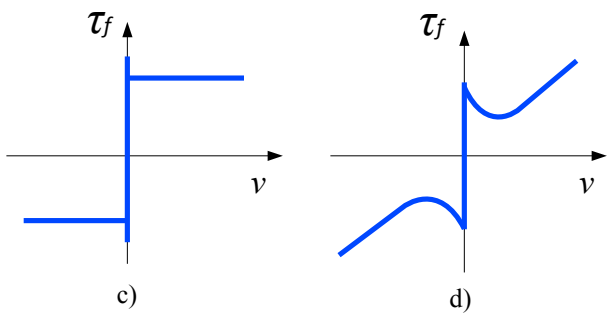

Figure 5.3: Representation of a) Static+Coulomb + viscous, b)Static +Coulomb + viscous + stribeck friction.

5.1.2 Dynamic friction

In this section, we will show several dynamic friction models in literature.

5.1.2.1 The Dahl model

Dahl [36] formulates the model for rolling and sliding friction simulations, which is related to pre sliding regime. The model idea is started with observation of bearing pre-rolling friction results close to solid material internal friction. In addition, meaning of the model is fixed friction in sliding regime such as static friction. The general Dahl model [37] can be written as

$$\frac{\mathrm{d}\tau_f}{\mathrm{d}x} = \sigma \left| 1 - \frac{\tau_f}{\tau_C} sgn(v) \right|^i sgn\left(1 - \frac{\tau_f}{\tau_C} sgn(v) \right), \tag{5.11}$$

where τ_C is the Coulomb friction force σ is the initial stiffness at velocity reversal, v is velocity, and i is the model exponent parameter that defines hysteresis shape. Using the the Dahl model as shown Eq. 5.11, we can obtain position dependent hysteresis loops. However, the model does not contain Stribeck effect, friction lag and break away force. There are several studies with using the directly basic model or the modified models in literature.

5.1.2.2 The LuGre model

The LuGre [38] model is one of the dynamic friction model to cover Stribeck friction effect in which the Dahl model has not contain. The general idea of the model is based on the fictitious bristles on which is stationary surface as shown in Fig. 5.4.

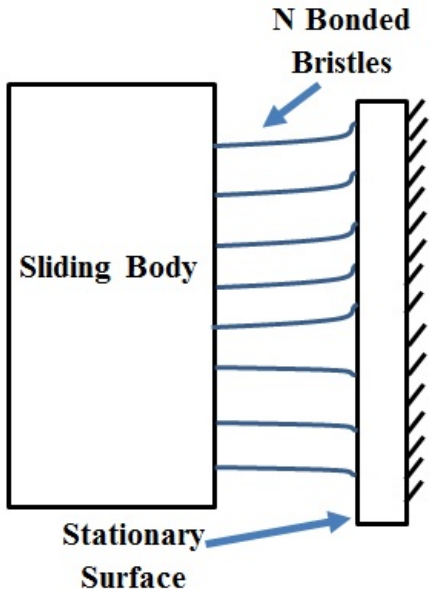

Figure 5.4: The bristle model.

Lets define the z as average deflection bristles and then, we can write derivation of the average deflection as follows

$$\frac{\mathrm{d}z}{\mathrm{d}t} = v - \frac{|v|}{g(v)}z, \tag{5.12}$$

where velocity of the sliding surface is called v and $g(v) > 0$ defines the Stribeck friction which is gradually decrease from $g(0)$ when the velocity get increase. In addition, it relates to material properties, temperature and lubricant.

The friction force can be written based on the fictitious bristles model as

$$\tau_f = \sigma_0 z + \sigma_1 \frac{\mathrm{d}z}{\mathrm{d}t} \tag{5.13}$$

where σ_0 is stiffness coefficient, σ_1 is the viscous damping coefficient. After adding the viscous friction term, the general friction force equation is

$$\tau_f = \sigma_0 z + \sigma_1 \frac{\mathrm{d}z}{\mathrm{d}t} + \sigma_2 v, \tag{5.14}$$

where σ_2 is the viscous friction coefficient.

Stribeck term can be written as follows

$$\sigma_0 g(v) = \tau_C + (\tau_S - \tau_C) e^{-|v/v_S|^2} \tag{5.15}$$

where τ_S is static friction, τ_C is Coulomb friction and v_S is Stribeck velocity.

In general, we can say the model contain Stribeck effect, friction lag and break away. However, friction forces do not only relates to current values of displacement but also it carries on with its past extremum values that can be called as the hysteresis behavior with nonlocal memory. [39].

5.1.2.3 The Leuven model

The Leuven Model is modeled to overcome the problem which is hysteresis behavior with nonlocal memory. Leuven model [40] can be written as

$$\tau_f = \tau_h(z) + \sigma_1 \frac{dz}{dt} + \sigma_2 v, \tag{5.16}$$

$$\frac{dz}{dt} = \left(1 - sgn\left(\frac{\tau_d}{s(v) - \tau_b}\right) \left|\frac{\tau_d}{s(v) - \tau_b}\right|^n\right), \tag{5.17}$$

where $\tau_h(z)$=τ_d+τ_b defines the hysteresis friction force is , τ_d, and τ_b are friction force at the starting of the transition curve and $s(v)$ is stribeck velocity.

We can say the model cover the Stribeck effect, friction lag, break away force and hysteresis behavior with nonlocal memory, however; the model could contain discontinuity in the friction force because of equality of τ_b to earlier values of $\tau_h(z)$. By replacing $\tau_d(z)/(s(v) - \tau_b)$ with $\tau_h(z)/s(v)$.

This problem was beat with modification which is using $\tau_h(z)/s(v)$ instead of $\tau_d(z)/(s(v)-\tau_b)$ in [41]. Thus, the Eq. (5.17) can be rewrite as

$$\frac{dz}{dt} = \left(1 - sgn\left(\frac{\tau_d}{s(v) - \tau_b}\right)\left|\frac{\tau_h(z)}{s(v)}\right|^n\right) \tag{5.18}$$

5.2 Parametric estimation and adaptive feedback control of planar cable robot

Adaptive motion control scheme involve on-line friction adaptive estimation and compensation, are shown in Figure 5.5.

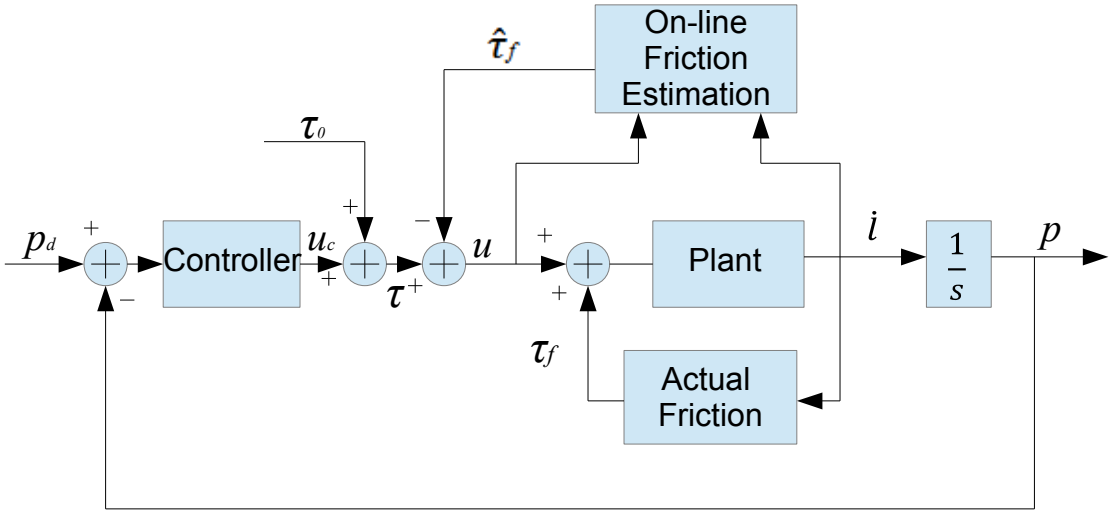

Figure 5.5: Parametric friction estimation and adaptive motion control scheme.

We use recursive least squares algorithm for estimation of friction parameters to their actual values.

5.2.1 Parametric model

5.2.1.1 Fully constrained planar cable robot

Consider Fig.5.5 the plant model as shown in Eq.(4.1) with adding friction force for fully constrained cable robot, that is,

$$\boldsymbol{M}_p\ddot{\boldsymbol{p}} = \boldsymbol{A}\boldsymbol{u} + \boldsymbol{A}\boldsymbol{\tau}_f = \boldsymbol{A}(\boldsymbol{\tau} - \hat{\boldsymbol{\tau}}_{\boldsymbol{f}}) + \boldsymbol{A}\boldsymbol{\tau}_f \tag{5.19}$$

where $\boldsymbol{\tau}_f = [\tau_{f1}, \tau_{f2}, \tau_{f3}]^T$ is the matrix of friction forces, $\boldsymbol{M}_p = [diag(m_p, m_p)]$ denotes mass matrix, $\boldsymbol{\tau} = [\tau_1, \tau_2, \tau_3]^T$ represents resultant control input, $\boldsymbol{A}$ is structural 2×3 matrix and acceleration of end effector can be represented as $\ddot{\boldsymbol{p}} = [\ddot{p}_x, \ddot{p}_y]^T$, $\boldsymbol{u}$=$[u_1, u_2, u_3]$ is combination of resultant control input and estimated friction force $\hat{\boldsymbol{\tau}}_f$.

In Eq. (5.19), $\ddot{\boldsymbol{p}}$ and $\boldsymbol{\tau}$ are known signals. The general static parametric model (SPM) is obtained as

$$\boldsymbol{z}_i = \boldsymbol{\theta}_i^{*T}\boldsymbol{\phi}_i \tag{5.20}$$

where

$$\boldsymbol{z} = [z_1, z_2, z_3]^T = \boldsymbol{A}^{\dagger}(\boldsymbol{M}_p\ddot{\boldsymbol{p}} - \boldsymbol{A}\boldsymbol{u}) \tag{5.21}$$

$$\boldsymbol{\theta}_{\boldsymbol{i}}^{*} = \left[\tau_{si}^{-},\ \ \tau_{ci}^{-},\ \ \tau_{si}^{+},\ \ \tau_{ci}^{+},\ \ \tau_{vi}\right]^T, \forall i = 1, 2, 3. \tag{5.22}$$

$$\boldsymbol{\phi}_i = \begin{bmatrix} g^{-}(w_{li})f_1^{-}(w_{li}) \\ g^{-}(w_{li})f_2^{-}(w_{li}) \\ g^{+}(w_{li})f_1^{+}(w_{li}) \\ g^{+}(w_{li})f_2^{+}(w_{li}) \\ g^{0}(w_{li})w_{li} \end{bmatrix}, \forall i = 1, 2, 3. \tag{5.23}$$

$$f_1^{+}(w_{li}) = e^{-w_{li}/v_{S1}^{+}} \ \ , \ \ \forall i = 1, 2, 3.$$
$$f_2^{+}(w_{li}) = 1 - e^{-w_{li}/v_{S2}^{+}} \ \ , \ \ \forall i = 1, 2, 3.$$
$$f_1^{-}(w_{li}) = e^{-w_{li}/v_{S1}^{-}} \ \ , \ \ \forall i = 1, 2, 3.$$
$$f_2^{-}(w_{li}) = 1 - e^{-w_{li}/v_{S2}^{-}} \ \ , \ \ \forall i = 1, 2, 3.$$

$$g^{o}(w_{li}) = \begin{cases} 1 & |w_{li}| \geq \psi \\ 0 & |w_{li}| < \psi \end{cases} \ \ , \ \ \forall i = 1, 2, 3.$$

$$g^{-}(w_{li}) = \begin{cases} 1 & w_{li} < -\psi \\ 0 & w_{li} \geq -\psi \end{cases}, \quad \forall i = 1, 2, 3.$$

$$g^{+}(w_{li}) = \begin{cases} 0 & w_{li} < \psi \\ 1 & w_{li} \geq \psi \end{cases} \quad \forall i = 1, 2, 3.$$

Here, $\boldsymbol{z}$ and $\boldsymbol{\phi}$ are available for measurements. τ_s^+ and τ_c^+ are static and Coulomb friction parameters which are in direction of positive motion, τ_s^- and τ_c^- are in direction of negative motion. In addition, viscous term is called as τ_v and w_l defines cable velocity.

The constant v_{s1} and v_{s2} can be selected in terms of the system and v_{s1} and v_{s2} are assumed they are available and can be selected different values in terms of the system. Also, we use threshold term, ψ to avoid the direction misinterpretations.

5.2.2 Estimation model

Estimation model can be written as

$$\hat{\boldsymbol{z}}_i = \boldsymbol{\theta}_i(t)^T \boldsymbol{\phi}_i, \quad \forall i = 1, 2, 3. \tag{5.24}$$

where $\boldsymbol{\theta_i(t)}$ is the estimate of $\boldsymbol{\theta_i^*}$ at time t.

5.2.3 PI algorithm (Adaptive laws)

5.2.3.1 Recursive Least squares algorithm

$$\dot{\boldsymbol{\theta}}_i = \boldsymbol{P}_i \epsilon_i \boldsymbol{\phi_i}, \quad \boldsymbol{\theta}_i(0) = \boldsymbol{\theta}_{0i} \tag{5.25}$$

$$\dot{\boldsymbol{P}}_i = \beta \boldsymbol{P}_i - \boldsymbol{P}_i \boldsymbol{\phi}_i^T \boldsymbol{P}_i, \quad \boldsymbol{P}_i(0) = \boldsymbol{P}_{0i} = \boldsymbol{Q}_{0i}^{-1}, \quad \forall i = 1, 2, 3. \tag{5.26}$$

where $\boldsymbol{P}$ is the covariance matrix and β is the forgetting factor. The estimation error term ϵ is given by

$$\epsilon_i = \frac{z_i - \hat{z}_i}{m_s^2} = \frac{z_i - \boldsymbol{\theta}_i^T(t)}{m_s^2}, \quad \forall i = 1, 2, 3. \tag{5.27}$$

$m_s^2 \geq 1$ is a normalization signal designed to guarantee that

$$\frac{\boldsymbol{\phi_i}}{m_s^2} \in \ with \quad m_s^2 = 1 + \alpha \boldsymbol{\phi_i}^T \boldsymbol{\phi_i}, \ \alpha > 0. \ \forall i = 1, 2, 3. \tag{5.28}$$

5.2.3.2 Backstepping adaptive control

Let us consider dynamic equation with perfect compensation assumption, we can rewrite the system equations in state-space form as

$$\begin{aligned} \dot{\boldsymbol{p}}_1 &= \boldsymbol{p}_2 \\ \dot{\boldsymbol{p}}_2 &= \boldsymbol{M}_{\boldsymbol{p}}^{-1}\boldsymbol{A}\boldsymbol{u}_c \end{aligned} \tag{5.29}$$

where the output of this system is $\boldsymbol{p_1} = \boldsymbol{p}$ which follow the reference signal. The defining intended errors can be expressed as $\boldsymbol{e}_1 = \boldsymbol{p}_1 - \boldsymbol{p}_d$, $\boldsymbol{e_2} = \dot{\boldsymbol{p}}_1 - \dot{\boldsymbol{p}}_d$. Then, the state equation of these tracking errors is written as fs

$$\begin{cases} \dot{\boldsymbol{e}}_1 = \boldsymbol{e}_2 \\ \dot{\boldsymbol{e}}_2 = \boldsymbol{M}_{\boldsymbol{p}}^{-1}\boldsymbol{A}\boldsymbol{u_c} - \ddot{\boldsymbol{p}}_d \end{cases} \tag{5.30}$$

where $\boldsymbol{M}_{\boldsymbol{p}}^{-1}\boldsymbol{A}\boldsymbol{u}_c = \bar{\boldsymbol{u}}$

Define the following new state variables for the design backstepping controller.

$$\begin{aligned} \boldsymbol{z}_1 &= \boldsymbol{p}_1 - \boldsymbol{p}_d = \boldsymbol{e}_1, \\ \boldsymbol{z}_2 &= \boldsymbol{e}_2 - \boldsymbol{e}_{2d} = \boldsymbol{e}_2 + \boldsymbol{K}\boldsymbol{e}_1. \end{aligned} \tag{5.31}$$

where $\boldsymbol{e}_{2d} = -K\boldsymbol{e}_1$ is the desired value of the e_2. Taking the derivation of the Eq. (5.31),

$$\begin{aligned} \dot{\boldsymbol{z}}_1 &= \boldsymbol{e}_2 \\ \dot{\boldsymbol{z}}_2 &= \dot{\boldsymbol{e}}_2 + K\dot{\boldsymbol{e}}_1. \end{aligned} \tag{5.32}$$

Substituting the Eq. (5.31) into Eq. (5.32), the new state variable can be written as follows

$$\begin{aligned} \dot{\boldsymbol{z}}_1 &= -K\boldsymbol{z}_1 + \boldsymbol{z}_2 \\ \dot{\boldsymbol{z}}_2 &= \bar{\boldsymbol{u}} - \ddot{\boldsymbol{p}}_{\boldsymbol{d}} + K(-K\boldsymbol{z}_1 + \boldsymbol{z}_2) = -K^2\boldsymbol{z}_1 + K\boldsymbol{z}_2 + \bar{\boldsymbol{u}} - \ddot{\boldsymbol{p}}_d. \end{aligned} \tag{5.33}$$

Selecting the $\bar{\boldsymbol{u}} = a_1\boldsymbol{z_1} + a_2\boldsymbol{z_2} + \ddot{\boldsymbol{p}}_{\boldsymbol{d}}$ to remove $\ddot{\boldsymbol{p}}_d$ and the $\dot{\boldsymbol{z}}$ can rewrite as

$$\dot{\boldsymbol{z}}_2 = (a_1 - K^2)\boldsymbol{z}_1 + (a_2 + K)\boldsymbol{z}_2. \tag{5.34}$$

We can express the new derivation of the state variable with matrix form as

$$\begin{bmatrix} \dot{\boldsymbol{z}}_1 \\ \dot{\boldsymbol{z}}_2 \end{bmatrix} = \begin{bmatrix} -K & 1 \\ (a_1 - K^2) & (a_2 + K) \end{bmatrix} \begin{bmatrix} z_1 \\ z_2 \end{bmatrix} \tag{5.35}$$

Lets propose $a_1 = K^2$ and $a_2 = -2K$. Then, we can rewrite as

$$\begin{bmatrix} \dot{\boldsymbol{z}}_1 \\ \dot{\boldsymbol{z}}_2 \end{bmatrix} = E \begin{bmatrix} \boldsymbol{z}_1 \\ \boldsymbol{z}_2 \end{bmatrix} \tag{5.36}$$

where $\boldsymbol{E} = \begin{bmatrix} -K & 1 \\ 0 & -K \end{bmatrix}$.

Backstepping controller back-steps the control Ke_1 through the integrator as mentioned above. Backstepping controller can be completed by using the following Lyapunov function and its derivative as

$$V(\boldsymbol{z}_1, \boldsymbol{z}_2) = \frac{1}{2}(\boldsymbol{z}_1^T \boldsymbol{z}_1 + \boldsymbol{z}_2^T \boldsymbol{z}_2) \tag{5.37}$$

$$\begin{aligned} \dot{V}(\boldsymbol{z}_1, \boldsymbol{z}_2) &= \boldsymbol{z}_1^T \dot{\boldsymbol{z}}_{\boldsymbol{1}} + \boldsymbol{z}_2^T \dot{\boldsymbol{z}}_{\boldsymbol{2}} < 0 \\ &= \begin{bmatrix} \boldsymbol{z}_{\boldsymbol{1}}^T & \boldsymbol{z}_{\boldsymbol{2}}^T \end{bmatrix} \begin{bmatrix} \dot{\boldsymbol{z}}_1 \\ \dot{\boldsymbol{z}}_2 \end{bmatrix} < 0 \\ &= \begin{bmatrix} \boldsymbol{z}_1^T & \boldsymbol{z}_2^T \end{bmatrix} \boldsymbol{E} \begin{bmatrix} \boldsymbol{z}_1 \\ \boldsymbol{z}_2 \end{bmatrix} < 0. \end{aligned} \tag{5.38}$$

where $\boldsymbol{E} < 0 \rightarrow$ negative definition. Substituting the equations (5.31) and (5.32) into Eq. (5.38) the derivation of Lyapunov function can be rewritten as

$$\dot{V} = -K^3 \boldsymbol{e}_1^2 - K\boldsymbol{e}_2^2 + (1 - 2K^2)\boldsymbol{e}_1 \boldsymbol{e}_2 < 0 \tag{5.39}$$

Recalling the $\bar{u}$ in Eq. (5.30) and (5.33), the equilibrium can be defined as follows

$$\bar{\boldsymbol{u}} = \boldsymbol{M}_{\boldsymbol{p}}^{-1} \boldsymbol{A} \boldsymbol{u}_{\boldsymbol{c}} = K^2 \boldsymbol{z}_1 - 2K\boldsymbol{z}_2 + \ddot{\boldsymbol{p}}_{\boldsymbol{d}} \tag{5.40}$$

Thus,

$$\boldsymbol{u}_{\boldsymbol{c}} = \boldsymbol{A}^{\dagger} \boldsymbol{M}_{\boldsymbol{p}} (K^2 \boldsymbol{z}_1 - 2K\boldsymbol{z}_2 + \ddot{\boldsymbol{p}}_d) \tag{5.41}$$

The internal cable tension vector $\boldsymbol{\tau}_0$, is added to the control law in order to ensure the always positive cable tension conditions. The below resultant control law is valid if all parameters are known.

$$\boldsymbol{\tau} = \boldsymbol{A}^{\dagger} \boldsymbol{M}_{\boldsymbol{p}} (-K^2 \boldsymbol{e}_1 - 2K\boldsymbol{e}_2 + \ddot{\boldsymbol{p}}_d) + \boldsymbol{\tau}_{\boldsymbol{0}} \tag{5.42}$$

5.3 Simulation

In this section, simulation results are presented. Using a fully constrained planar cable robot, two type of computer simulations are conducted by using MATLAB and a trajectory is given for all motor rotations have both positive and negative directions. Recursive least squares algorithm is taken from [20] develops a estimation of friction parameters. Then, a Dormond-Prince method is used for evaluation the controller with friction compensation and without compensation. The mass of the end effector is m_p= 30 kg and initial position of end effector is in origin point. In addition, we assume the desired position of the mobile platform belongs to the feasible workspace of the cable robot and the pseudo inverse of structure matrix exists.

There are two scenarios in this study. First scenario is when the controller, actual friction and parametric friction estimator simultaneously are activated. This scenario can be called adaptive estimation and compensation scheme. Second scenario consists of the controller and actual friction force but not parameter estimator.

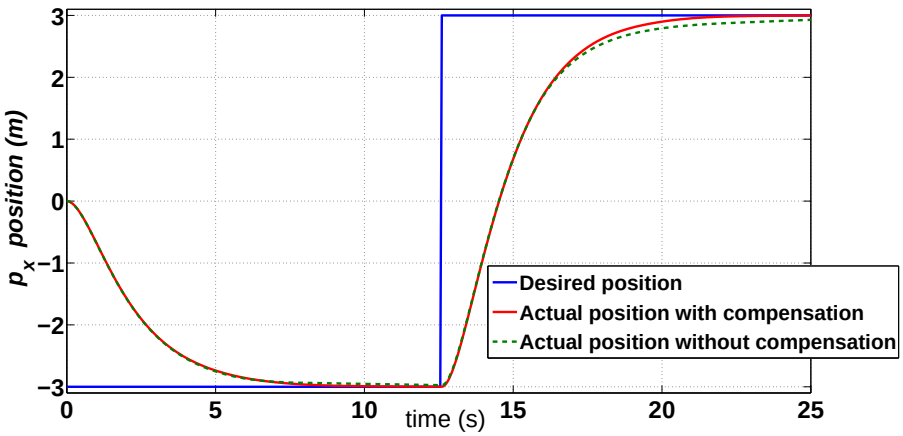

(a)

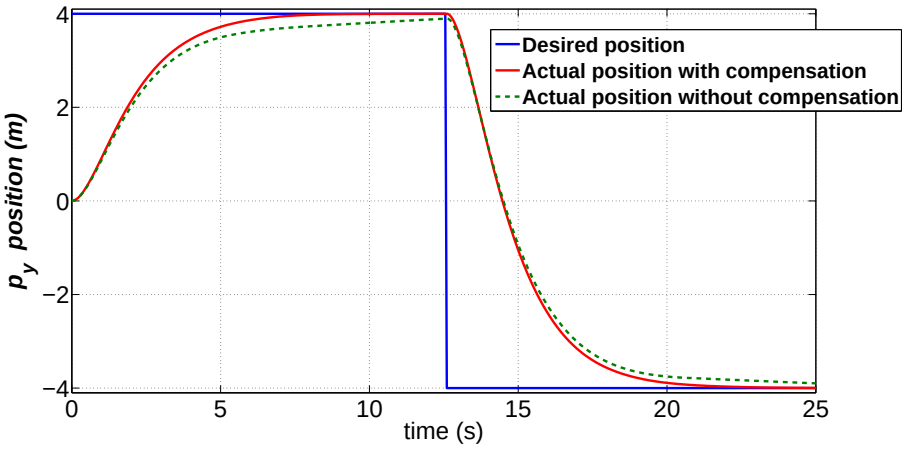

(b)

Figure 5.6: a)p_x and b)p_y position controller comparison for the three-cable robot with friction compensation and without compensation.

Fig. 5.6 depicts that tracking errors go to almost zero with compensation in eight seconds for each cycle in Fig. 5.6. However, the tracking errors without compensation in Fig. 5.6 do not reach to zero because of friction force.

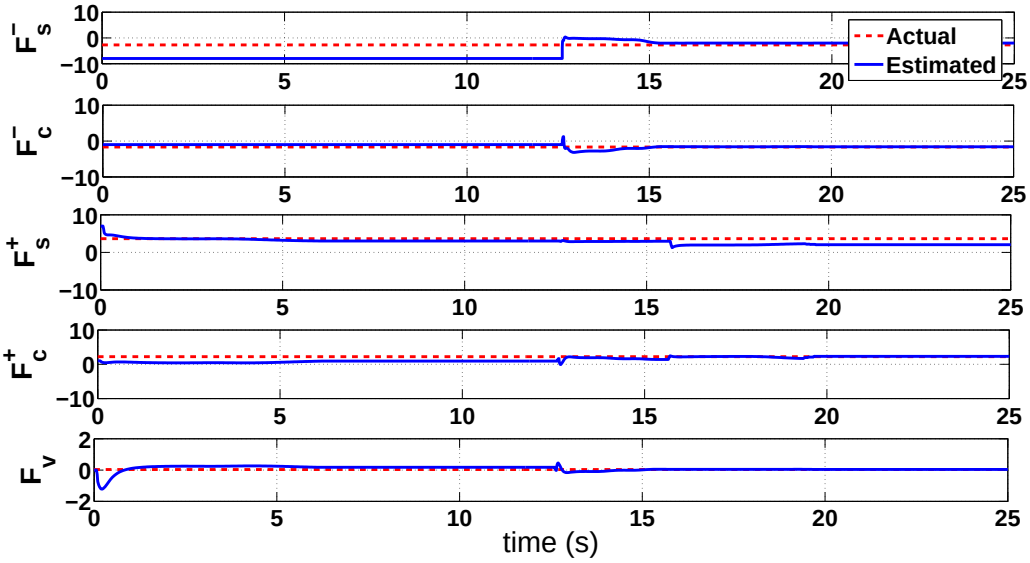
Actual
Estimated
F_s^-
F_c^-
F_s^+
F_c^+
F_v
time (s)

(a)

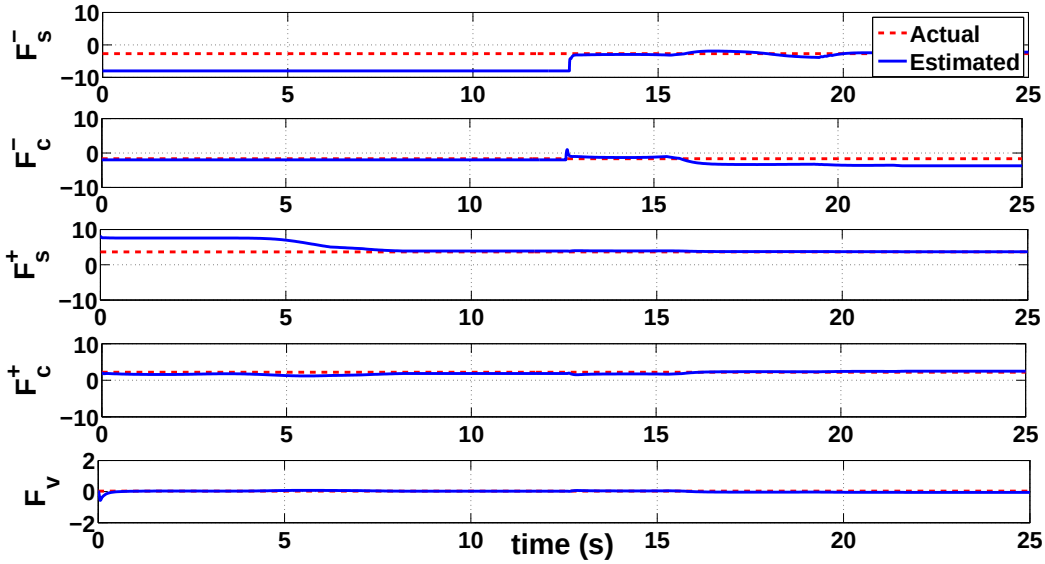
Actual
Estimated
F_s^-
F_c^-
F_s^+
F_c^+
F_v
time (s)

(b)

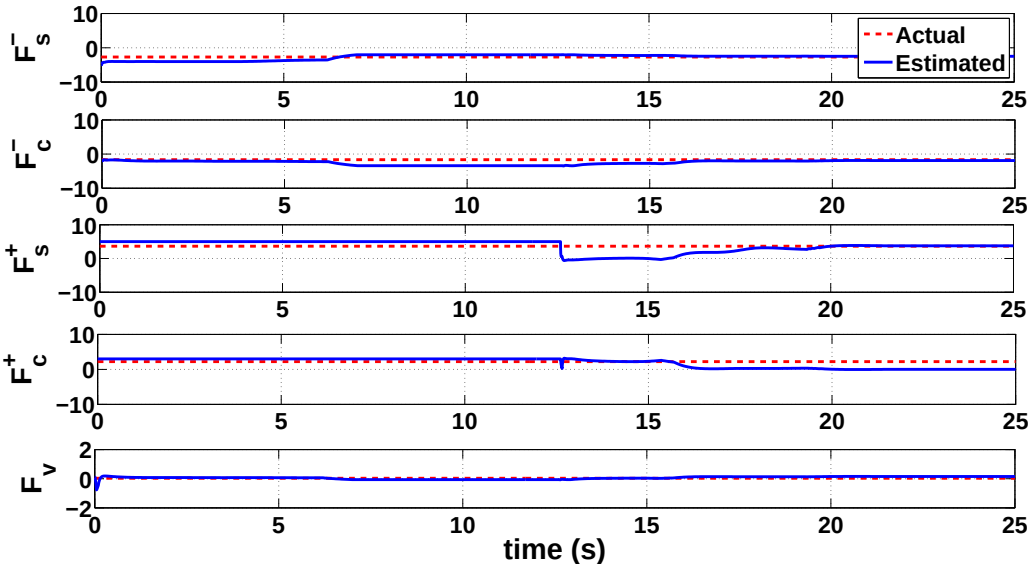

(c)

Figure 5.7: Friction parameter estimation results for adaptive backstepping control scheme a) motor-1, b) motor-2, c) motor-3, respectively.

In addition, it can be seen from Fig. 5.7, recursive least squares algorithm almost converge actual values of friction parameters after 20 seconds for a) motor-1, b) motor-2, c) motor-3, respectively.

Chapter 6

Discussions and Conclusion

In this study, a comparison study among the four controllers, SMsatA, Backstepping, PDA and PID, are developed for a fully-constrained and redundant planar cable robot. In other words, the well-known PID benefits, such as simplicity and robustness, are evaluated against the adaptive control formulations that require the construction of a parametric model and a parameter estimation algorithm. The proposed adaptive controllers were designed for an uncertain structure matrix which results of error in the measured anchor points. In addition, feasible workspace for both configurations are studied and depicted for a given set of bounded cable tensions.

Numerical simulations have shown a concordance with the theory; that is, adaptive controllers are shown to be asymptotically stable. However, an experimental validation might give a more reliable sight to the adaptation problem.

Three quantifiable indexes are established for comparison purpose; that is, the L_2 norm of position errors during the first and the last 5 seconds of each simulation. It is observed that both the consumed kinetic energy and the position errors during the first 5 seconds have similar values in each controller, which allows a fair comparison between the controllers.

Simulations in Chapter 4 have shown that the PDA controller presents both advantages: robustness and convergence at the desired point when under the presence of a uncertain structure matrix; moreover, the all-positive cable tensions is achieved with minimum values.

Finally, simulation results in Chapter 5 show on-line parameter estimation algorithms and adaptive control schemes have achieved desired performance.

References

[1] S. Behzadipour. Kinematics and dynamics of a self-stressed cartesian cable-driven mechanism. *Journal of Mechanical Design*, 131(6):1487–1509, 2009.

[2] H. Kino. Principle of orthohonalization for completely restrained parallel wire driven robot. In *Proc. of the IEEE/ASME International Conference on Advanced Intelligent Mechatronics*, pages 509–514. AIM, 2003.

[3] S. Kawamura, H. Kino, and C. Won. High-speed manipulation by using parallel wire-driven robots. *Robotica*, 18(1):13–21, 2000.

[4] J. Albus, R. Bostelman, and N. Dagalakis. The nist robocrane. *Journal of Robotic Systems*, 10(5):709–724, 1992.

[5] S. Kawamura, W. Choe, S. Tanaka, and S. Pandian. Development of an ultrahigh speed robot falcon using wire drive system. In *Proc. IEEE ICRA, Nagoya, Japan*, volume 1, page 215220. IEEE, 1995.

[6] M. Zarebidoki, A. Lotfavar, and H.R. Fahham. Dynamic modeling and adaptive control of a cable-suspended robot. In *Proc. of the World Congress on Engineering*, volume 3, pages 215–220. WCE, 2011.

[7] S. Lahouar, E. Ottaviano, S. Zeghoul, and L. Romdhane. Collision free path-planning for cable-driven parallel robots. *Robotics and Autonomous Systems*, pages 1083–1093.

[8] M. Hiller, S. Fang, S. Mielczarek, R. Verhoeven, and D. Franitza. Design, analysis and realization of tendon-based parallel manipulators. *Mechanism and Machine Theory*, 40:429–445, 2005.

[9] P. D. Campbell, P. L. Swaim, and C. J. Thompson. Charlotte robot technology for space and terrestrial applications. In *Proc. 25th International Conference on Environmental Systems, San Diego*. SAE Paper 951520, 1993.

[10] S. Oh and S. K. Agrawal. Cable-suspended planar parallel robots with redundant cables: controllers with positive cable tensions. In *Proc. International Conference Robotics and Automation*, volume 3, pages 3023–3028. IEEE, 2003.

[11] P. Gholami, M. M. Aref, and H. D. Taghirad. On the control of the kntu cdrpm: A cable driven redundant parallel manipulator. In *Proc. of Internationl Conference on Intelligent Robots and Systems (IROS)*, pages 2404–2409. IEEE/RSJ, 2008.

[12] A. Ming and T. Higuchi. Study on multiple degree-of-freedom positioning mechanism using wires (part 1) - concept, design and control. *International Journal of the Japan Society for Precision Engineering*, 28(2).

[13] R. G Roberts, T. Graham, and T. Lippitt. On the inverse kinematics, statics, and fault tolerance of cable-suspended robots. *Journal of Robotic Systems*, 15(10).

[14] X. Diao and O. Ma. A method of verifying force-closure condition for general cable manipulators with seven cables. *Mechanism and Machine Theory*, 42(12).

[15] M. Hassan and A. Khajepour. Minimum-norm solution for the actuator forces in cable-based parallel manipulators based on convex optimization. In *Proc. 2007 IEEE International Conference on Robotics and Automation*, pages 1498–1503. IEEE, 2007.

[16] C. B. Pham, G. Yang, and S. H. Yeo. Dynamic analysis of cable-driven parallel mechanisms. In *Proc. 2005 Advanced Intelligent Mechatronics*, pages 612–617. IEEE/ASME, 2005.

[17] S. Fang, D. Franitza, and M. Torlo. Motion control of a tendon-based parallel manipulator using optimal tension distribution. *IEEE/ASME Transactions on Mechatronics*, 9(3).

[18] H. Kino, T. Yahiro, and F. Takemura. Adaptive position control for fully constrained parallel wire driven systems. In *Proc. Intelligent Robots and Systems*, pages 79–84. IEEE/RSJ, 2006.

[19] G. Tao. *Adaptive Control Design and Analysis*. John Wiley and Sons Inc., Hoboken, NJ, USA, 2004.

[20] P. Ioannou and B. Fidan. *Adaptive Control Tutorial*. Society for Industrial Mathematics, 2006.

[21] J. Angeles. *Rational Kinematics*. Springer, 1988.

[22] S. Behzadipour and A. Khajepour. Stiffness of cable-based parallel manipulators with application to stability analysis. *Transactions of the ASME*, 128(1):303–310, 2006.

[23] S. J. Torres Mendez. Low mobility cable robot with application to robotic warehousing, phd thesis.

[24] S. J. Torres Mendez, G. Gungor, B. Fidan, and A. Khajepour. Comparison of adaptive and robust controllers for fully-constrained and redundant planar cable robots. In *Proc. of International Mechanical Engineering Congress and Exposition*. ASME, 2014.

[25] G. Gungor, S. J. Torres Mendez, B. Fidan, and A. Khajepour. Estimation of anchor points for fully-constrained and redundant planar cable robots. In *Proc. of International Mechanical Engineering Congress and Exposition*. ASME, 2014.

[26] H. D. Taghirad. *Parallel Robots; Mechanics and Control*. CRC Press, 2011.

[27] V.I. Utkin. Variable structure systems with sliding modes. *IEEE Transaction on Automatic Control*, 22(2):212–222, 1977.

[28] N. N. Krasovskii. Some problems of the theory of stability of motion. *[English translation Stanford]*, 1963.

[29] J. Lamaury and M. Gouttefarde. Control of a large redundantly actuated cable-suspended parallel robot. In *Proc. of IEEE International Conference on Robotics and Automation (ICRA)*, pages 383–396. IEEE, May 6-10, 2013.

[30] J. Cazalilla, M. Valls, V. Mata, M. Daz-Rodrguez, and A. Valera. Adaptive control of a 3-dof parallel manipulator considering payload handling and relevant parameter models. *Robotics and Computer-Integrated Manufacturing, Elsevier*, 30:468–477, 2014.

[31] H. M. Turhan. System identification and adaptive compensation of friction in manufacturing automation systems, *MASc Thesis*.

[32] W. Stephen Attaway. The mechanics of friction in rope rescue. In *International Technical Rescue Symposium*, 1999.

[33] C. Canudas de Wit, K. Astrom, and K. Braun. Adaptive friction compensation in dc-motor drives. *IEEE Journal of Robotics and Automation*, 3(6):681–685, 1987.

[34] H. Olsson, K. J. Åström, C. Canudas De Wit, M. Gäfvert, and P. Lischinsky. Friction models and friction compensation. *European journal of control*, 4:176–195, 1998.

[35] K. Erkorkmaz and Y. Altintas. High speed cnc system design. part ii: modeling and identification of feed drives. *International Journal of Machine Tools and Manufacture*, 41(10):1487–1509, 2001.

[36] P. R. Dahl. A solid friction model. *The Aerospace Corporation*, 1968.

[37] P. R. Dahl. Measurement of solid friction parameters of ball bearings. *The Aerospace Corporation*, 1977.

[38] C. Canudas de Wit, H. Olsson, K. J. Astrom, and P. Lischinsky. A new model for control of systems with friction. *Automatic Control*, 40(3):419–425, 1995.

[39] I. D. Mayergoyz. *Mathematical Models of Hysteresis and Their Applications*. Academic Press, 2003.

[40] J. Swevers, F. Al-Bender, C. G. Ganseman, and T. Projogo. An integrated friction model structure with improved presliding behavior for accurate friction compensation. *Automatic Control, IEEE Transactions on*, 45(4):675–686, 2000.

[41] V. Lampaert, J. Swevers, and F. Al-Bender. Modification of the leuven integrated friction model structure. *Automatic Control, IEEE Transactions on*, 47(4):683–687, 2002.

[42] E. Levin. Friction experiments with a capstan. *Am. J. Phys*, 1991.

[43] D. A. Haessig Jr and B. Friedland. Modeling and simulation of friction. In *Orlando, FL*, pages 383–396. International Society for Optics and Photonics, 1991.

[44] S. J. Torres-Mendez and A. Khajepour. Design optimization of a warehousing cable-based robot. In *Proc. of the ASME 2014 International Design Technical Conference and Computers and Information in Engineering Conference IDETC/CIE*, pages 383–396. ASME, August 17-20, 2014.

[45] S. J. Torres-Mendez and A. Khajepour. Analysis of a high stiffness warehousing cable-based robot. In *Proc. of the ASME 2014 International Design Technical Conference and Computers and Information in Engineering Conference IDETC/CIE*, pages 383–396. ASME, August 17-20, 2014.